AN EFFICIENT INTERFERENCE-AWARE CONSTRAINED BEAMFORMING AND RECEIVER DESIGN FOR MM-WAVE HYBRID MASSIVE MIMO WITH NON-ORTHOGONAL MULTIPLE ACCESS

A THESIS SUBMITTED TO
THE GRADUATE SCHOOL OF NATURAL AND APPLIED SCIENCES
OF
MIDDLE EAST TECHNICAL UNIVERSITY

BY

MURAT BAYRAKTAR

IN PARTIAL FULFILLMENT OF THE REQUIREMENTS
FOR
THE DEGREE OF MASTER OF SCIENCE
IN
ELECTRICAL AND ELECTRONICS ENGINEERING

JULY 2021

Approval of the thesis:

AN EFFICIENT INTERFERENCE-AWARE CONSTRAINED BEAMFORMING AND RECEIVER DESIGN FOR MM-WAVE HYBRID MASSIVE MIMO WITH NON-ORTHOGONAL MULTIPLE ACCESS

submitted by **MURAT BAYRAKTAR** in partial fulfillment of the requirements for the degree of **Master of Science in Electrical and Electronics Engineering Department, Middle East Technical University** by,

Prof. Dr. Halil Kalıpçılar
Dean, Graduate School of **Natural and Applied Sciences** _____

Prof. Dr. İlkay Ulusoy
Head of Department, **Electrical and Electronics Engineering** _____

Assist. Prof. Dr. Gökhan Muzaffer Güvensen
Supervisor, **Electrical and Electronics Engineering, METU** _____

Examining Committee Members:

Prof. Dr. Ali Özgür Yılmaz
Electrical and Electronics Engineering, METU _____

Assist. Prof. Dr. Gökhan Muzaffer Güvensen
Electrical and Electronics Engineering, METU _____

Prof. Dr. Çağatay Candan
Electrical and Electronics Engineering, METU _____

Assoc. Prof. Dr. Ayşe Melda Yüksel Turgut
Electrical and Electronics Engineering, TOBB University _____

Assoc. Prof. Dr. Berkan Dülek
Electrical and Electronics Engineering, Hacettepe University _____

Date: 13.07.2021

I hereby declare that all information in this document has been obtained and presented in accordance with academic rules and ethical conduct. I also declare that, as required by these rules and conduct, I have fully cited and referenced all material and results that are not original to this work.

Name, Surname: Murat Bayraktar

Signature :

ABSTRACT

AN EFFICIENT INTERFERENCE-AWARE CONSTRAINED BEAMFORMING AND RECEIVER DESIGN FOR MM-WAVE HYBRID MASSIVE MIMO WITH NON-ORTHOGONAL MULTIPLE ACCESS

Bayraktar, Murat
M.S., Department of Electrical and Electronics Engineering
Supervisor: Assist. Prof. Dr. Gökhan Muzaffer Güvensen

July 2021, 92 pages

This thesis investigates efficient interference-aware beamformer design for mm-wave massive multiple-input and multiple-output (MIMO) systems. Furthermore, adaptation of code-domain non-orthogonal multiple access (NOMA) to mm-wave massive MIMO is studied. The first part of the thesis concentrates on interference-aware pre-beamformer (analog beamformer) design for joint spatial division and multiplexing (JSDM) which is a user-grouping based two-stage beamforming method. Single-carrier frequency domain equalization (SC-FDE) is employed in uplink wideband channels. First, unconstrained statistical analog beamformer of each group, namely, generalized eigenbeamformer (GEB) which has strong interference suppression capability is designed. Then, constant-modulus constrained approximations of unconstrained beamformer are obtained by utilizing alternating minimization algorithms. Moreover, a dynamic subarray algorithm is proposed where the connections between radio frequency (RF) chains and antennas are dynamically changed. Minimum mean square error (MMSE) criterion based iterative block decision feedback equalization (IB-DFE) method, which takes the residual interference in reduced dimension into account, is proposed for intra-group processing. Simulation results verify the superi-

ority of the proposed interference-aware constrained design over existing approaches in terms of beampattern, spectral efficiency, outage capacity, bit-error rate (BER) and channel estimation accuracy. The second part of the thesis is devoted to the development of a novel wideband signal model in beamspace for code-domain NOMA with SC-FDE transmission in JSDM framework. Based on this signal model, a code-beamspace IB-DFE receiver is proposed for joint equalization and multiuser detection, and it is shown that code-domain NOMA is beneficial, especially for mm-wave massive MIMO systems with limited number of RF chains and spatial correlation.

Keywords: mm-wave systems, massive MIMO, dynamic subarray, constrained beamformer, code-domain NOMA

ÖZ

DİK OLMAYAN ÇOKLU ERİŞİMLİ MİLİMETRE DALGA HİBRİT MASİF MIMO İÇİN EFEKTİF BİR GİRİŞİM DUYARLI HÜZME ŞEKİLLENDİRME VE ALICI TASARIMI

Bayraktar, Murat
Yüksek Lisans, Elektrik ve Elektronik Mühendisliği Bölümü
Tez Yöneticisi: Dr. Öğr. Üyesi. Gökhan Muzaffer Güvensen

Temmuz 2021 , 92 sayfa

Bu tez milimetre dalga masif MIMO için verimli ve girişime duyarlı hüzme şekillendirici tasarımını incelemektedir. Buna ek olarak, kod alanı NOMA'nın milimetre dalga masif MIMO sistemlerine adaptasyonu üzerine çalışılmıştır. Tezin ilk kısmı, kullanıcı gruplamasına dayalı iki aşamalı hüzme şekillendirme yöntemi olan JSDM için girişime duyarlı ön hüzme şekillendirici (analog hüzme şekillendirici) tasarımına odaklanmaktadır. SC-FDE, yer-uydu bağı geniş bantlı kanallar için kullanılmıştır. İlk olarak, her bir grubun kısıtsız istatistiksel analog hüzme şekillendiricisi, güçlü girişim bastırma kabiliyetine sahip GEB, tasarlanmıştır. Ardından alternatif minimizasyon algoritmaları kullanılarak kısıtsız hüzme şekillendiricinin sabit değer kısıtlı yaklaşımları elde edilmiştir. Ayrıca, RF zincirleri ile antenler arasındaki bağlantıların değiştirildiği dinamik bir alt dizin algoritması önerilmiştir. Dijital hüzme şekillendirme aşaması için MMSE kriteri tabanlı azaltılmış boyuttaki artık girişimi dikkate alan IB-DFE yöntemi önerilmektedir. Simülasyon sonuçları, ışın modeli, spektral verimlilik, kesinti kapasitesi, bit-hata oranı ve kanal kestirimi doğruluğu açısından önerilen

girişime duyarlı kısıtlı tasarımın mevcut yaklaşımlara göre üstünlüğünü doğrulamaktadır. Tezin ikinci kısmı, JSDM çerçevesinde SC-FDE iletimi ile kod alanlı NOMA için hüzme uzayında yeni bir geniş bantlı sinyal modelinin geliştirilmesine ayrılmıştır. Bu sinyal modeline dayalı olarak, ortak eşitleme ve çok kullanıcılı algılama için bir kod-hüzme-uzaylı IB-DFE alıcısı önerilmiş ve kod alanı NOMA'nın, özellikle sınırlı sayıda RF zincirine ve uzaysal korelasyona sahip milimetre dalga masif MIMO sistemlerinde faydalı olduğu gösterilmiştir.

Anahtar Kelimeler: milimetre dalga sistemleri, masif MIMO, dinamik alt dizin, kısıtlı hüzme şekillendirici, kod alanı NOMA

To my loved ones

ACKNOWLEDGMENTS

I would like to express my gratitude to my supervisor Assist. Prof. Gökhan Muzaffer Güvensen for his endless support and guidance. This thesis would not have been possible without the insightful discussions we had throughout the course of my research. I am grateful to have him as my supervisor during my MSc studies.

I would also like to thank Prof. Ali Özgür Yılmaz for his valuable suggestions and guidance during my studies.

I want to thank Scientific and Technological Research Council of Turkey (TUBİTAK) for supporting my studies through 2210-A National Scholarship Programme for MSc Students. I also thank Information and Communication Technologies Authority and Turkcell for the research support they provided at the beginning of my MSc studies.

I would like to thank my friends Berk Ataeli and Eren Berk Kama for their encouragement, suggestions and friendship throughout my undergraduate and graduate education at METU.

I am eternally indebted to my family for their support throughout my life. It would not have been possible for me to even set my goals let alone achieving them without their endless encouragement.

Finally, I give my best gratitude to my loving wife, Yağmur, for being patient and supporting throughout my life, including the times I spent for the preparation of this thesis. She has always encouraged me when I encountered obstacles both in life and in my research, and I am grateful to her.

TABLE OF CONTENTS

LIST OF TABLES

TABLES

LIST OF FIGURES

FIGURES

LIST OF ABBREVIATIONS

AoA	Angle of arrival
AoD	Angle of departure
AS	Angular spread
BER	Bit-error rate
BS	Base station
CCM	Channel covariance matrix
CDF	Cumulative density function
CFO	Carrier-frequency-offset
CSI	Channel state information
FD	Fully digital
FDE	Frequency domain equalization
GEB	Generalized eigenbeamformer
IB-DFE	Iterative block decision feedback equalization
IDMA	Interleave division multiple access
ISI	Inter-symbol interference
JSDM	Joint spatial division and multiplexing
LDS	Low density spreading
LMMSE	Linear minimum mean square error
LS	Least squares
MC	Multicarrier
MFB	Matched filter bound
MIMO	Multiple-input multiple-output
mm-Wave	Millimeter wave
MSE	Mean square error

MMSE	Minimum mean square error
MPA	Message passing algorithm
MPC	Multipath component
MUSA	Multi-user shared access
nMSE	Normalized mean square error
NOMA	Non-orthogonal multiple access
OFDM	Orthogonal frequency division multiplexing
PAPR	Peak-to-average power ratio
PE	Phase extraction
PE-AM	Phase extraction with alternating minimization
POCS	Projections onto convex sets
RF	Radio frequency
SC	Single-carrier
SC-FDE	Single-carrier frequency domain equalization
SCMA	Sparse code multiple access
SIC	Successive interference canccellation
SINR	Signal-to-interference-plus-noise ratio
SNR	Signal-to-noise ratio
TDD	Time division duplexing
ULA	Uniform linear array
WMMSE	Weighted minimum mean square error
ZF	Zero-forcing

NOMENCLATURE

Scalars

α	Multiplier of Q-function in the theoretical BER expression for QAM modulation
$\beta^{(g_u),i}$	Complex amplitude of user u in group g at the output of i^{th} DFE iteration
$\Delta_l^{(g_u)}$	Angular spread of user u in group g at l^{th} MPC
$\gamma^{(g_u)}$	Channel gain of user u in group g
$\hat{a}_m^{(g),i}$	Time domain estimates of NOMA symbols of user u in group g at m^{th} interval at the output of i^{th} DFE iteration
$\hat{a}_{f,k}^{(g),i}$	Frequency domain estimates of NOMA symbols of user u in group g at k^{th} frequency bin at the output of i^{th} DFE iteration
$\hat{x}_n^{(g),i}$	Time domain estimates of symbols of user u in group g at n^{th} time instance at the output of i^{th} DFE iteration
$\hat{x}_{f,k}^{(g),i}$	Frequency domain estimates of symbols of user u in group g at k^{th} frequency bin at the output of i^{th} DFE iteration
κ	Multiplier in the argument of Q-function in the theoretical BER expression for QAM modulation
$\lambda^{(g)}$	MIMO-NOMA loading of group g
$\mu_l^{(g_u)}$	Mean AoA of user u in group g at l^{th} MPC
$\nu_i^{(g)}$	Phase of non-zero entry in the i^{th} row of $\mathbf{S}_c^{(g)}$ for partially connected arrays
$\nu_i^{(g)}$	Phase of the non-zero entry in the i^{th} row of $\mathbf{S}_c^{(g)}$ for fixed subarrays
$\overline{SINR}^{(g)}$	Statistical SINR of group g

ϕ	Shifting angle of Group-1 for the mobile scenario
$\rho_l^{(g_u)}(\theta)$	Angular power profile of user u in group g at l^{th} MPC as a function of incident angle θ
θ	Incident angle in azimuth
$\tilde{a}_m^{(g),i}$	Time domain NOMA soft decisions of user u in group g at m^{th} interval at the output of i^{th} DFE iteration
$\tilde{a}_{f,k}^{(g),i}$	Frequency domain NOMA soft decisions of user u in group g at k^{th} frequency bin at the output of i^{th} DFE iteration
$\tilde{x}_n^{(g),i}$	Time domain soft decisions of user u in group g at n^{th} time instance at the output of i^{th} DFE iteration
$\tilde{x}_{f,k}^{(g),i}$	Frequency domain soft decisions of user u in group g at k^{th} frequency bin at the output of i^{th} DFE iteration
$\xi_n^{(g_u),i}$	Residual interference of user u in group g at n^{th} time instant at the output of i^{th} DFE iteration
$a_m^{(g_u)}$	Transmitted NOMA symbol of user u in group g at m^{th} interval
$a_{f,k}^{(g)}$	Frequency domain transmitted NOMA symbol of user u in group g at k^{th} frequency bin
$B(\theta)$	Beampattern as a function of incident angle θ
$C_i^{(g_u)}$	Ergodic capacity of user u in group g at the output of i^{th} DFE iteration
D	Total number of RF chains at the BS
D_g	Number of RF chains allocated to group g
E_b	Bit energy per user
$E_s^{(g)}$	Total symbol energy of group g
G	Number of user groups
g	User group index

g_u	User u in group g
i	IB-DFE iteration index
i_{max}	Number of IB-DFE iterations
$j(i)$	Column where i^{th} of row of the analog beamformer has the non-zero entry for partially connected arrays
k	Frequency bin index
L	Total number of MPCs
l	MPC index
L_{eff}	Number of effective MPCs
M	Number of antennas at the BS
m	NOMA symbol index
N	Block length
n	Time index
N_0	Noise variance
N_c	Spreading sequence length
N_s	Number of NOMA symbols transmitted in a block of length N
N_{iter}	Number of times Algorithm 3 is repeated
n_{max}	Number of iterations of alternating minimization algorithm
$nMSE^{(g)}$	nMSE of beamspace channel estimation of group g
p	Effective MPC index
$P_b^{(g),i}$	Theoretical BER of group g at the output of i^{th} DFE iteration
$SINR_i^{(g_u)}$	SINR of user u in group g at the output of i^{th} DFE iteration
$SNR^{(g)}$	SNR of group g
T	Training sequence length

U	Total number of users
u	User index
U_g	Number of users in group g
$x_n^{(g_u)}$	Transmitted signal of user u in group g at n^{th} time instance
$x_{f,k}^{(g)}$	Frequency domain transmitted signal of user u in group g at k^{th} frequency bin

Vectors

$\bar{\boldsymbol{\eta}}_m^{(g)}$	Equivalent NOMA interference vector of group g at m^{th} interval
$\bar{\boldsymbol{\eta}}_{f,k}^{(g)}$	Normalized DFT of $\bar{\boldsymbol{\eta}}_m^{(g)}$ at k^{th} frequency bin
$\bar{\mathbf{h}}_{eff}^{(g,g')}$	Overall effective channel vector of group g' at the output of the analog beamformer of group g
$\bar{\mathbf{n}}_n$	Overall noise vector at the BS during uplink training for channel estimation
$\bar{\mathbf{x}}_m^{(g)}$	Equivalent transmitted NOMA signal vector of group g at m^{th} interval
$\bar{\mathbf{y}}^{(g)}$	Overall received signal in reduced dimension at the BS during uplink training for channel estimation
$\bar{\mathbf{y}}_m^{(g)}$	Equivalent received NOMA signal vector of group g at m^{th} interval
$\bar{\mathbf{y}}_{f,k}^{(g)}$	Normalized DFT of $\bar{\mathbf{y}}_m^{(g)}$ at k^{th} frequency bin
$\boldsymbol{\eta}_n^{(g)}$	Full dimensional sum of inter-group signals and noise of group g at n^{th} time instance
$\hat{\bar{\mathbf{h}}}_{eff}^{(g,g)}$	Estimate of $\bar{\mathbf{h}}_{eff}^{(g,g)}$
$\hat{\mathbf{a}}_m^{(g),i}$	Time domain estimates of NOMA symbols of group g at m^{th} interval at the output of i^{th} DFE iteration
$\hat{\mathbf{a}}_{f,k}^{(g),i}$	Frequency domain estimates of NOMA symbols of group g at k^{th} frequency bin at the output of i^{th} DFE iteration

$\hat{\mathbf{x}}_n^{(g),i}$	Time domain estimates of symbols of group g at n^{th} time instance at the output of i^{th} DFE iteration
$\hat{\mathbf{x}}_{f,k}^{(g),i}$	Frequency domain estimates of symbols of group g at k^{th} frequency bin at the output of i^{th} DFE iteration
$\mathbf{a}_m^{(g)}$	Transmitted NOMA symbol vector of group g at m^{th} interval
$\mathbf{a}_{f,k}^{(g)}$	Frequency domain transmitted NOMA symbol vector of group g at k^{th} frequency bin
$\mathbf{e}_i$	Unitary vector with a specified dimension whose i^{th} entry is one whereas others are zero
$\mathbf{f}_n$	Arbitrary vector at time instance n
$\mathbf{f}_{f,k}$	Normalized DFT of $\mathbf{f}_n$ at k^{th} frequency bin
$\mathbf{h}_l^{(g_u)}$	Channel vector of user u in group g at l^{th} MPC
$\mathbf{h}_{eff,l}^{(g,g')}$	Overall effective channel vector of all users user in group g' at the output of analog beamformer of group g
$\mathbf{h}_{eff,l}^{(g,g'_u)}$	Effective channel vector of user u in group g' at the output of analog beamformer of group g at l^{th} MPC
$\mathbf{n}_n$	Noise vector at the BS at n^{th} time instance
$\mathbf{q}^{(g_u)}$	Unit norm spreading code of user u in group g with length N_c
$\mathbf{s}_n^{(g)}$	Full dimensional intra-group signals of group g at n^{th} time instance
$\mathbf{u}(\theta)$	Unit norm steering vector for incident angle θ
$\mathbf{v}_i$	i^{th} most dominant eigenvector of the generalized eigenvalue problem
$\mathbf{x}_n^{(g)}$	Transmitted signal vector of group g at n^{th} time instance
$\mathbf{x}_{f,k}^{(g)}$	Frequency domain transmitted signal vector of group g at k^{th} frequency bin
$\mathbf{y}_n$	Received signal at the BS at n^{th} time instance

$\mathbf{z}_l^{(g_u)}$ Random $M \times 1$ vector which has zero-mean circularly symmetric complex Gaussian entries with unit variance

$\tilde{\boldsymbol{\eta}}_{f,k}^{(g)}$ Normalized DFT of $\tilde{\boldsymbol{\eta}}_n^{(g)}$ at k^{th} frequency bin

$\tilde{\boldsymbol{\eta}}_n^{(g)}$ Sum of inter-group signals and interference of group g in reduced dimension at n^{th} time instance

$\tilde{\mathbf{a}}_m^{(g),i}$ Time domain NOMA soft decisions of group g at m^{th} interval at the output of i^{th} DFE iteration

$\tilde{\mathbf{a}}_{f,k}^{(g),i}$ Frequency domain NOMA soft decisions of group g at k^{th} frequency bin at the output of i^{th} DFE iteration

$\tilde{\mathbf{n}}_n^{(g)}$ Noise vector at the output of analog beamformer of g at n^{th} time instance

$\tilde{\mathbf{n}}_{f,k}^{(g)}$ Normalized DFT of $\tilde{\mathbf{n}}_n^{(g)}$ at k^{th} frequency bin

$\tilde{\mathbf{s}}_n^{(g)}$ Intra-group signals of group g in reduced dimension at n^{th} time instance

$\tilde{\mathbf{s}}_{f,k}^{(g)}$ Normalized DFT of $\tilde{\mathbf{s}}_n^{(g)}$ at k^{th} frequency bin

$\tilde{\mathbf{x}}_n^{(g),i}$ Time domain soft decisions of group g at n^{th} time instance at the output of i^{th} DFE iteration

$\tilde{\mathbf{x}}_{f,k}^{(g),i}$ Frequency domain soft decisions of group g at k^{th} frequency bin at the output of i^{th} DFE iteration

$\tilde{\mathbf{y}}_n^{(g)}$ Signal vector at the output of analog beamformer of group g at n^{th} time instance

$\tilde{\mathbf{y}}_{f,k}^{(g)}$ Normalized DFT of $\tilde{\mathbf{y}}_n^{(g)}$ at k^{th} frequency bin

Matrices

$\bar{\mathbf{H}}_{eff,p}^{(g,g)}$ Augmented effective channel matrix of group g for p^{th} effective MPC

$\boldsymbol{\Delta}_i^{(g)}$ Consequence of the constraint on feedback filters for the solution of optimum filters of IB-DFE receiver

$\boldsymbol{\Gamma}^{(g)}$ Matrix carrying the spreading information in group g

$\mathbf{\Lambda}_{eff,k}^{(g,g')}$	Frequency domain effective channel matrix of group g' at the output of analog beamformer of group g at k^{th} frequency bin
$\mathbf{\Lambda}_{f,k}^{(g,g)}$	Frequency domain equivalent NOMA channel matrix of group g at k^{th} frequency bin
$\mathbf{\Pi}^{(g)}$	Binary connection matrix of group g showing the connections between antennas and RF chains
$\mathbf{\Psi}_{p}^{(g,g)}$	Equivalent NOMA channel matrix of group g for p^{th} effective MPC
$\mathbf{A}$	Arbitrary invertible matrix
$\mathbf{A}^{(g)}$	Arbitrary unitary matrix
$\mathbf{A}_{k}^{(g),i}$	A solution matrix used to find optimum filters for group g at k^{th} frequency bin at i^{th} DFE iteration
$\mathbf{C}_{k}^{(g),i}$	Feedback filter of IB-DFE receiver of group g for k^{th} frequency bin at i^{th} iteration
$\mathbf{D}_{k}^{(g),i}$	A solution matrix used to find optimum filters for group g at k^{th} frequency bin at i^{th} DFE iteration
$\mathbf{E}^{(g)}$	Column selection matrix of group g for DFT beamformer
$\mathbf{H}_{eff,l}^{(g,g')}$	Effective channel matrix of group g' at the output of analog beamformer of group g at l^{th} MPC
$\mathbf{H}_{l}^{(g)}$	Channel matrix of group g at l^{th} MPC
$\mathbf{P}_{1}^{(g),i}$	Correlation matrix between transmitted symbols and soft decisions of group g for i^{th} DFE iteration
$\mathbf{P}_{2}^{(g),i}$	Correlation matrix of soft decisions of group g for i^{th} DFE iteration
$\mathbf{Q}$	DFT matrix
$\mathbf{R}_{l}^{(g_u)}$	CCM of user $u$group g at l^{th} MPC
$\mathbf{R}_{\hat{\mathbf{h}}_{eff}^{(g,g)}\bar{\mathbf{h}}_{eff}^{(g,g)}}$	Covariance between $\hat{\bar{\mathbf{h}}}_{eff}^{(g,g)}$ and $\bar{\mathbf{h}}_{eff}^{(g,g)}$

$\mathbf{R}_{\hat{\bar{\mathbf{h}}}_{eff}^{(g,g)}}$	Covariance matrix of $\hat{\bar{\mathbf{h}}}_{eff}^{(g,g)}$
$\mathbf{R}_{\bar{\boldsymbol{\eta}}_f}^{(g)}$	Covariance matrix of $\bar{\boldsymbol{\eta}}_f^{(g)}$
$\mathbf{R}_{\bar{\mathbf{h}}_{eff}^{(g,g)}}$	Covariance matrix of $\bar{\mathbf{h}}_{eff}^{(g,g)}$
$\mathbf{R}_{\bar{\mathbf{y}}^{(g)}\bar{\mathbf{h}}_{eff}^{(g,g)}}$	Covariance between $\bar{\mathbf{y}}^{(g)}$ and $\bar{\mathbf{h}}_{eff}^{(g,g)}$
$\mathbf{R}_{\bar{\mathbf{y}}^{(g)}}$	Covariance matrix of $\bar{\mathbf{y}}^{(g)}$
$\mathbf{R}_{\bar{\mathbf{y}}_{f,k}^{(g)}}$	Covariance matrix of $\bar{\mathbf{y}}_{f,k}^{(g)}$
$\mathbf{R}_{\boldsymbol{\eta}}^{(g)}$	Covariance matrix of $\boldsymbol{\eta}_n^{(g)}$
$\mathbf{R}_{\mathbf{s}}^{(g)}$	Covariance matrix of $\mathbf{s}_n^{(g)}$
$\mathbf{R}_{\tilde{\boldsymbol{\eta}}_f}^{(g)}$	Covariance matrix of $\tilde{\boldsymbol{\eta}}_{f,k}^{(g)}$
$\mathbf{R}_{\tilde{\mathbf{s}}_f}^{(g)}$	Covariance matrix of $\tilde{\mathbf{s}}_{f,k}^{(g)}$
$\mathbf{R}_{\tilde{\mathbf{y}}_{f,k}^{(g)}}$	Covariance matrix of $\tilde{\mathbf{y}}_{f,k}^{(g)}$
$\mathbf{S}^{(g)}$	Analog beamformer of group g
$\mathbf{S}_{cm}^{(g)}$	Compensation matrix of group g
$\mathbf{S}_{c}^{(g)}$	Constrained analog beamformer of group g
$\mathbf{S}_{GEB}^{(g)}$	GEB of group g
$\mathbf{W}_{k}^{(g),i}$	Feedforward filter of IB-DFE receiver of group g for k^{th} frequency bin at i^{th} iteration
$\mathbf{X}^{(g)}$	Equivalent pilot matrix of group g
$\mathbf{X}^{(g_u)}$	Equivalent pilot matrix of user u in group g
$\mathbf{Z}^{(g)}$	Channel estimator matrix of group g
$\tilde{\mathbf{S}}_{c}^{(g)}$	Partially connected constrained beamformer whose non-zero entry locations are unknown

CHAPTER 1

INTRODUCTION

1.1 Motivation

Massive multiple-input multiple-output (MIMO) at mm-wave bands is the frontier technology for next generation wireless communication systems due to the availability of vast spectrum [1, 2]. Hybrid analog/digital structure is an efficient approach for these systems as it has lower hardware complexity and energy consumption compared to fully digital beamforming, and mm-wave bands exhibit joint angle-delay sparsity [3]. Hence, researchers have been working on low-complexity beamformer design for hybrid systems [4–8]. Joint spatial division and multiplexing (JSDM) is a user-grouping based two-stage beamforming method where analog beamformers are designed by using slowly varying channel statistics, i.e., channel covariance matrices (CCMs) [9, 10]. User-grouping reduces signal processing complexity since digital processing of each group becomes independent from each other. In addition, only instantaneous intra-group channels in reduced dimension need to be learned which reduces channel estimation overhead.

Most of the existing researches for massive MIMO systems adopt flat-fading channel model by considering the use of orthogonal frequency division multiplexing (OFDM) [2]. The reason to prefer single-carrier (SC) modulation over OFDM in this thesis is its superiority for systems having non-linearities, such as quantized MIMO [11, 12], owing to its lower peak-to-average power ratio (PAPR) [13] and robustness to carrier-frequency-offset (CFO) errors [14]. Having lower PAPR is a critical property for systems with non-linear elements [15], where the advantages of SC transmission over the multicarrier (MC) are demonstrated. Moreover, even for unquantized linear

systems, there are many recent studies that motivate the use of SC especially for MIMO systems in mm-wave bands [16–19]. In these studies, the mitigation of inter-symbol interference (ISI) is fulfilled via reduced complexity signal processing.

On the other hand, non-orthogonal multiple access (NOMA) is another technology that has received great attention recently due to its ability to support massive connectivity [20–22]. Unlike conventional orthogonal multiple access methods, NOMA schemes use non-orthogonal physical resources (e.g., time and frequency) where overloading can be realized. In NOMA schemes, overlapped resources are allocated to several users resulting in controlled multiuser interference that can be suppressed in power- or code-domain. Combination of NOMA and massive MIMO is a critical issue as they have distinct advantages.

In this thesis, we adopt JSDM framework in frequency-selective channels where we employ single-carrier frequency domain equalization (SC-FDE) for uplink transmission. There are two main motivations of the thesis. The first one is to design practical interference-aware pre-beamformers for JSDM framework while considering constant-modulus constraint. The second motivation of the thesis is to efficiently carry out the adaptation of code-domain NOMA to SC massive MIMO systems, specifically to JSDM.

1.2 Beamformer Design for Hybrid Massive MIMO Systems

Analog beamformer design for JSDM framework is a critical task since inter-group interference should be mitigated at this stage. There are several papers that find unconstrained analog beamformers that take interference into account [9, 10, 23]. However, they do not suppress inter-group interference perfectly. In [23], a weighted minimum mean square error (WMMSE) type digital beamformer is proposed to suppress residual interference. A near-optimal generalized eigenbeamformer (GEB), which has strong interference suppression capability, is proposed for SC transmission at mm-wave bands in [18, 19]. However, none of these analog beamformers obey constant-modulus constraint. For two-stage beamforming concept, DFT beamformer and phase of unconstrained beamformers are considered as state-of-the-art

constrained analog beamformer alternatives [9, 24–27].

On the other hand, constrained analog beamformer design for hybrid analog/digital systems is a well-studied research area [5–7]. These papers use the instantaneous full dimensional channel state information (CSI) for beamformer design with fully connected arrays. In [26], two-stage beamforming approach is adopted where columns of the unconstrained analog beamformer are selected as eigenvectors of sum of CCMs of users. Furthermore, constrained analog beamformer is obtained via alternating minimization algorithm, and a compensation matrix is applied in digital baseband to orthogonalize the overall analog beamformer. On the other hand, compared to fully connected arrays, partially connected ones require much less phase shifters at the expense of spectral efficiency. Compromise between spectral efficiency and energy consumption for fully connected arrays and fixed subarrays is extensively studied in [6, 28].

Recently, a challenging problem called dynamic subarray design is studied where the aim is to obtain the optimal connection between radio frequency (RF) chains and antennas for partially connected arrays [27, 29–34]. In these papers, it is shown that dynamic subarrays outperform fixed ones in terms of several metrics such as spectral efficiency. [27, 29–31] consider a point-to-point hybrid analog/digital system, whereas [32–34] consider multiple users. In [32], frequency-selective channels are considered in uplink transmission where ISI is mitigated with frequency domain iterative block decision feedback equalization (IB-DFE), which is similar to our work. However, dynamic connections in that paper depend on instantaneous CSI, which is not practical, whereas other papers on dynamic subarray design and our work make use of slowly changing parameters (e.g., CCMs) to find optimal connections. For dynamic subarrays, connection change can be realized with switches which are shown to be energy-efficient components for mm-wave massive MIMO systems [35, 36].

Table 1.1 summarizes the contributions of the existing work on constrained beamformer design. None of them are interested in constrained pre-beamformer (analog beamformer) design even for fully connected arrays where mitigation of interference is realized at this stage. That is, interference nulling capability of statistical pre-beamformers is ignored while considering constant-modulus constraint in prior work.

Furthermore, dynamic subarray design is not considered for interference-aware pre-beamformers in the literature.

Table 1.1: Summary of existing work on constrained beamformer design with fully connected and partially connected arrays (fixed and dynamic subarrays)

Papers	[5]	[6]	[7]	[9, 10, 23]	[18, 19]	[26]	[27]	[28]	[29]	[30, 31]	[32]	[33, 34]	This Work
Frequency-Selectivity	✗	✓	✗	✗	✓	✗	✓	✗	✗	✓	✓	✗	✓
Multiuser	✗	✗	✓	✓	✓	✓	✗	✗	✗	✗	✓	✓	✓
Two-Stage Beamforming	✗	✗	✓	✓	✓	✓	✓	✓	✗	✗	✗	✓	✓
Interference-Aware Pre-Beamformer	✗	✗	✗	✓	✓	✗	✗	✓	✗	✗	✗	✗	✓
Constrained Analog Beamformer	✓	✓	✓	✗	✗	✓	✗	✓	✓	✓	✓	✓	✓
Fully Connected Array	✓	✓	✓	✓	✓	✓	✓	✗	✗	✗	✗	✗	✓
Fixed Subarray	✗	✓	✗	✗	✗	✗	✓	✓	✓	✓	✓	✓	✓
Dynamic Subarray	✗	✗	✗	✗	✗	✗	✓	✗	✓	✓	✓	✓	✓

1.3 Non-Orthogonal Multiple Access and Adaptation to Massive MIMO

NOMA schemes are initially introduced for single-antenna systems and their extension to MIMO systems is an important research direction. In addition, low-complexity interference cancellation algorithms should be developed so that NOMA schemes become more practical [22]. High complexity of message passing algorithm (MPA) and error propagation of successive interference cancellation (SIC) are the two main problems of current receiver architectures. There are some studies that propose novel low-complexity receivers. Conventional and advanced receivers for some NOMA schemes are described in [37] and references therein. In [38], graph based iter-

ative receivers for downlink MIMO-SCMA system with cooperation is proposed and performance comparison with existing receivers is provided where number of antennas is equal to number of physical resources. Overloaded and coded massive MIMO-NOMA systems and capacity-achieving low-complexity linear minimum mean square error (LMMSE) detection based receivers are studied in [39, 40]. Gaussian message passing algorithm is proposed for an overloaded massive MIMO system in [41].

In the literature, there are many studies on integration of power-domain NOMA and massive MIMO [21, 22, 42]. In [43], NOMA is integrated with beamspace MIMO in order to support more users than the available RF chains. In [44], users are divided into groups where each group has one RF chain. Multiple analog beams are created for each NOMA group by dynamically dividing antenna array into subarrays, which is called beam splitting. In [45], a joint optimization of user-grouping and hybrid beamformer design along with power allocation is provided.

On the other hand, there is limited work where code-domain NOMA is considered with massive MIMO systems. In [46], benefits of code-domain NOMA in underloaded massive MIMO systems are investigated, where short spreading sequences are utilized similar to our work. It is shown that code-domain NOMA outperforms classical massive MIMO when users are spatially close to each other, especially when spatial user-grouping is utilized. However, this work considers a flat-fading channel model and uses a fully digital architecture with linear precoders/combiners. Massive MIMO is integrated with interleave division multiple access (IDMA) along with iterative data-aided channel estimation and suboptimal detection methods in [47]. Low density spreading (LDS) signatures are applied in massive MIMO system in [48]. Belief propagation based receiver is applied without using any CSI. In [49], beamspace MIMO at mm-wave bands is integrated with sparse code multiple access (SCMA) where the number of RF chains is equal to the number of physical resources.

Furthermore, NOMA schemes are generally considered with MC transmission, even though SC provides lower PAPR, which is critical for uplink transmission. Power-domain NOMA can be considered with both SC and MC transmission, whereas code-domain NOMA is considered with only MC transmission as ISI caused by frequency-

selective channels would disrupt the codewords if they were transmitted in temporal domain. In [50], power-domain NOMA is considered with SC-FDE in massive MIMO systems, where IB-DFE is used for joint equalization and multiuser detection. To the author's best knowledge, SC transmission is used with code-domain NOMA for the first time in our previous work [51], where code-domain NOMA is shown to be beneficial for JSDM, since users in the same group have spatially correlated channels. In that work, we showed that code-domain NOMA schemes, namely SCMA and multi-user shared access (MUSA), perform well with extremely low number of RF chains. Although SC was utilized for uplink transmission, equalization and multiuser detection were performed at different stages which degrades the performance. In contrast, we apply joint equalization and multiuser detection in this work.

Although there is some effort to combine NOMA with massive MIMO systems, there is lack of literature for the adaptation of practical NOMA schemes such as MUSA to massive MIMO hybrid beamforming architecture employing SC in wideband mm-wave channels. In this thesis, one of our aims is to present how code-domain NOMA can be useful in practical massive MIMO systems with limited number of RF chains where users are closely spaced.

1.4 Contributions and Outline of the Thesis

In the first part of this thesis, which is compromised of Chapters 2, 3 and 4, we design interference-aware analog beamformers for JSDM framework utilizing SC-FDE in uplink transmission. Our contributions for the first part are as follows:

- In Chapter 2, we design a near-optimal unconstrained analog beamformer that considers interference. Unlike most prior work, we concentrate on analog beamformers which are updated with slowly varying CCMs. We try to maximize mutual information between the frequency domain received signal and intended group's signal in reduced dimension, i.e., after the analog beamformer. Although we employ a frequency-selective channel model, cost function turns out to be independent of frequency bin for spatial-narrowband arrays. Near-optimal unconstrained analog beamformer that maximizes the mutual informa-

tion in reduced dimension coincides with GEB concept. This type of beamformers have strong interference capability, and their optimality can be shown with respect to several criteria [18, 19].

- We propose algorithms to obtain constant-modulus constrained approximations of GEB for both fully and partially connected arrays in Chapter 3. We decompose the analog beamformer into two stages, namely, constrained analog beamformer and compensation matrix. Compensation matrix is applied in the digital baseband just before digital beamformers. Compensation matrix increases the degrees of freedom in the optimization problem which is formulated as minimization of the Euclidean distance between GEB and combination of constrained analog beamformer and compensation matrix. We obtain a constrained solution for fully connected arrays by utilizing an alternating minimization-based algorithm. Then, we present the algorithm to find the constrained solution for partially connected arrays with any fixed connection structure. Furthermore, we propose a low-complexity algorithm to find the optimal partially connected array structure that yields the maximum expected signal-to-interference-plus-noise ratio (SINR) in reduced dimension by exploiting the properties of GEB. The last problem is known as dynamic subarray design. To the authors' best knowledge, this is the first dynamic subarray algorithm for slowly varying statistical analog beamformers in JSDM framework.

- In Chapter 4, we promote the usage of minimum mean square error (MMSE) criterion based iterative equalizers for digital beamforming stage where the residual interference after constrained analog beamformers, which cannot mitigate the inter-group interference completely, is considered. We adopt IB-DFE method that is shown to be an effective approach for SC transmission [52]. In this way, interference is taken into account in both analog and digital beamforming stages.

- In JSDM framework, users usually have single antenna elements [10], and multiantenna user extension of statistical analog beamforming with spatially correlated channels is not studied in the literature. We provide an analysis to address this issue by showing that proposed unconstrained GEB and constrained analog beamformer design algorithms can be readily extended to multiantenna user

scenario. Moreover, our analysis imply that digital beamforming and channel estimation schemes would be unchanged.

- We provide a comprehensive analysis by using several performance measures; beampattern, spectral efficiency, outage capacity, bit-error rate (BER) and accuracy of channel estimation in reduced dimension. Beampattern analysis of constrained analog beamformers, especially partially connected arrays, is lacking in the literature. Our analysis provides novel insights about the interference suppression capabilities of constrained analog beamformers.

In summary, we design interference-aware slowly varying analog beamformers in JSDM framework unlike most prior work as it can be seen from Table 1.1. However, our design can be used in any framework with the presence of interference whose covariance matrix is known. In addition, proposed algorithms are evaluated with simulations by using the provided analysis tools. We consider a scenario where a group is assumed to be mobile so that its multipath components (MPCs) can be overlapped with angular regions of other groups, which leads to increase in inter-group interference at certain situations. In this way, interference suppression capabilities of constrained analog beamformers can be observed. The results show that proposed fully connected array algorithm is superior to DFT beamformer and phase of GEB which are considered as state-of-the-art. Proposed algorithm attains the performance of GEB with moderate interference strength. Furthermore, proposed dynamic subarray algorithm outperforms commonly used fixed subarray structures. The first part of the thesis is based on our paper [53].

In the second part of the thesis (Chapter 5), we integrate code-domain NOMA, specifically MUSA, to JSDM in order to investigate the potential gains that can be achieved with the use of code-domain NOMA in massive MIMO systems. We apply joint equalization and multiuser detection, in contrast to our previous work in [51]. Contributions of the second part of the thesis are as follows:

- Adaptation of code-domain NOMA to uplink SC-FDE with mm-wave massive MIMO, specifically with JSDM, is achieved through a novel NOMA signal model in beamspace.

- A joint code-beamspace IB-DFE receiver is proposed based on the developed signal model for performing the task of joint equalization and multiuser detection.
- It is shown that theoretical performance bounds can be achieved even for very limited number of RF chains and high NOMA loading. Moreover, advantages of code-domain NOMA aided JSDM over conventional JSDM are clearly demonstrated in terms of BER, especially for spatially correlated channels in overloaded mm-wave massive MIMO.

Finally, Chapter 6 is devoted to discussion and conclusions which provide a summary of the thesis and future research directions.

1.5 Notations

This section shows the notations for the mathematical operations that are used throughout the thesis. Scalars, column vectors and matrices are denoted by lowercase (e.g., x), lower-case boldface (e.g., $\mathbf{x}$) and uppercase boldface (e.g., $\mathbf{X}$) letters, respectively. $|x|$ and x^* are the magnitude and complex conjugate of scalar x, respectively. $\mathbf{X}^T$, $\mathbf{X}^H$, $\mathbf{X}^{-1}$ and $|\mathbf{X}|$ represent the transpose, Hermitian, inverse and determinant of matrix $\mathbf{X}$, respectively. $[\mathbf{X}]_{(i,j)}$ is the entry of matrix $\mathbf{X}$ at i^{th} row and j^{th} column. $[\mathbf{X}]_{(i,:)}$ and $[\mathbf{X}]_{(:,j)}$ are used to extract i^{th} row and j^{th} column of matrix $\mathbf{X}$, respectively. $\mathsf{E}\{\cdot\}$ and $\mathrm{Tr}\{\cdot\}$ are the expectation and trace operators, respectively. $\|\mathbf{x}\|$ and $\|\mathbf{X}\|_F$ denote the Euclidean norm of vector $\mathbf{x}$ and Frobenius norm of matrix $\mathbf{X}$, respectively. diag$\{\cdot\}$ and blkdiag$\{\cdot\}$ are used to construct diagonal and block diagonal matrices, respectively. $\mathbf{I}_N$ is the identity matrix with size $N \times N$, $\measuredangle(\cdot)$ extracts the phase of given input, vec$(\mathbf{X})$ represents the vectorization of matrix $\mathbf{X}$, $\mathcal{CN}\big(\mathbf{x}, \mathbf{R}\big)$ is a complex Gaussian random vector with mean $\mathbf{x}$ and covariance $\mathbf{R}$, $P(\cdot)$ represents the probability value, $\otimes$ denote the Kronecker product between two matrices, and δ_{ij} is the Kronecker delta function.

CHAPTER 2

WIDEBAND SYSTEM MODEL AND UNCONSTRAINED STATISTICAL PRE-BEAMFORMING FOR HYBRID MASSIVE MIMO

We consider an uplink SC-FDE system where the base station (BS) with M antennas serves U single-antenna users[1]. Total number of RF chains is denoted by D where $D \leq M$. Users are partitioned into G groups according to their channel covariance eigenspaces[2]. Number of users in group g is denoted by U_g, and number of RF chains allocated to this group is D_g. For conventional hybrid analog/digital systems $U_g \leq D_g$ relation should be satisfied to successfully separate intra-group user signals. Considering $U = \sum_{g=1}^{G} U_g$ and $D = \sum_{g=1}^{G} D_g$, the constraint on total number of RF chains can be stated as $U \leq D \leq M$. In contrast, this limitation can be circumvented with the use of code-domain NOMA as it will be shown in this thesis. This chapter provides a system model for the conventional massive MIMO without NOMA (i.e., $U_g \leq D_g$), while adaptation to NOMA is provided in Chapter 5.

2.1 Wideband SC-FDE Uplink Transmission

Received signal vector $\mathbf{y}_n \in \mathsf{C}^{M\times 1}$ at the BS at n^{th} time instance is expressed as

$$\mathbf{y}_n = \sum_{g=1}^{G} \sum_{l=0}^{L-1} \mathbf{H}_l^{(g)} \mathbf{x}_{(n-l)_N}^{(g)} + \mathbf{n}_n, \tag{2.1}$$

for $n = 0, 1, \ldots, N-1$, where block length is denoted by N. In (2.1), $\mathbf{H}_l^{(g)} \triangleq$

[1] Users are assumed have single-antenna elements for simplicity. However, this framework can be extended to multi-antenna users and proposed methods in this thesis can be used as it is shown in Appendix B.

[2] The design of user grouping algorithms is out of scope of this thesis. Efficient user-grouping procedures can be found in [54, 55].

$\left[\mathbf{h}_l^{(g_1)}, \ldots, \mathbf{h}_l^{(g_{U_g})}\right] \in \mathsf{C}^{M \times U_g}$ represents the channel matrix of group g at l^{th} MPC where the channel vector of user u in group g is denoted by $\mathbf{h}_l^{(g_u)}$, and the total number of MPCs is denoted by L. A cyclic prefix with length larger than L is used to obtain circulant channel matrices while preventing the inter-block interference. Transmitted symbol vector of group g is defined as $\mathbf{x}_n^{(g)} \triangleq \left[x_n^{(g_1)}, \ldots, x_n^{(g_{U_g})}\right]^T \in \mathsf{C}^{U_g \times 1}$ with

$$\mathsf{E}\left\{x_n^{(g_u)}\left(x_{n'}^{(g'_{u'})}\right)^*\right\} = \frac{E_s^{(g)}}{U_g}\delta_{gg'}\delta_{uu'}\delta_{nn'} \tag{2.2}$$

where $x_n^{(g_u)}$ is the transmitted symbol of user u in group g. Total transmit energy of group g is denoted by $E_s^{(g)}$, which is shared equally among users in the same group, i.e., intra-group near-far effect is not considered. Noise vector $\mathbf{n}_n$ is comprised of zero-mean circularly symmetric complex Gaussian random variables with variance N_0.

Channel vectors obey the spatially correlated Rayleigh channel model with $\mathbf{h}_l^{(g_u)} \sim \mathcal{CN}\left(\mathbf{0}, \mathbf{R}_l^{(g_u)}\right)$ where $\mathbf{R}_l^{(g_u)}$ is the CCM of user u in group g at l^{th} MPC [9, 10, 18, 19, 23, 26]. User channel vectors are assumed to be mutually uncorrelated among MPCs and users which is expressed as

$$\mathsf{E}\left\{\mathbf{h}_l^{(g_u)}\left[\mathbf{h}_{l'}^{(g'_{u'})}\right]^H\right\} = \mathbf{R}_l^{(g_u)}\delta_{gg'}\delta_{uu'}\delta_{ll'}. \tag{2.3}$$

Without loss of generality, channel vectors can be written as $\mathbf{h}_l^{(g_u)} = \left[\mathbf{R}_l^{(g_u)}\right]^{\frac{1}{2}}\mathbf{z}_l^{(g_u)}$ where $\mathbf{z}_l^{(g_u)} \in \mathsf{C}^{M \times 1}$ has zero-mean circularly symmetric complex Gaussian entries with unit variance. Considering the one-ring scattering model [9, 10, 26], CCM of a user at l^{th} MPC can be defined as

$$\mathbf{R}_l^{(g_u)} \triangleq \gamma^{(g_u)} \int_{\mu_l^{(g_u)} - \frac{\Delta_l^{(g_u)}}{2}}^{\mu_l^{(g_u)} + \frac{\Delta_l^{(g_u)}}{2}} \rho_l^{(g_u)}(\theta)\mathbf{u}(\theta)\mathbf{u}(\theta)^H d\theta, \tag{2.4}$$

where $\sqrt{\gamma^{(g_u)}}$ is the channel gain of user u in group g satisfying $\sum_{l=0}^{L-1} \mathrm{Tr}\left\{\mathbf{R}_l^{(g_u)}\right\} = \gamma^{(g_u)}$ relation. For l^{th} MPC of user u in group g, angular power profile function, mean angle of arrival (AoA) and angular spread (AS) are denoted by $\rho_l^{(g_u)}(\theta)$, $\mu_l^{(g_u)}$ and

$\Delta_l^{(g_u)}$, respectively. Unit norm steering vector $\mathbf{u}(\theta) \in \mathsf{C}^{M\times 1}$ of a uniform linear array (ULA) with half the wavelength spacing corresponding to azimuth angle θ is defined as

$$\mathbf{u}(\theta) \triangleq \frac{1}{\sqrt{M}}\left[1 \; e^{j\pi sin(\theta)} \cdots \; e^{j(M-1)\pi sin(\theta)}\right]^T. \tag{2.5}$$

We considered ULA for simplicity, however, formulations in this thesis can be used for other array structures such as uniform planar arrays. The only parameter that would be different for other array structures is the steering vector. Moreover, the BS observes a sparse angle-delay profile at mm-wave frequencies [3]. That is, users have a few active MPCs with narrow angular spread which makes user-grouping feasible. In this thesis, it is assumed that users in the same group have the same active MPCs with similar mean AoAs constituting MPC clusters.

2.2 Two-Stage Beamforming Concept

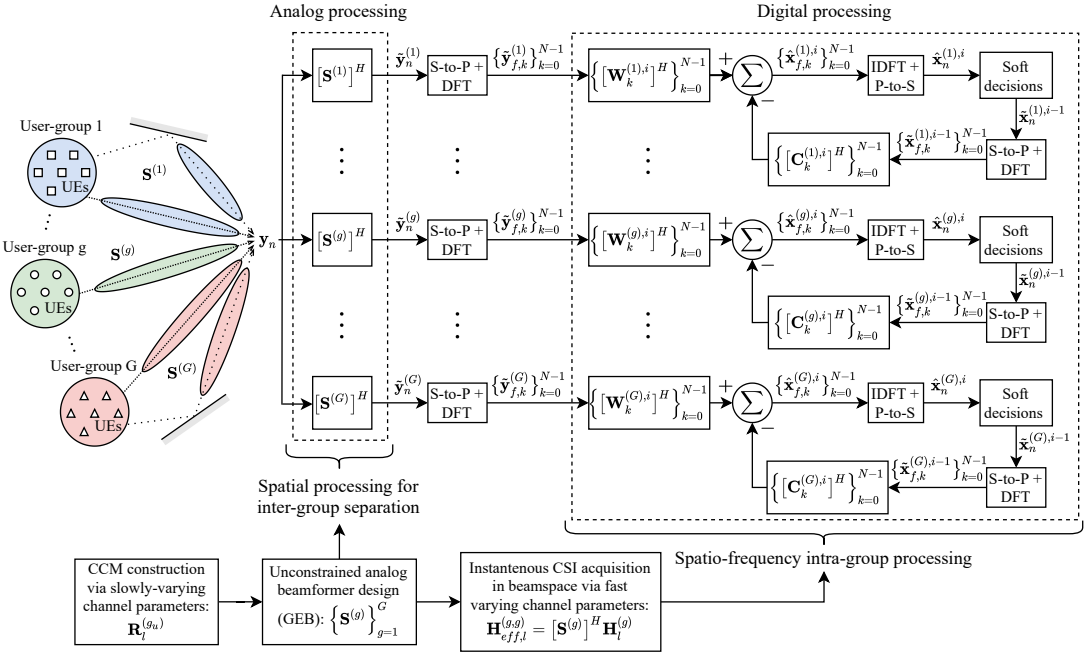

Figure 2.1: Block diagram of the overall system design for JSDM with SC-FDE

This thesis considers a two-stage beamforming architecture based on JSDM where there is an analog beamformer $\mathbf{S}^{(g)} \in \mathsf{C}^{M\times D_g}$ for each group suppressing channels of

users in other groups. Let the received signal in (2.1) is rewritten as

$$\mathbf{y}_n = \underbrace{\sum_{l=0}^{L-1} \mathbf{H}_l^{(g)} \mathbf{x}_{(n-l)_N}^{(g)}}_{\mathbf{s}_n^{(g)}\text{: Intra-Group Signals}} + \underbrace{\sum_{g' \neq g} \sum_{l=0}^{L-1} \mathbf{H}_l^{(g')} \mathbf{x}_{(n-l)_N}^{(g')} + \mathbf{n}_n}_{\boldsymbol{\eta}_n^{(g)}\text{: Inter-Group Signals + Noise Terms}}, \tag{2.6}$$

where intra-group and inter-group signals are separated for group g. Then, signal vector of group g after its analog beamformer, $\tilde{\mathbf{y}}_n^{(g)} \in \mathsf{C}^{D_g \times 1}$, can be expressed as

$$\tilde{\mathbf{y}}_n^{(g)} = \left[\mathbf{S}^{(g)}\right]^H \mathbf{y}_n = \underbrace{\sum_{l=0}^{L-1} \mathbf{H}_{eff,l}^{(g,g)} \mathbf{x}_{(n-l)_N}^{(g)}}_{\tilde{\mathbf{s}}_n^{(g)}\text{: Intra-Group Signals in Reduced Dimension}} + \underbrace{\sum_{g' \neq g} \sum_{l=0}^{L-1} \mathbf{H}_{eff,l}^{(g,g')} \mathbf{x}_{(n-l)_N}^{(g')} + \left[\mathbf{S}^{(g)}\right]^H \mathbf{n}_n}_{\tilde{\boldsymbol{\eta}}_n^{(g)}\text{: Inter-Group Signals + Noise Terms in Reduced Dimension}}, \tag{2.7}$$

where effective channel matrices at l^{th} MPC are denoted by $\mathbf{H}_{eff,l}^{(g,g')} \triangleq \left[\mathbf{S}^{(g)}\right]^H \mathbf{H}_l^{(g')} \in \mathsf{C}^{D_g \times U_{g'}}$, which represents the effective channel of group g' at the output of analog beamformer of group g. For an optimal analog beamformer, entries of $\mathbf{H}_{eff,l}^{(g,g')}$ should be zero for $g \neq g'$. In (2.7), intra-group signals and sum of inter-group signals and noise in reduced dimension are denoted by $\tilde{\mathbf{s}}_n^{(g)} = \left[\mathbf{S}^{(g)}\right]^H \mathbf{s}_n^{(g)} \in \mathsf{C}^{D_g \times 1}$ and $\tilde{\boldsymbol{\eta}}_n^{(g)} = \left[\mathbf{S}^{(g)}\right]^H \boldsymbol{\eta}_n^{(g)} \in \mathsf{C}^{D_g \times 1}$, respectively.

Assuming inter-group interference is completely mitigated at analog beamforming stage, digital processing of each group is implemented independently. In this thesis, frequency domain equalization (FDE) is employed to mitigate ISI caused by SC transmission. Since FDE is employed, DFT operation is applied to the sequence $\left\{\tilde{\mathbf{y}}_n^{(g)}\right\}_{n=0}^{N-1}$. Using the circularity in (2.7), one can obtain the signal at the k^{th} frequency bin after the DFT operation as

$$\tilde{\mathbf{y}}_{f,k}^{(g)} = \underbrace{\boldsymbol{\Lambda}_{eff,k}^{(g,g)} \mathbf{x}_{f,k}^{(g)}}_{\tilde{\mathbf{s}}_{f,k}^{(g)}} + \underbrace{\sum_{g' \neq g} \boldsymbol{\Lambda}_{eff,k}^{(g,g')} \mathbf{x}_{f,k}^{(g')} + \tilde{\mathbf{n}}_{f,k}^{(g)}}_{\tilde{\boldsymbol{\eta}}_{f,k}^{(g)}}, \tag{2.8}$$

for $k = 0, 1, \ldots, N-1$, where the DFT of effective channel matrices are denoted by

$$\mathbf{\Lambda}_{eff,k}^{(g,g')} = \sum_{l=0}^{L-1} \mathbf{H}_{eff,l}^{(g,g')} e^{-j\frac{2\pi}{N}kl}. \tag{2.9}$$

In (2.8), $\tilde{\mathbf{y}}_{f,k}^{(g)}$, $\tilde{\mathbf{s}}_{f,k}^{(g)}$, $\mathbf{x}_{f,k}^{(g)}$, $\tilde{\boldsymbol{\eta}}_{f,k}^{(g)}$ and $\tilde{\mathbf{n}}_{f,k}^{(g)}$ are normalized DFTs of vector sequences $\tilde{\mathbf{y}}_{n}^{(g)}$, $\tilde{\mathbf{s}}_{n}^{(g)}$, $\mathbf{x}_{n}^{(g)}$, $\tilde{\boldsymbol{\eta}}_{n}^{(g)}$ and $\tilde{\mathbf{n}}_{n}^{(g)} = \left[\mathbf{S}^{(g)}\right]^{H}\mathbf{n}_n$, respectively. Note that normalized DFT of any vector sequence $\{\mathbf{f}_n\}_{n=0}^{N-1}$ can be calculated as

$$\mathbf{f}_{f,k} \triangleq \frac{1}{\sqrt{N}} \sum_{n=0}^{N-1} \mathbf{f}_n e^{-j\frac{2\pi}{N}kn}, \quad k = 0, 1, \ldots, N-1. \tag{2.10}$$

Digital beamformers are used to separate intra-group signals of users in JSDM framework. Since we employed FDE structure, digital beamformers are applied in frequency domain where IB-DFE method is utilized via feedforward and feedback filters which are updated at each iteration. Feedforward and feedback filters of group g for k^{th} frequency bin at the i^{th} equalizer iteration are denoted by $\mathbf{W}_{k}^{(g),i} \in \mathsf{C}^{D_g \times U_g}$ and $\mathbf{C}_{k}^{(g),i} \in \mathsf{C}^{U_g \times U_g}$, respectively. The output of DFE at the i^{th} iteration, which is found by using (2.8) and soft decisions of previous iteration, is expressed as follows:

$$\hat{\mathbf{x}}_{f,k}^{(g),i} = \left[\mathbf{W}_{k}^{(g),i}\right]^{H} \tilde{\mathbf{y}}_{f,k}^{(g)} - \left[\mathbf{C}_{k}^{(g),i}\right]^{H} \tilde{\mathbf{x}}_{f,k}^{(g),i-1}, \tag{2.11}$$

$$\hat{\mathbf{x}}_{n}^{(g),i} = \frac{1}{\sqrt{N}} \sum_{k=0}^{N-1} \hat{\mathbf{x}}_{f,k}^{(g),i} e^{j\frac{2\pi}{N}kn} \tag{2.12}$$

for $k, n = 0, 1, \ldots, N-1$. Time-domain estimates $\hat{\mathbf{x}}_{n}^{(g),i} \triangleq \left[\hat{x}_{n}^{(g_1),i}, \ldots, \hat{x}_{n}^{(g_{U_g}),i}\right]^{T}$ are used to demodulate the transmitted symbols, where $\hat{x}_{n}^{(g_u),i}$ is the estimate of $x_{n}^{(g_u)}$. In (2.11), $\tilde{\mathbf{x}}_{f,k}^{(g),i-1}$ is the soft decision vector of group g obtained from the previous iteration. Block diagram summarizing the overall two-stage beamforming architecture described in this section is given in Fig. 2.1.

2.3 Optimal Pre-Beamformer: Generalized Eigenbeamformer (GEB)

In JSDM framework, analog beamformers are designed by using CCMs, which are assumed to be known perfectly in this thesis[3]. In this section, we find a near-optimal unconstrained analog beamformer structure for JSDM framework where frequency-selectivity of channels are considered. We approach the analog beamformer design as a dimension reduction problem. That is, we aim to find a near-optimal unconstrained analog beamformer, which results in a linear transformation, that preserves the mutual information in reduced dimension. The cost function that needs to be maximized in reduced dimension is the mutual information between $\tilde{\mathbf{y}}_{f,k}^{(g)}$ and $\tilde{\mathbf{s}}_{f,k}^{(g)}$ in (2.8) which can be expressed as

$$I\left(\tilde{\mathbf{s}}_{f,k}^{(g)};\tilde{\mathbf{y}}_{f,k}^{(g)}\right)=\log_2\left(\left|\mathbf{I}_{D_g}+\left[\mathbf{R}_{\tilde{\boldsymbol{\eta}}_f}^{(g)}\right]^{-1}\mathbf{R}_{\tilde{\mathbf{s}}_f}^{(g)}\right|\right), \tag{2.13}$$

if $\tilde{\mathbf{y}}_{f,k}^{(g)}$ and $\tilde{\mathbf{s}}_{f,k}^{(g)}$ are assumed to be Gaussian random vectors. Covariance matrices of $\tilde{\mathbf{s}}_{f,k}^{(g)}$ and $\tilde{\boldsymbol{\eta}}_{f,k}^{(g)}$ are denoted by $\mathbf{R}_{\tilde{\mathbf{s}}_f}^{(g)}=\mathsf{E}\left\{\tilde{\mathbf{s}}_{f,k}^{(g)}\left[\tilde{\mathbf{s}}_{f,k}^{(g)}\right]^H\right\}$ and $\mathbf{R}_{\tilde{\boldsymbol{\eta}}_f}^{(g)}=\mathsf{E}\left\{\tilde{\boldsymbol{\eta}}_{f,k}\left[\tilde{\boldsymbol{\eta}}_{f,k}\right]^H\right\}$ for $k=0,1,\ldots,N-1$, respectively. Note that these covariance matrices are independent of frequency bin index k according to Appendix A[4]. Hence, there will be a single cost function to maximize. Furthermore, it is easy to see that maximization of mutual information is equivalent to maximization of the determinant inside the logarithm in (2.13). If we replace $\mathbf{R}_{\tilde{\mathbf{s}}_f}^{(g)}$ and $\mathbf{R}_{\tilde{\boldsymbol{\eta}}_f}^{(g)}$ with their expressions given in Appendix A, the cost function that needs to be maximized under the constraint that $\mathbf{S}^{(g)}$ is a full column

[3] CCM estimation is out of scope of this thesis. However, there are several papers proposing efficient methods for CCM estimation [56–59]. It can be assumed that CCMs can be learned by using the methods mentioned in these papers. It is important to note that CCMs depend on slowly varying parameters such as AoAs, which is the reason why they do not need to be updated frequently. Hence, CCM estimation overhead does not cause a significant increase in overall system complexity.

[4] In this thesis, although frequency-wideband effect is taken into account, spatial-wideband (beam-squint) effect is ignored as bandwidth is assumed to be not that wide [60]. If a spatial-wideband system was considered, spatial covariance matrices of signals would depend on the frequency bin index. However, proposed analog beamforming could still be used either by using the mean spatial covariance matrices, which are averaged over frequency bins, to find the unconstrained analog beamformer as in [30, 61] (which do not consider the interference rejection capability of pre-beamformer) or by finding the unconstrained analog beamformer with spatial-narrowband assumption and applying a beam-squint compensation in digital domain [62].

matrix can be written as

$$\begin{aligned} &\underset{\mathbf{S}^{(g)}}{\text{maximize}} \ \left|\mathbf{I}_{D_g}+\left([\mathbf{S}^{(g)}]^H\mathbf{R}_{\boldsymbol{\eta}}^{(g)}\mathbf{S}^{(g)}\right)^{-1}\left([\mathbf{S}^{(g)}]^H\mathbf{R}_{\mathbf{s}}^{(g)}\mathbf{S}^{(g)}\right)\right| \\ &\text{subject to } \ \text{rank}\left(\mathbf{S}^{(g)}\right)=D_g \end{aligned} \tag{2.14}$$

where covariance matrix of intra-group signals and covariance matrix of sum of inter-group signals and noise terms in (2.6) are expressed as $\mathsf{E}\left\{\mathbf{s}_n^{(g)}\left[\mathbf{s}_{n'}^{(g)}\right]^H\right\}=\mathbf{R}_{\mathbf{s}}^{(g)}\delta_{nn'}$ and $\mathsf{E}\left\{\boldsymbol{\eta}_n^{(g)}\left[\boldsymbol{\eta}_{n'}^{(g)}\right]^H\right\}=\mathbf{R}_{\boldsymbol{\eta}}^{(g)}\delta_{nn'}$, respectively. Considering the uncorrelated nature of transmitted symbols among users and time in addition to the uncorrelated channel vectors in (2.3), these two covariance matrices are computed as

$$\mathbf{R}_{\mathbf{s}}^{(g)}=\frac{E_s^{(g)}}{U_g}\sum_{u=1}^{U_g}\sum_{l=0}^{L-1}\mathbf{R}_l^{(g_u)}, \tag{2.15}$$

$$\mathbf{R}_{\boldsymbol{\eta}}^{(g)}=\sum_{g'\neq g}\frac{E_s^{(g')}}{U_{g'}}\sum_{u=1}^{U_{g'}}\sum_{l=0}^{L-1}\mathbf{R}_l^{(g'_u)}+N_0\mathbf{I}_M. \tag{2.16}$$

Lemma 1*:* If multiantenna users were considered, design of statistical analog beamformer $\mathbf{S}^{(g)}$, which is based on the optimization problem in (2.14), would remain the same with additional knowledge of scaling constants that appear in (2.15) and (2.16). Although these constants depend on the precoding applied at the user side, they can be learned via training or their statistical mean can be used.

Proof. See Appendix B. ■

Analog beamformer $\bar{\mathbf{S}}^{(g)}$ that maximizes the cost function is found as [63]

$$\bar{\mathbf{S}}^{(g)}=\left[\mathbf{v}_1,\mathbf{v}_2,\cdots,\mathbf{v}_{D_g}\right], \tag{2.17}$$

where $\mathbf{v}_i$ is the eigenvector corresponding to the i^{th} most dominant eigenvalue (i.e., λ_i) of the generalized eigenvalue problem which is defined as

$$\mathbf{R}_{\mathbf{s}}^{(g)}\mathbf{v}_i=\lambda_i\mathbf{R}_{\boldsymbol{\eta}}^{(g)}\mathbf{v}_i, \quad i=1,2,\ldots,M. \tag{2.18}$$

This solution is known as generalized eigenbeamformer which creates deep nulls for interfering signals. It is meaningful to use $\mathbf{R}_{\mathbf{s}}^{(g)}$, which covers CCMs of all MPCs of the intended group, in the generalized eigenvalue problem in (2.18) since SC-FDE is employed. In order to obtain orthonormalized analog beamformers, QR decomposition of GEB in (2.17) is found as $\bar{\mathbf{S}}^{(g)} = \mathbf{S}^{(g)}\bar{\mathbf{R}}^{(g)}$, which is permissible according to Lemma 2. Equivalent analog beamformer $\mathbf{S}^{(g)}$ found by QR decomposition is used as GEB for the rest of the thesis.

Lemma 2: Using $\mathbf{S}^{(g)}\mathbf{A}$ instead of $\mathbf{S}^{(g)}$ does not change the cost function where $\mathbf{A} \in \mathsf{C}^{D_g \times D_g}$ is any invertible matrix.

Proof. Replacing $\mathbf{S}^{(g)}$ with $\mathbf{S}^{(g)}\mathbf{A}$ results in a similarity transformation for the second term in the determinant in (2.14), that can be expressed as

$$\big([\mathbf{S}^{(g)}\mathbf{A}]^H \mathbf{R}_{\boldsymbol{\eta}}^{(g)} \mathbf{S}^{(g)\mathbf{A}}\big)^{-1} \big([\mathbf{S}^{(g)}\mathbf{A}]^H \mathbf{R}_{\mathbf{s}}^{(g)} \mathbf{S}^{(g)}\mathbf{A}\big) = \mathbf{A}^{-1}\big([\mathbf{S}^{(g)}]^H \mathbf{R}_{\boldsymbol{\eta}}^{(g)} \mathbf{S}^{(g)}\big)^{-1} \big([\mathbf{S}^{(g)}]^H \mathbf{R}_{\mathbf{s}}^{(g)} \mathbf{S}^{(g)}\big)\mathbf{A}. \quad (2.19)$$

Similarity transformation does not affect the cost function since generalized eigenvectors diagonalize the second term in the determinant in (2.14), as it is shown in [63]. Hence, alternative representations of GEB can be used without loss of performance. ■

CHAPTER 3

CONSTRAINED ANALOG BEAMFORMER DESIGN

In this thesis, optimality is imposed at the analog beamforming stage. A near-optimal analog beamformer GEB was designed in Section 2.3, where the cost function was maximized with high inter-group interference suppression capability, which is critical for JSDM framework since residual interference should be close to zero so that multiuser detection of each group can be considered separately at the digital beamforming stage. Although near-optimal GEB satisfies this requirement, it is an unconstrained beamformer, i.e., it does not obey constant-modulus constraint. However, phase-shifter networks are preferred for the analog beamforming stage in practice [3]. There are two possible alternatives to obtain constant-modulus constrained analog beamformers. The first one is to consider this constraint in the original optimization problem which was given in (2.14). However, this constraint makes the optimization problem intractable. Second alternative is to start from the optimal unconstrained analog beamformer and construct a new optimization problem to find another analog beamformer that satisfies constant-modulus constraint. We follow the latter alternative which is widely used in the literature [5, 6, 26]. Thus, our goal is to find a constant-modulus approximation of near-optimal GEB of each group.

Firstly, we propose methods to find constrained approximations of GEB for fully connected array architectures. Then, we provide strategies to find approximations of GEB for both fixed and dynamic partially connected arrays. In this chapter, near-optimal GEB of group g found in (2.17) in Section 2.3 and its constant-modulus constrained equivalent are denoted by $\mathbf{S}_{GEB}^{(g)} \in \mathsf{C}^{M \times D_g}$ and $\mathbf{S}_{c}^{(g)} \in \mathsf{C}^{M \times D_g}$, respectively.

3.1 Fully Connected Array

Fully connected arrays require connections between all antennas and RF chains, which means that there is a phase shifter in between any antenna and RF chain pair. This architecture is the most commonly considered one for the constant-modulus constrained analog beamformers. We firstly provide a simple DFT beamformer structure as a benchmark. This type of beamformer is obtained by using AoAs belonging to MPC clusters of user groups. Then, we present two different approaches to find approximations of nearly-optimal GEB for fully connected arrays.

3.1.1 DFT Beamformer

DFT beamformer is widely used for mm-wave communications by leveraging the sparsity in angle-delay domain [9, 24, 25]. However, it is not an interference aware beamformer. In other words, it only considers the AoAs of MPC clusters in the intended group and does not consider the channels or signals of other groups. Let $\mathbf{Q} \in \mathsf{C}^{M \times M}$ be the normalized DFT matrix with entries

$$[\mathbf{Q}]_{(m,n)} \triangleq \frac{1}{\sqrt{M}} e^{-j\frac{2\pi}{M}\pi mn} \tag{3.1}$$

for $m, n = 0, 1, \ldots, M-1$. Then, DFT beamformer of group g is defined as

$$\mathbf{S}_c^{(g)} \triangleq \mathbf{Q}\mathbf{E}^{(g)}, \tag{3.2}$$

where $\mathbf{E}^{(g)} = [\mathbf{e}_{g,1}, \mathbf{e}_{g,2}, \ldots, \mathbf{e}_{g,D_g}] \in \mathsf{Z}^{M \times D_g}$ is used as the column selection matrix for group g. Columns of $\mathbf{E}^{(g)}$ are denoted by $\mathbf{e}_i \in \mathsf{Z}^{M \times 1}$ which is a binary vector whose i^{th} entry is one whereas others are zero. This vector selects the columns of the DFT matrix for the analog beamformer. For any group, firstly, closest DFT vectors to mean AoAs of active MPCs are selected. If the number of available RF chains is greater than the number of active MPCs, which is the desired case, remaining columns are selected from the adjacent DFT vectors to the ones closest to mean AoAs. Analog beamformer used in practice is expressed as $\mathbf{S}^{(g)} = \mathbf{S}_c^{(g)}$.

3.1.2 Phase Extraction (PE)

Constrained analog beamformer $\mathbf{S}_c^{(g)}$ has only constant-modulus constraint for the fully connected structure, i.e., RF chains are connected to all the antennas. Since our goal is to find the best approximation to GEB, an optimization problem can be constructed as follows:

$$\begin{aligned} \underset{\mathbf{S}_c^{(g)}}{\text{minimize}} \quad & \left\| \mathbf{S}_{GEB}^{(g)} - \mathbf{S}_c^{(g)} \right\|_F^2 \\ \text{subject to} \quad & \left| [\mathbf{S}_c^{(g)}]_{(i,j)} \right| = \frac{1}{\sqrt{M}}, \forall i, j, \end{aligned} \tag{3.3}$$

which has the simple phase extraction solution where optimum constrained analog beamformer can be expressed as

$$\mathbf{S}_c^{(g)\star} = \frac{1}{\sqrt{M}} e^{j\angle\left(\mathbf{S}_{GEB}^{(g)}\right)}. \tag{3.4}$$

This solution is used in the literature due to its simplicity. If hybrid massive MIMO without user-grouping is considered, phase extraction offers acceptable performance [26, 27]. However, deep nulls introduced by GEB may disappear which results in increase in inter-group interference for JSDM. Similar to DFT beamformer, practical analog beamformer is expressed as $\mathbf{S}^{(g)} = \mathbf{S}_c^{(g)}$.

3.1.3 Phase Extraction with Alternating Minimization (PE-AM)

In order to improve the accuracy of approximation, we introduce a compensation matrix $\mathbf{S}_{cm}^{(g)} \in \mathbb{C}^{D_g \times D_g}$ which will be applied in the digital baseband after the constrained analog beamformer $\mathbf{S}_c^{(g)}$. This can be considered as dividing the analog beamformer into two stages. A new optimization problem with the compensation matrix can be constructed as

$$\begin{aligned} \underset{\mathbf{S}_c^{(g)}, \mathbf{S}_{cm}^{(g)}}{\text{minimize}} \quad & \left\| \mathbf{S}_{GEB}^{(g)} - \mathbf{S}_c^{(g)} \mathbf{S}_{cm}^{(g)} \right\|_F^2 \\ \text{subject to} \quad & \left| [\mathbf{S}_c^{(g)}]_{(i,j)} \right| = \frac{1}{\sqrt{M}}, \forall i, j. \end{aligned} \tag{3.5}$$

Optimization problem given above can be solved with manifold optimization-based algorithms which have high complexity [6]. However, it is possible to modify the optimization problem in (3.5) and construct another problem which has a simpler solution. Columns of near-optimal GEB are mutually orthonormal whereas there is no constraint on the compensation matrix. Although optimum structure of the compensation matrix is not known, orthogonality constraint on compensation matrix is imposed to obtain a simplified optimization problem. It can be shown that the cost function in (3.5) is upper-bounded by

$$\left\| \mathbf{S}_{GEB}^{(g)} \left[\mathbf{S}_{cm}^{(g)} \right]^H - \mathbf{S}_c^{(g)} \right\|_F^2, \tag{3.6}$$

if the orthogonality constraint is imposed on the compensation matrix. It is feasible to use (3.6) as the cost function and modify the optimization problem in (3.5) with this upper bound, which results in the following optimization problem:

$$\begin{aligned} \underset{\mathbf{S}_c^{(g)}, \mathbf{S}_{cm}^{(g)}}{\text{minimize}} \quad & \left\| \mathbf{S}_{GEB}^{(g)} \left[\mathbf{S}_{cm}^{(g)} \right]^H - \mathbf{S}_c^{(g)} \right\|_F^2 \\ \text{subject to} \quad & \left| [\mathbf{S}_c^{(g)}]_{(i,j)} \right| = \frac{1}{\sqrt{M}}, \forall i, j; \quad \left[\mathbf{S}_{cm}^{(g)} \right]^H \mathbf{S}_{cm}^{(g)} = \mathbf{I}_{D_g}. \end{aligned} \tag{3.7}$$

Note that $\mathbf{S}_{GEB}^{(g)} \left[\mathbf{S}_{cm}^{(g)} \right]^H$ is an equivalent generalized eigenbeamformer according to Lemma 2 since $\left[\mathbf{S}_{cm}^{(g)} \right]^H$ is invertible. Given $\mathbf{S}_{cm}^{(g)}$, optimum solution for the constrained analog beamformer $\mathbf{S}_c^{(g)\star}$ is a phase extraction of the equivalent beamformer that is expressed as

$$\mathbf{S}_c^{(g)\star} = \frac{1}{\sqrt{M}} e^{j \measuredangle \left(\mathbf{S}_{GEB}^{(g)} [\mathbf{S}_{cm}^{(g)}]^H \right)}. \tag{3.8}$$

For given constrained analog beamformer $\mathbf{S}_c^{(g)}$, optimization problem given in (3.7) reduces to

$$\begin{aligned} \underset{\mathbf{S}_{cm}^{(g)}}{\text{minimize}} \quad & \left\| \mathbf{S}_{GEB}^{(g)} \left[\mathbf{S}_{cm}^{(g)} \right]^H - \mathbf{S}_c^{(g)} \right\|_F^2 \\ \text{subject to} \quad & \left[\mathbf{S}_{cm}^{(g)} \right]^H \mathbf{S}_{cm}^{(g)} = \mathbf{I}_{D_g}. \end{aligned} \tag{3.9}$$

which is similar to the orthogonal Procrustes problem [64]. Optimal compensation matrix can be found as

$$\mathbf{S}_{cm}^{(g)\star} = \mathbf{V}^{(g)}\left[\mathbf{U}^{(g)}\right]^H, \tag{3.10}$$

which is obtained by using the SVD of the equivalent generalized eigenbeamformer $\left[\mathbf{S}_{GEB}^{(g)}\right]^H \mathbf{S}_c^{(g)}$ [6], that can be expressed as

$$\left[\mathbf{S}_{GEB}^{(g)}\right]^H \mathbf{S}_c^{(g)} = \mathbf{U}^{(g)}\mathbf{\Sigma}^{(g)}\left[\mathbf{V}^{(g)}\right]^H \tag{3.11}$$

Alternating minimization algorithm is adopted in order to obtain optimum solutions where $\mathbf{S}_c^{(g)\star}$ is calculated for given $\mathbf{S}_{cm}^{(g)}$, and $\mathbf{S}_{cm}^{(g)\star}$ is calculated by using given $\mathbf{S}_c^{(g)}$ repeatedly until the convergence is achieved for the cost function. This solution strategy is also known as projections onto convex sets (POCS) or alternating projection method in the literature. Summary of the described solution is given in Algorithm 1.

Algorithm 1 PE-AM

Input: $\mathbf{S}_{GEB}^{(g)}$

Initialize: $\mathbf{S}_{c,0}^{(g)} = \frac{1}{\sqrt{M}} e^{j\angle\left(\mathbf{S}_{GEB}^{(g)}\right)}$, iteration index $n = 0$

1: **repeat**

2: Fix $\mathbf{S}_{c,n}^{(g)}$, find $\left[\mathbf{S}_{GEB}^{(g)}\right]^H \mathbf{S}_{c,n}^{(g)} = \mathbf{U}_n^{(g)}\mathbf{\Sigma}_n^{(g)}\left[\mathbf{V}_n^{(g)}\right]^H$

3: $\mathbf{S}_{cm,n}^{(g)} = \mathbf{V}_n^{(g)}\left[\mathbf{U}_n^{(g)}\right]^H$

4: Fix $\mathbf{S}_{cm,n}^{(g)}$, find $\mathbf{S}_{c,n+1}^{(g)} = \frac{1}{\sqrt{M}} e^{j\angle\left(\mathbf{S}_{GEB}^{(g)}[\mathbf{S}_{cm,n}^{(g)}]^H\right)}$

5: $n \leftarrow n + 1$

6: **until** $\left\|\mathbf{S}_{GEB}^{(g)}\left[\mathbf{S}_{cm,n}^{(g)}\right]^H - \mathbf{S}_{c,n+1}^{(g)}\right\|_F$ converges

Output: $\mathbf{S}_c^{(g)} = \mathbf{S}_{c,n+1}^{(g)}$ and $\mathbf{S}_{cm}^{(g)} = \mathbf{S}_{cm,n}^{(g)}$

For compensation matrix-based design, constrained beamformer $\mathbf{S}_c^{(g)}$ is applied in analog domain whereas compensation matrix $\mathbf{S}_{cm}^{(g)}$ is applied in digital baseband just before the digital beamformers. Thus, overall analog beamformer of group g becomes $\mathbf{S}^{(g)} = \mathbf{S}_c^{(g)}\mathbf{S}_{cm}^{(g)}$ as it is seen from Fig. 3.1.

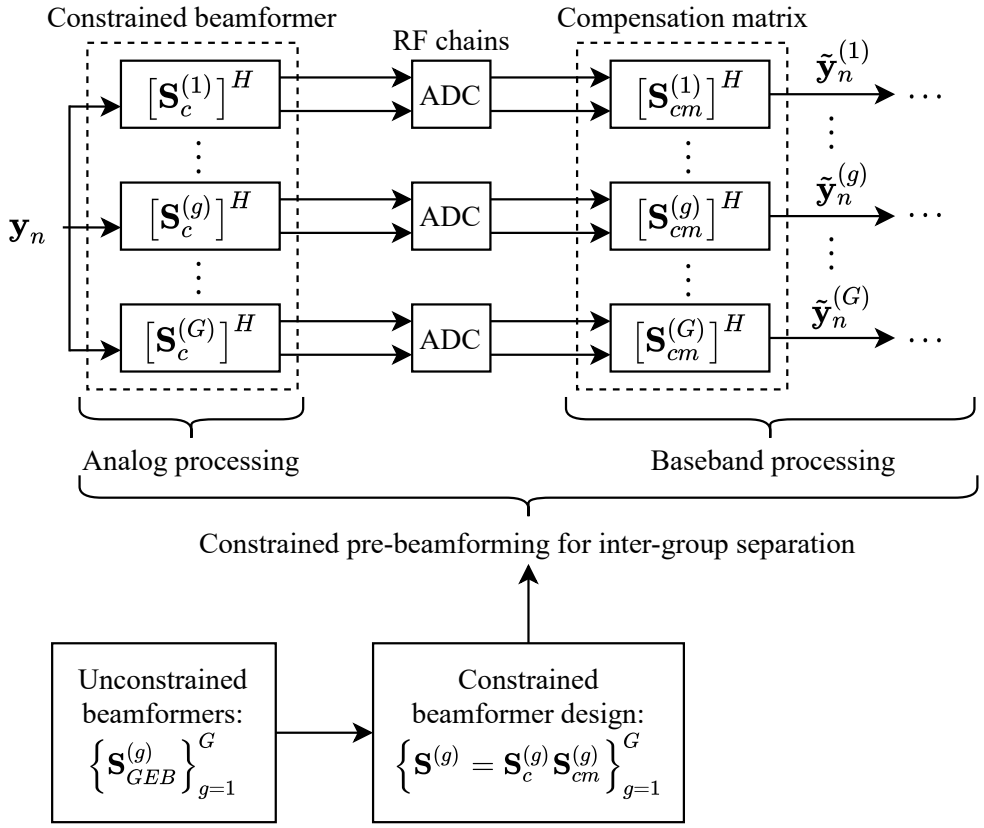

Figure 3.1: Block diagram of the proposed constrained pre-beamforming design

3.2 Partially Connected Array

Unlike fully connected arrays, each antenna element is connected to only one RF chain for partially connected designs. In other words, analog beamformer has a sparse structure resulting in less phase shifters. Let the binary connection matrix of group g is denoted by $\mathbf{\Pi}^{(g)} \in \mathsf{Z}^{M \times D_g}$ where each row contains only one non-zero entry. Column where i^{th} row has the non-zero entry is denoted by $j(i)$. Constrained beamforming matrix $\mathbf{S}_c^{(g)}$ has non-zero entries where the connection matrix $\mathbf{\Pi}^{(g)}$ has non-zero entries. Similar to PE-AM algorithm, we consider joint optimization of constrained beamformer and compensation matrix. There are two types of partially connected arrays. In the first one, optimization problem is solved by using a fixed connection matrix. The second one considers finding the optimum connection matrix for a given unconstrained beamformer.

3.2.1 Fixed Subarray Design

Joint optimization problem of constrained analog beamformer with partially connected array and compensation matrix can be written as

$$\begin{aligned} \underset{\mathbf{S}_c^{(g)},\mathbf{S}_{cm}^{(g)}}{\text{minimize}} \quad & \left\| \mathbf{S}_{GEB}^{(g)} - \mathbf{S}_c^{(g)} \mathbf{S}_{cm}^{(g)} \right\|_F^2 \\ \text{subject to} \quad & \left| [\mathbf{S}_c^{(g)}]_{(i,j)} \right| = \frac{1}{\sqrt{M}} [\mathbf{\Pi}^{(g)}]_{(i,j)}, \forall i, j, \end{aligned} \tag{3.12}$$

for a given connection matrix $\mathbf{\Pi}^{(g)}$. Note that since there is only one non-zero element in each row of $\mathbf{S}_c^{(g)}$, non-zero element in i^{th} row is multiplied with $j(i)^{th}$ row of the compensation matrix $\mathbf{S}_{cm}^{(g)}$. By using this property, optimization problem in (3.12) is simplified as

$$\underset{\{\nu_i^{(g)}\}_{i=1}^M}{\text{minimize}} \quad \left\| \left[\mathbf{S}_{GEB}^{(g)}\right]_{(i,:)} - \frac{1}{\sqrt{M}} e^{j\nu_i^{(g)}} \left[\mathbf{S}_{cm}^{(g)}\right]_{(j(i),:)} \right\|_F^2 \tag{3.13}$$

for given compensation matrix $\mathbf{S}_{cm}^{(g)}$, where $\nu_i^{(g)}$ is the phase of non-zero entry in the i^{th} row of $\mathbf{S}_c^{(g)}$. It can be seen that optimization of phase values is decoupled. Hence, optimum phase values $\left\{\nu_i^{(g)\star}\right\}_{i=1}^M$ are found as

$$\nu_i^{(g)\star} = \measuredangle\left(\left[\mathbf{S}_{GEB}^{(g)}\right]_{(i,:)} \left[\mathbf{S}_{cm}^{(g)}\right]_{(j(i),:)}^H \right). \tag{3.14}$$

Given constrained beamformer $\mathbf{S}_c^{(g)}$, optimization problem to find the compensation matrix becomes

$$\underset{\mathbf{S}_{cm}^{(g)}}{\text{minimize}} \quad \left\| \mathbf{S}_{GEB}^{(g)} - \mathbf{S}_c^{(g)} \mathbf{S}_{cm}^{(g)} \right\|_F^2. \tag{3.15}$$

As there is no constraint on the compensation matrix, optimum solution is the least squares (LS) solution given as

$$\mathbf{S}_{cm}^{(g)\star} = \left(\left[\mathbf{S}_c^{(g)}\right]^H \mathbf{S}_c^{(g)} \right)^{-1} \left[\mathbf{S}_c^{(g)}\right]^H \mathbf{S}_{GEB}^{(g)}. \tag{3.16}$$

Alternating minimization approach is adopted as in PE-AM algorithm to find constrained analog beamformer and compensation matrix. Summary of the fixed partially connected array design is given in Algorithm 2.

Algorithm 2 Fixed Subarray Design

Input: $\mathbf{S}_{GEB}^{(g)}, \mathbf{\Pi}^{(g)}$

Initialize: Set random phases to $\mathbf{S}_{c,0}^{(g)}$, iteration index $n = 0$

1: **repeat**

2: Fix $\mathbf{S}_{c,n}^{(g)}$

3: Find $\mathbf{S}_{cm,n}^{(g)} = \left(\left[\mathbf{S}_{c,n}^{(g)} \right]^H \mathbf{S}_{c,n} \right)^{-1} \left[\mathbf{S}_{c,n}^{(g)} \right]^H \mathbf{S}_{GEB}^{(g)}$

4: Fix $\mathbf{S}_{cm,n}^{(g)}$, find $\mathbf{S}_{c,n+1}^{(g)}$ by (3.14)

5: $n \leftarrow n + 1$

6: **until** $\left\| \mathbf{S}_{GEB}^{(g)} - \mathbf{S}_{c,n+1}^{(g)} \mathbf{S}_{cm,n}^{(g)} \right\|_F$ converges

Output: $\mathbf{S}_{c}^{(g)} = \mathbf{S}_{c,n+1}^{(g)}$ and $\mathbf{S}_{cm}^{(g)} = \mathbf{S}_{cm,n}^{(g)}$

3.2.2 Dynamic Subarray Design

This section aims to find an algorithm that finds the optimum connection matrix $\mathbf{\Pi}^{(g)}$ for a given GEB. Let $\tilde{\mathbf{S}}_{c}^{(g)} \in \mathsf{C}^{M \times D_g}$ be a partially connected constrained beamformer whose non-zero entry locations are unknown. This matrix needs to satisfy following constraints

$$\left| [\tilde{\mathbf{S}}_{c}^{(g)}]_{(i,j)} \right| \in \{0, 1\}, \forall i, j, \tag{3.17a}$$

$$\sum_{j=1}^{D_g} \left| [\tilde{\mathbf{S}}_{c}^{(g)}]_{(i,j)} \right| = 1, \forall i, \tag{3.17b}$$

$$\sum_{i=1}^{M} \left| [\tilde{\mathbf{S}}_{c}^{(g)}]_{(i,j)} \right| \geq 1, \forall j, \tag{3.17c}$$

where the first one is constant-modulus constraint while second one needs to be satisfied to make sure that each antenna is connected to only one RF chain. The third

constraint should be satisfied so that each RF chain is connected to at least one antenna. Let the equivalent near-optimal generalized eigenbeamformer be $\mathbf{S}_{GEB}^{(g)}\mathbf{A}^{(g)}$ where $\mathbf{A}^{(g)} \in \mathsf{C}^{D_g \times D_g}$ is an arbitrary unitary matrix. Note that $\mathbf{S}_{GEB}^{(g)}\mathbf{A}^{(g)}$ can replace $\mathbf{S}_{GEB}^{(g)}$ as long as $\mathbf{A}^{(g)}$ is invertible according to Lemma 2. Let us ignore the constraint in (3.17c) for now and construct an optimization problem given as

$$\begin{aligned} \underset{\mathbf{A}^{(g)} \in \mathcal{A}, \tilde{\mathbf{S}}_c^{(g)}}{\text{minimize}} \quad & \left\| \mathbf{S}_{GEB}^{(g)}\mathbf{A}^{(g)} - \tilde{\mathbf{S}}_c^{(g)} \right\|_F^2 \\ \text{subject to} \quad & \left| [\tilde{\mathbf{S}}_c^{(g)}]_{(i,j)} \right| \in \{0,1\}, \forall i,j; \\ & \sum_{j=1}^{D_g} \left| [\tilde{\mathbf{S}}_c^{(g)}]_{(i,j)} \right| = 1, \forall i, \end{aligned} \tag{3.18}$$

where $\mathcal{A}$ is the set of unitary matrices which are invertible. Given $\mathbf{A}^{(g)}$, entries of optimal constrained analog beamformer can be found as

$$[\tilde{\mathbf{S}}_c^{(g)\star}]_{(i,j)} = \begin{cases} e^{j\angle\left([\mathbf{S}_{GEB}^{(g)}\mathbf{A}^{(g)}]_{(i,j)}\right)}, & \text{if } j = j^\star(i) \\ 0, & \text{otherwise,} \end{cases} \tag{3.19}$$

where $j^\star(i) = \arg\max_{1 \le j \le D_g} |[\mathbf{S}_{GEB}^{(g)}\mathbf{A}^{(g)}]_{(i,j)}|$ for $i = 1, 2, \ldots, M$ [29]. For given $\tilde{\mathbf{S}}_c^{(g)}$, optimization problem in (3.18) reduces to orthogonal Procrustes problem expressed as

$$\underset{\mathbf{A}^{(g)} \in \mathcal{A}}{\text{minimize}} \quad \left\| \mathbf{S}_{GEB}^{(g)}\mathbf{A}^{(g)} - \tilde{\mathbf{S}}_c^{(g)} \right\|_F^2 \quad , \tag{3.20}$$

which has the same solution as in the PE-AM algorithm. Optimum unitary matrix is found as

$$\mathbf{A}^{(g)\star} = \mathbf{V}^{(g)}\left[\mathbf{U}^{(g)}\right]^H, \tag{3.21}$$

where the following SVD is used: $\left[\mathbf{S}_{GEB}^{(g)}\right]^H \tilde{\mathbf{S}}_c^{(g)} = \mathbf{U}^{(g)}\mathbf{\Sigma}^{(g)}\left[\mathbf{V}^{(g)}\right]^H$. Similar to previous algorithms, alternating minimization is applied to find partially connected constrained beamformer which is summarized in Algorithm 3.

Algorithm 3 Dynamic Connection Design

Input: $\mathbf{S}_{GEB}^{(g)}$

Initialize: Set random phases to $\tilde{\mathbf{S}}_{c,0}^{(g)}$, iteration index $n = 0$

1: **repeat**

2: Fix $\tilde{\mathbf{S}}_{c,n}^{(g)}$, find $\left[\mathbf{S}_{GEB}^{(g)}\right]^H \tilde{\mathbf{S}}_{c,n}^{(g)} = \mathbf{U}_n^{(g)} \mathbf{\Sigma}_n^{(g)} \left[\mathbf{V}_n^{(g)}\right]^H$

3: $\mathbf{A}_n^{(g)} = \mathbf{V}_n^{(g)} \left[\mathbf{U}_n^{(g)}\right]^H$

4: Fix $\mathbf{A}_n^{(g)}$, find $\tilde{\mathbf{S}}_{c,n+1}^{(g)}$ by (3.19)

5: $n \leftarrow n + 1$

6: **until** $\left\| \mathbf{S}_{GEB}^{(g)} \mathbf{A}_n^{(g)} - \tilde{\mathbf{S}}_{c,n+1}^{(g)} \right\|_F$ converges

Output: $\tilde{\mathbf{S}}_c^{(g)} = \tilde{\mathbf{S}}_{c,n+1}^{(g)}$

Remark 1*:* The result of Algorithm 3, which solves a non-convex problem, depends on the initial random phases which leads to different antenna connections for each result. Hence, this algorithm should be repeated several times with different initial phases and the result yielding the maximum expected SINR for group g in reduced dimension, which is the SINR after statistical pre-beamformer $\mathbf{S}^{(g)}$ (i.e., just before digital beamforming), should be used. Expression for the expected SINR is given in (C.1) in Appendix C, where we denote the expected SINR of group g by $\overline{SINR}^{(g)}$.

Remark 2*:* Constraint (3.17c) is not considered in Algorithm 3 which is repeated several times as stated in Remark 1. Optimum connection matrix should be selected from the results where there is a connection between any RF chain and at least one antenna to satisfy this constraint.

It is important to note that only constrained analog beamformer can be found by using Algorithm 3. However, we need to find a compensation matrix to improve the result. We propose that result of Algorithm 3 should be used in order to find the connection matrix as $\mathbf{\Pi}^{(g)} = \left|\tilde{\mathbf{S}}_c^{(g)}\right|$. Then, this connection matrix should be used as an input to Algorithm 2 which jointly optimizes constrained analog beamformer and compensation matrix. Furthermore, initial phases of constrained analog beamformer for Algorithm 2 is selected as the phases of $\tilde{\mathbf{S}}_c^{(g)}$. Therefore, it can be seen that Algorithm 3 is used to find the connection matrix. Summary of the overall dynamic

subarray design is given in Algorithm 4 where N_{iter} is the number of times Algorithm 3 is repeated.

Algorithm 4 Dynamic Subarray Design

Input: $\mathbf{S}_{GEB}^{(g)}, N_{iter}$

Initialize: Iteration index $t = 0$

1: **repeat**
2: $t \leftarrow t + 1$
3: Run Algorithm 3 to find $\tilde{\mathbf{S}}_c^{(g)}$ and set $\tilde{\mathbf{S}}_{c,t}^{(g)} \leftarrow \tilde{\mathbf{S}}_c^{(g)}$
4: **if** $\sum_{i=1}^{M} \left|[\tilde{\mathbf{S}}_{c,t}^{(g)}]_{(i,j)}\right| \geq 1, \forall j$ **then**
5: Calculate $\overline{SINR}_t^{(g)}$ by setting $\mathbf{S}^{(g)} \leftarrow \tilde{\mathbf{S}}_{c,t}^{(g)}$ in (C.1)
6: **else**
7: Set $\overline{SINR}_t^{(g)}$ to 0
8: **end if**
9: **until** $t = N_{iter}$
10: $t^\star = \arg\max_{1 \leq t \leq N_{iter}} \overline{SINR}_t^{(g)}$
11: Run Algorithm 2 with $\mathbf{\Pi}^{(g)} = \left|\tilde{\mathbf{S}}_{c,t^\star}^{(g)}\right|$ and initial phases of $\tilde{\mathbf{S}}_{c,t^\star}^{(g)}$ to find $\mathbf{S}_c^{(g)}$ and $\mathbf{S}_{cm}^{(g)}$.

Output: $\mathbf{S}_c^{(g)}$ and $\mathbf{S}_{cm}^{(g)}$

3.3 Convergence and Complexity Analysis

3.3.1 Convergence Analysis

Alternating minimization approach is employed to obtain both fully and partially connected constrained analog beamformers. Convergence of given algorithms is guaranteed since cost functions, which are bounded below, are monotonically decreasing at each iteration. Considering these two facts, algorithms given in this thesis converge to local minima [5, 29].

3.3.2 Complexity Analysis

Constrained beamformer design algorithms that are described in this chapter are based on GEB found by generalized eigenvalue problem in (2.18) where matrices with size $M \times M$ are involved. In the literature, Lanczos algorithm and its variations are used to find a few most dominant generalized eigenvectors [65]. Although the exact computational complexity of this algorithm is not clear due to the iterative solutions, its complexity can roughly be taken as $O(M^3)$.

On the other hand, alternating minimization based algorithms require additional computation over GEB. Phase extraction has the same complexity order with GEB as it only requires the phases of GEB. Algorithm 1 and Algorithm 3 has the same solution steps which involve phase extraction of matrix multiplication at one step. Another step includes SVD of a matrix with size $D_g \times D_g$ which has a complexity order of $O(D_g^3)$. Since these computations are repeated several times, complexity of PE-AM and dynamic connection design becomes $O(n_{max}D_g^3)$ where n_{max} is the number of iterations until the convergence. Algorithm 2 only includes phase extraction from a vector multiplication and a LS solution which requires the inverse of a $D_g \times D_g$ matrix with complexity order of $O(D_g^3)$. Complexity of fixed subarray design becomes $O(n_{max}D_g^3)$ due to the alternating minimization method. Algorithm 4, which is used to find the dynamic constrained analog beamformers, involves execution of Algorithm 2 once and Algorithm 3 N_{iter} times. Therefore, computational complexity of dynamic subarray design becomes $O((N_{iter}+1)n_{max}D_g^3)$. It can be understood that complexity orders of proposed alternating minimization-based algorithms are not high as number of RF chains D_g is limited in hybrid systems. Moreover, recall that unconstrained analog beamformers are designed based on slowly varying CCMs. Hence, constrained beamformers and dynamic connections are updated infrequently. Computational complexity orders of proposed unconstrained and constrained analog beamformer design algorithms are summarized in Table 3.1.

Table 3.1: Computational complexity orders of proposed analog beamforming algorithms

Beamformer Type	Computational Complexity
GEB	$O(M^3)$
PE	$O(M^3)$
PE-AM	$O(M^3 + n_{max}D_g^3)$
Fixed Subarray	$O(M^3 + n_{max}D_g^3)$
Dynamic Subarray	$O(M^3 + (N_{iter} + 1)n_{max}D_g^3)$

CHAPTER 4

INTRA-GROUP PROCESSING FOR CONVENTIONAL HYBRID MASSIVE MIMO: $U \leq D$ CASE

In this chapter, the digital processing architecture for classical hybrid massive MIMO case without NOMA, i.e., $U \leq D$ will be described. The two-stage beamforming architecture, which includes the intra-group processing via IB-DFE, was introduced in Chapter 2. As digital processing of each user group is independent from each other, only intra-group effective channels of users are required for digital beamformer design. Effective channel vectors are learned in time division duplexing (TDD) mode as in Section 4.2.2. Intra-group channel estimation in reduced dimension reduces the channel estimation overhead significantly. In addition, dimensions of feedforward and feedback filters are reduced with the help of user-grouping since IB-DFE is used to separate intra-group user signals.

Firstly, optimal feedforward and feedback filters will be obtained for the IB-DFE receiver while taking the residual inter-group interference into account. Then, performance measures, namely, ergodic capacity and channel estimation accuracy in reduced dimension will be derived. Lastly, numerical results of proposed constrained beamforming methods for both fully and partially connected arrays will be discussed.

4.1 Digital Beamformer Design: IB-DFE

Frequency domain equalizer output at i^{th} iteration was defined in (2.11), where feedforward and feedback filters were utilized. Optimal filters at each iteration can be found by using MMSE criterion where the total mean square error (MSE) of a block

for group g at i^{th} iteration is defined as

$$MSE_i^{(g)} = \mathsf{E}\left\{ \sum_{k=0}^{N-1} \left\| \hat{\mathbf{x}}_{f,k}^{(g),i} - \mathbf{x}_{f,k}^{(g),i} \right\|^2 \right\}. \tag{4.1}$$

In addition, following constraint is imposed on feedback filters to avoid self cancellation:

$$\sum_{k=0}^{N-1} \left[\mathbf{C}_k^{(g),i} \right]_{(u,u)} = 0 \tag{4.2}$$

for $u = 1, 2, \ldots, U_g$. In [52], it is shown that minimization of (4.1) with the given constraint reduces to following N parallel equations

$$\mathbf{R}_{\tilde{\mathbf{y}}_{f,k}^{(g)}} \mathbf{W}_k^{(g),i} = \mathbf{\Lambda}_{eff,k}^{(g,g)} \left(\frac{E_s^{(g)}}{U_g} \mathbf{I}_{U_g} + \mathbf{P}_1^{(g),i} \mathbf{C}_k^{(g),i} \right), \tag{4.3}$$

$$\mathbf{P}_2^{(g),i} \mathbf{C}_k^{(g),i} = \left[\mathbf{P}_1^{(g),i} \right]^H \left(\left[\mathbf{\Lambda}_{eff,k}^{(g,g)} \right]^H \mathbf{W}_k^{(g),i} - \mathbf{I}_{U_g} \right) + \mathbf{\Delta}_i^{(g)} \tag{4.4}$$

for $k = 0, 1, \ldots, N-1$, where $\mathbf{\Delta}_i^{(g)} = \mathrm{diag}\{\Delta_i^{(g_1)}, \ldots, \Delta_i^{(g_{U_g})}\}$ is a consequence of the constraint on feedback filters. In (4.3) and (4.4), correlation matrices $\mathbf{P}_1^{(g),i} \in \mathsf{C}^{U_g \times U_g}$ and $\mathbf{P}_2^{(g),i} \in \mathsf{C}^{U_g \times U_g}$ are expressed

$$\mathbf{P}_1^{(g),i} = \mathsf{E}\left\{ \mathbf{x}_n^{(g)} \left[\tilde{\mathbf{x}}_n^{(g),i-1} \right]^H \right\}, \tag{4.5a}$$

$$\mathbf{P}_2^{(g),i} = \mathsf{E}\left\{ \tilde{\mathbf{x}}_n^{(g),i-1} \left[\tilde{\mathbf{x}}_n^{(g),i-1} \right]^H \right\}, \tag{4.5b}$$

which show the reliability of the estimates. Note that exact calculation of $\mathbf{P}_1^{(g),i}$ requires the knowledge of transmitted symbols, which is not available at the receiver. A practical approach is to assume that $\mathbf{P}_1^{(g),i} = \mathbf{P}_2^{(g),i} = \mathrm{diag}\left\{ \mathsf{E}\left\{ \tilde{\mathbf{x}}_n^{(g),i} \left[\tilde{\mathbf{x}}_n^{(g),i} \right]^H \right\} \right\}$ as done in [52]. Considering the fact that transmitted symbol vectors of users are uncorrelated and independent from the noise vector, covariance matrix of $\tilde{\mathbf{y}}_{f,k}^{(g)}$ in (2.8)

can be expressed as

$$\mathbf{R}_{\tilde{\mathbf{y}}_{f,k}^{(g)}} = \mathsf{E}\Big\{\tilde{\mathbf{y}}_{f,k}^{(g)}\big[\tilde{\mathbf{y}}_{f,k}^{(g)}\big]^H\Big\} = \frac{E_s^{(g)}}{U_g}\mathbf{\Lambda}_{eff,k}^{(g,g)}\big[\mathbf{\Lambda}_{eff,k}^{(g,g)}\big]^H + \mathbf{R}_{\tilde{\boldsymbol{\eta}}_f}^{(g)}, \tag{4.6}$$

for given frequency-domain intra-group channel matrix $\mathbf{\Lambda}_{eff,k}^{(g,g)}$. Recall that intra-group channels are available at the BS whereas inter-group channel matrices $\mathbf{\Lambda}_{eff,k}^{(g,g')}$ are not known. That is why inter-group channel matrices are treated as random matrices in (4.6) and covariance matrix of sum of inter-group interference and noise terms in reduced dimension $\mathbf{R}_{\tilde{\boldsymbol{\eta}}_f}^{(g)}$, whose expression is given in Appendix A, is used[1].

With the given definitions, feedforward and feedback filters can be computed. If $\mathbf{W}_k^{(g),i}$ is substituted in (4.4) for each frequency bin while considering the constraint on feedback filters, $\mathbf{C}_k^{(g),i}$ and $\Delta_i^{(g_u)}$ can be found as

$$\mathbf{C}_k^{(g),i} = \mathbf{A}_k^{(g),i}\Big(\mathbf{D}_k^{(g),i} + \mathbf{\Delta}_i^{(g)}\Big), \tag{4.7}$$

$$\Delta_i^{(g_u)} = \frac{-\sum_{k=0}^{N-1}\big[\mathbf{A}_k^{(g),i}\big]_{(u,:)}\big[\mathbf{D}_k^{(g),i}\big]_{(:,u)}}{\sum_{k=0}^{N-1}\big[\mathbf{A}_k^{(g),i}\big]_{(u,u)}}, \tag{4.8}$$

where

$$\mathbf{A}_k^{(g),i} = \Big(\mathbf{P}_2^{(g),i} - \big[\mathbf{P}_1^{(g),i}\big]^H\big[\mathbf{\Lambda}_{eff,k}^{(g,g)}\big]^H\mathbf{R}_{\tilde{\mathbf{y}}_{f,k}^{(g)}}^{-1}\mathbf{\Lambda}_{eff,k}^{(g,g)}\mathbf{P}_1^{(g),i}\Big)^{-1}, \tag{4.9}$$

$$\mathbf{D}_k^{(g),i} = \big[\mathbf{P}_1^{(g),i}\big]^H\big[\mathbf{\Lambda}_{eff,k}^{(g,g)}\big]^H\mathbf{R}_{\tilde{\mathbf{y}}_{f,k}^{(g)}}^{-1}\mathbf{\Lambda}_{eff,k}^{(g,g)}\frac{E_s^{(g)}}{U_g} - \big[\mathbf{P}_1^{(g),i}\big]^H. \tag{4.10}$$

Lastly, feedforward filters can be found by substituting $\mathbf{C}_k^{(g),i}$ in (4.3) for each frequency bin. At initialization stage, correlation matrices are set to $\mathbf{P}_1^{(g),0} = \mathbf{P}_2^{(g),0} =$

[1] Estimation of only intra-group effective channels reduces the channel estimation overhead. Furthermore, there may be other sources of interference with known spatial covariance matrices such as inter-cell interference. In that case, instantaneous channel estimation for the interfering source would not be possible, yet our framework would still be applicable.

$\mathrm{diag}\{\mathbf{0}_{U_g}\}$ where $\mathbf{0}_{U_g}$ is a zero vector with length U_g. Consequently, there is no feedback at initialization while feedforward filters are reduced to LMMSE type digital beamformers that can be expressed as

$$\mathbf{W}_k^{(g),0} = \frac{E_s^{(g)}}{U_g} \mathbf{R}_{\tilde{\mathbf{y}}_{f,k}^{(g)}}^{-1} \mathbf{\Lambda}_{eff,k}^{(g,g)}. \tag{4.11}$$

If analog beamformers are properly designed, inter-group interference terms in (2.8) will be close to zero. In this case, zero-forcing (ZF) approach can be adopted at initialization. ZF type digital beamformer of group g is expressed as

$$\mathbf{W}_k^{(g),0} = \mathbf{\Lambda}_{eff,k}^{(g,g)} \left(\left[\mathbf{\Lambda}_{eff,k}^{(g,g)} \right]^H \mathbf{\Lambda}_{eff,k}^{(g,g)} \right)^{-1}. \tag{4.12}$$

The main advantage of ZF is its computation complexity since it involves inversion of matrices with size $U_g \times U_g$ per frequency bin resulting in a complexity order of $O(NU_g^3)$, whereas LMMSE involves inversion of covariance matrix of $\tilde{\mathbf{y}}_{f,k}^{(g)}$ per frequency bin that results in a complexity order of $O(ND_g^3)$. On the other hand, IB-DFE structure requires the calculation of feedforward and feedback filters at each iteration. Computation complexity of feedforward filters is equivalent to LMMSE filter while feedback filters require inversion of matrices with size $U_g \times U_g$ and $D_g \times D_g$ per frequency bin which results in a complexity order of $O(ND_g^3)$ as $U_g \leq D_g$. Thus, overall complexity of IB-DFE becomes $O(i_{max} ND_g^3)$ where i_{max} is the number of equalizer iterations. It is important to note that complexity order of described digital beamforming design scales with the third power of either U_g or D_g which are limited in JSDM framework. Hence, signal processing complexity of digital beamforming is highly reduced via user-grouping and two-stage beamforming approach.

4.2 Performance Measures

In order to show the effectiveness of proposed constrained design, we should define some performance measures. We firstly introduce ergodic capacity which is the most commonly used performance measure. Then, we describe a channel estimation method in reduced dimension and define the normalized mean square error (nMSE)

that shows the accuracy of channel estimation.

4.2.1 Ergodic Capacity

Ergodic capacity of user u in group g at the output of i^{th} equalizer iteration is defined as

$$C_i^{(g_u)} = \mathsf{E}_{\left\{\mathbf{H}_{eff,l}^{(g,g)}\right\}_{l=0}^{L-1}}\left\{\log_2\left(1+SINR_i^{(g_u)}\right)\middle|\mathbf{S}^{(g)}\right\}, \tag{4.13}$$

where expectation is taken over different instantaneous channel realizations while keeping the analog beamformer constant, i.e., user locations and CCMs are kept constant. Output SINR of user u in group g at the output of i^{th} equalizer iteration is denoted by $SINR_i^{(g_u)}$. Let the Bussgang decomposition of the soft output for decoding transmitted symbols given in (2.12) is expressed as [66]

$$\hat{x}_n^{(g_u),i} = \beta^{(g_u),i} x_n^{(g_u)} + \xi_n^{(g_u),i}, \tag{4.14}$$

for $n = 0, 1, \ldots, N-1$ and $u = 1, 2, \ldots, U_g$, where $\beta^{(g_u),i}$ and $\xi_n^{(g_u),i}$ are the complex amplitude and residual interference of the transmitted symbol of user u in group g, respectively. Then the output SINR of this user for given $\left\{\mathbf{H}_{eff,l}^{(g,g)}\right\}_{l=0}^{L-1}$ is calculated as

$$SINR_i^{(g_u)} = \frac{|\beta^{(g_u),i}|^2 \mathsf{E}\left\{|x_n^{(g_u)}|^2\right\}}{\mathsf{E}\left\{|\xi_n^{(g_u),i}|^2\right\}} = \frac{E_s^{(g)}}{U_g}\frac{|\beta^{(g_u),i}|^2}{\mathsf{E}\left\{|\xi_n^{(g_u),i}|^2\right\}}. \tag{4.15}$$

By using (2.8), (2.11) and (2.12), complex amplitude can be computed as

$$\begin{aligned}\beta^{(g_u),i} &= \mathsf{E}\left\{\hat{x}_n^{(g_u),i}\left(x_n^{(g_u)}\right)^*\right\} / \mathsf{E}\left\{|x_n^{(g_u)}|^2\right\} \\ &= \frac{1}{N}\sum_{k=0}^{N-1}\left[\mathbf{W}_k^{(g),i}\right]_{(:,u)}^H \mathbf{\Lambda}_{eff,k}^{(g,g)} \mathbf{e}_u,\end{aligned} \tag{4.16}$$

where $\mathbf{e}_u \in \mathsf{Z}^{U_g \times 1}$ is a binary vector whose u^{th} entry is one whereas others are zero. On the other hand, residual interference power can be calculated as $\mathsf{E}\left\{|\xi_n^{(g_u),i}|^2\right\} =$

$\left\{|\hat{x}_n^{(g_u),i}|^2\right\} - \frac{E_s^{(g)}}{U_g}|\beta^{(g_u),i}|^2$ where

$$\begin{aligned}\mathsf{E}\left\{|\hat{x}_n^{(g_u),i}|^2\right\} = &\frac{1}{N}\sum_{k=0}^{N-1}\left[\mathbf{W}_k^{(g),i}\right]_{(:,u)}^H \mathbf{R}_{\tilde{\mathbf{y}}_{f,k}^{(g)}}\left[\mathbf{W}_k^{(g),i}\right]_{(:,u)} \\ &+ \frac{1}{N}\sum_{k=0}^{N-1}\left[\mathbf{C}_k^{(g),i}\right]_{(:,u)}^H \mathbf{P}_2^{(g),i}\left[\mathbf{C}_k^{(g),i}\right]_{(:,u)} \\ &- \frac{2}{N}\sum_{k=0}^{N-1}\mathrm{Re}\left\{\left[\mathbf{W}_k^{(g),i}\right]_{(:,u)}^H \mathbf{\Lambda}_{eff,k}^{(g,g)}\mathbf{P}_1^{(g),i}\left[\mathbf{C}_k^{(g),i}\right]_{(:,u)}\right\},\end{aligned} \tag{4.17}$$

which can be obtained by using Parseval's relation for (2.11) and (2.12). Covariance matrix of $\tilde{\mathbf{y}}_{f,k}^{(g)}$ given in (4.6) is used for the calculation above. Since $\beta^{(g_u),i}$ and $\mathsf{E}\left\{|\xi_n^{(g_u),i}|^2\right\}$ do not depend on the time instance n, they can be calculated once for given instantaneous effective channel matrices.

Asymptotic Analysis

In IB-DFE framework, estimates are expected to be more reliable as the number of iterations increases. Asymptotically, if perfect knowledge of intra-group user symbols are obtained, correlation matrices approach to the maximum reliability case that can be expressed as $\mathbf{P}_1^{(g),i} = \mathbf{P}_2^{(g),i} = \frac{E_s^{(g)}}{U_g}\mathbf{I}_{U_g}$. In Appendix D, asymptotic SINR of user u in group g is obtained as

$$SINR^{(g_u)} = \frac{1}{N}\sum_{k=0}^{N-1}\frac{E_s^{(g)}}{U_g}\left[\mathbf{\Lambda}_{eff,k}^{(g,g)}\right]_{(:,u)}^H \mathbf{R}_{\tilde{\boldsymbol{\eta}}_f^{(g)}}^{-1}\left[\mathbf{\Lambda}_{eff,k}^{(g,g)}\right]_{(:,u)}. \tag{4.18}$$

It can be understood that the equalizer at each frequency bin becomes a whitening matched filter after perfect intra-group cancellation in frequency domain. Therefore, asymptotic SINR in (4.18) is called the matched filter bound (MFB) which is the maximum SINR that can be achieved by utilizing IB-DFE.

4.2.2 Beamspace-Aware Channel Estimation

In this thesis, channel estimation is realized in reduced dimension. Instantaneous intra-group effective channel matrices $\left\{\mathbf{H}_{eff,l}^{(g,g)}\right\}_{l=0}^{L-1}$ of each group are estimated during the uplink channel estimation phase in TDD mode where distinct pilot sequences with length T are assigned to each user in a group. Equivalent signal vector of group g at the BS at the end of the pilot sequence transmission is defined as

$$\begin{aligned}\bar{\mathbf{y}}^{(g)} &\triangleq \left[\left[\tilde{\mathbf{y}}_0^{(g)}\right]^H, \left[\tilde{\mathbf{y}}_1^{(g)}\right]^H, \cdots, \left[\tilde{\mathbf{y}}_{T-1}^{(g)}\right]^H\right]^H \\ &= \sum_{g'=1}^{G}\left(\mathbf{X}^{(g')} \otimes \mathbf{I}_{D_g}\right)\bar{\mathbf{h}}_{eff}^{(g,g')} + \left(\mathbf{I}_T \otimes \left[\mathbf{S}^{(g)}\right]^H\right)\bar{\mathbf{n}},\end{aligned} \tag{4.19}$$

where $\mathbf{X}^{(g)} \in \mathsf{C}^{T \times U_g L}$ is the equivalent pilot matrix of group g and $\bar{\mathbf{h}}_{eff}^{(g,g')} \in \mathsf{C}^{D_g U_{g'} L \times 1}$ is the overall effective channel vector of group g' after the analog beamformer of group g. Note that equivalent signal vector $\bar{\mathbf{y}}^{(g)} \in \mathsf{C}^{TD_g \times 1}$ is obtained by vertically concatenating received signal vectors after the analog beamformer $\left\{\tilde{\mathbf{y}}_n^{(g)}\right\}_{n=0}^{T-1}$ in (2.7). Similarly, equivalent noise vector $\bar{\mathbf{n}} \in \mathsf{C}^{TM \times 1}$ is constructed by vertically concatenating noise vectors $\{\mathbf{n}_n\}_{n=0}^{T-1}$. Equivalent pilot matrix is defined as

$$\mathbf{X}^{(g)} \triangleq \left[\mathbf{X}^{(g_1)}, \mathbf{X}^{(g_2)}, \cdots, \mathbf{X}^{(g_{U_g})}\right], \tag{4.20}$$

where $\left[\mathbf{X}^{(g_u)}\right]_{(i,j)} \triangleq x_{i-j}^{(g_u)}$, for $i = 0, 1, \ldots, T-1$ and $j = 0, 1, \ldots, L-1$. Pilot sequence entries of user u in group g are denoted by $x_n^{(g_u)}$. Note that entries with negative indices can be taken as cyclic prefix or previously decoded symbols. Overall effective channel vector of group g' for the analog beamformer of group g is defined as

$$\bar{\mathbf{h}}_{eff}^{(g,g')} \triangleq \left[\left[\bar{\mathbf{h}}_{eff}^{(g,g'_1)}\right]^H, \left[\bar{\mathbf{h}}_{eff}^{(g,g'_2)}\right]^H, \cdots, \left[\bar{\mathbf{h}}_{eff}^{(g,g'_{U_{g'}})}\right]^H\right]^H, \tag{4.21}$$

$$\bar{\mathbf{h}}_{eff}^{(g,g'_u)} \triangleq \left[\left[\mathbf{h}_{eff,0}^{(g,g'_u)}\right]^H, \left[\mathbf{h}_{eff,1}^{(g,g'_u)}\right]^H, \cdots, \left[\mathbf{h}_{eff,L-1}^{(g,g'_u)}\right]^H\right]^H, \tag{4.22}$$

where $\mathbf{h}_{eff,l}^{(g,g'_u)} \triangleq \left[\mathbf{S}^{(g)}\right]^H \mathbf{h}_l^{(g'_u)}$, or $\mathbf{h}_{eff,l}^{(g,g'_u)} \triangleq \left[\mathbf{H}_{eff,l}^{(g,g')}\right]_{(:,u)}$, for $l = 0, 1, \ldots, L-1$. It is important to note that we are only interested in intra-group channel vectors. In other words, our aim is to estimate $\bar{\mathbf{h}}_{eff}^{(g,g)}$ from (4.19) as

$$\hat{\bar{\mathbf{h}}}_{eff}^{(g,g)} = \left[\mathbf{Z}^{(g)}\right]^H \bar{\mathbf{y}}^{(g)} \tag{4.23}$$

where $\mathbf{Z}^{(g)} \in \mathbf{C}^{D_g U_g L \times T D_g}$ is the channel estimator matrix. In this thesis, LMMSE and LS channel estimators are considered. Expressions for these estimators can be found in Appendix E. In order to show the accuracy of channel estimation, we calculate nMSE which is defined as

$$\begin{aligned} nMSE^{(g)} &\triangleq \frac{\mathsf{E}\left\{\left\|\bar{\mathbf{h}}_{eff}^{(g,g)} - \hat{\bar{\mathbf{h}}}_{eff}^{(g,g)}\right\|^2\right\}}{\mathsf{E}\left\{\left\|\bar{\mathbf{h}}_{eff}^{(g,g)}\right\|^2\right\}} \\ &= \frac{\mathrm{Tr}\left\{\mathbf{R}_{\bar{\mathbf{h}}_{eff}^{(g,g)}}\right\} + \mathrm{Tr}\left\{\mathbf{R}_{\hat{\bar{\mathbf{h}}}_{eff}^{(g,g)}}\right\} - 2\mathrm{Re}\left\{\mathrm{Tr}\left\{\mathbf{R}_{\hat{\bar{\mathbf{h}}}_{eff}^{(g,g)}\bar{\mathbf{h}}_{eff}^{(g,g)}}\right\}\right\}}{\mathrm{Tr}\left\{\mathbf{R}_{\bar{\mathbf{h}}_{eff}^{(g,g)}}\right\}} \end{aligned} \tag{4.24}$$

where covariance matrix of $\hat{\bar{\mathbf{h}}}_{eff}^{(g,g)}$ and covariance between $\hat{\bar{\mathbf{h}}}_{eff}^{(g,g)}$ and $\bar{\mathbf{h}}_{eff}^{(g,g)}$ can be computed as

$$\mathbf{R}_{\hat{\bar{\mathbf{h}}}_{eff}^{(g,g)}} = \mathsf{E}\left\{\hat{\bar{\mathbf{h}}}_{eff}^{(g,g)}\left[\hat{\bar{\mathbf{h}}}_{eff}^{(g,g)}\right]^H\right\} = \left[\mathbf{Z}^{(g)}\right]^H \mathbf{R}_{\bar{\mathbf{y}}^{(g)}} \mathbf{Z}^{(g)}, \tag{4.25}$$

$$\mathbf{R}_{\hat{\bar{\mathbf{h}}}_{eff}^{(g,g)}\bar{\mathbf{h}}_{eff}^{(g,g)}} = \mathsf{E}\left\{\hat{\bar{\mathbf{h}}}_{eff}^{(g,g)}\left[\bar{\mathbf{h}}_{eff}^{(g,g)}\right]^H\right\} = \left[\mathbf{Z}^{(g)}\right]^H \mathbf{R}_{\bar{\mathbf{y}}^{(g)}\bar{\mathbf{h}}_{eff}^{(g,g)}}. \tag{4.26}$$

Expressions of $\mathbf{R}_{\bar{\mathbf{y}}^{(g)}\bar{\mathbf{h}}_{eff}^{(g,g)}}$, $\mathbf{R}_{\bar{\mathbf{y}}^{(g)}}$ and $\mathbf{R}_{\bar{\mathbf{h}}_{eff}^{(g,g)}}$ are given in (E.2), (E.3) and (E.4) in Appendix E, respectively. There are some concluding remarks for the described channel estimation scheme.

Remark 3: With the assumption that analog beamformer suppresses inter-group interference perfectly, training periods of groups does not have to be synchronized. In

this case, training symbols of other groups ($\mathbf{X}^{(g')}, g' \neq g$) can be assumed to be random. Furthermore, users in a group should use different training sequences whereas users in other groups can reuse the same sequences with properly designed analog beamformers. Hence, it can be inferred that this channel estimation scheme is robust against pilot contamination.

Remark 4: Analog beamforming method proposed in this thesis was shown to be applicable to multiantenna user case in Lemma 1. Similarly, channel estimation scheme described in this subsection can be extended to multiantenna user case by redefining effective channels as in (B.8) in Appendix B.

4.3 Numerical Results

In this section, proposed constrained analog beamformers are compared by using the performance measures in Section 4.2. BS has an ULA with $M = 128$ antennas whereas users have single-antenna elements. Carrier frequency is selected as 30GHz while the antenna spacing of the ULA is set to half the wavelength. A predetermined user-grouping is employed with $G = 4$ groups where each group has $U_g = 2$ users[2]. Although total number of delays is $L = 32$, users do not have active MPCs at every delay. In the simulations, angular spread $\Delta_l^{(g_u)}$ of all users is set to 2° for every MPC. Power profile function $\rho_l^{(g_u)}(\theta)$ is assumed to be uniform in the angular spread of the MPC and channel gain $\sqrt{\gamma^{(g_u)}}$ is set to 1 for all users. MPC cluster powers of users are assumed to be the same. Signal-to-noise ratio (SNR) of group g is denoted by $SNR^{(g)} = \frac{E_s^{(g)}}{N_0}$.

The scenario used for simulations is given in Table 4.1. This table shows the active MPC indices of groups and mean AoAs of users related to each active MPC. Group-1 is selected as the mobile group with shifting angle of ϕ which is swept from -45° to 45° with increments of 0.1° for simulation purposes. It is important to note that CCMs are slowly varying parameters. However, the reason to use a mobile group is to obtain results for different angular profiles and observe the effect of overlapping MPCs. Hence, we are only interested in the results of the mobile group which

[2] Here, we assume that users come in groups, either by nature or by the use of a proper user grouping algorithm [54, 55].

is Group-1. For each ϕ, CCMs and analog beamformer of Group-1 are calculated, then ergodic capacity, BER and nMSE are obtained. Ergodic capacity of user u in Group-1 and nMSE of Group-1 corresponding to shifting angle ϕ are denoted by $C_{\phi}^{(1_u)}$ and $nMSE_{\phi}^{(1)}$, respectively. Ergodic capacity and BER results are obtained with perfect CSI knowledge. Cardinality of the input alphabet is selected as 4 (i.e., QPSK) for BER simulations, whereas Gaussian alphabets are assumed for ergodic capacity calculations. Therefore, results related to ergodic capacity are shown for ZF and LMMSE type digital beamformers.

Table 4.1: Angle-delay profile of groups for the mobile scenario

Group	MPC index	Mean AoAs $\left(\mu_l^{(g_u)}\right)$ of users
1 (Mobile)	0	{ϕ-15.5°, ϕ-14.5°}
	5	{ϕ-2.5°, ϕ-1.5°}
	11	{ϕ+16.5°, ϕ+17.5°}
2	3	{40.5°, 41.5°}
	9	{20.5°, 21.5°}
3	8	{-10.5°, -9.5°}
	17	{-20.5°, -19.5°}
4	29	{-40.5°, -39.5°}

Angle-delay map of groups is given in Fig. 4.1 in order to visualize the scenario given in Table 4.1. In this figure, ϕ of the mobile group is set to $15°$. This is a typical mm-wave scenario where we observe a sparse angle-delay profile.

4.3.1 JSDM with Fully Connected Arrays

In this section, constrained fully connected array structures are compared. Fully digital (FD) beamformer and unconstrained near-optimal analog beamformer GEB introduced in Section 2.3 are used as benchmark. In order to make a fair comparison, FD is applied with the perfect knowledge of instantaneous effective intra-group CSI and inter-group CCMs. DFT beamformer, phase extraction and PE-AM in Algorithm 1

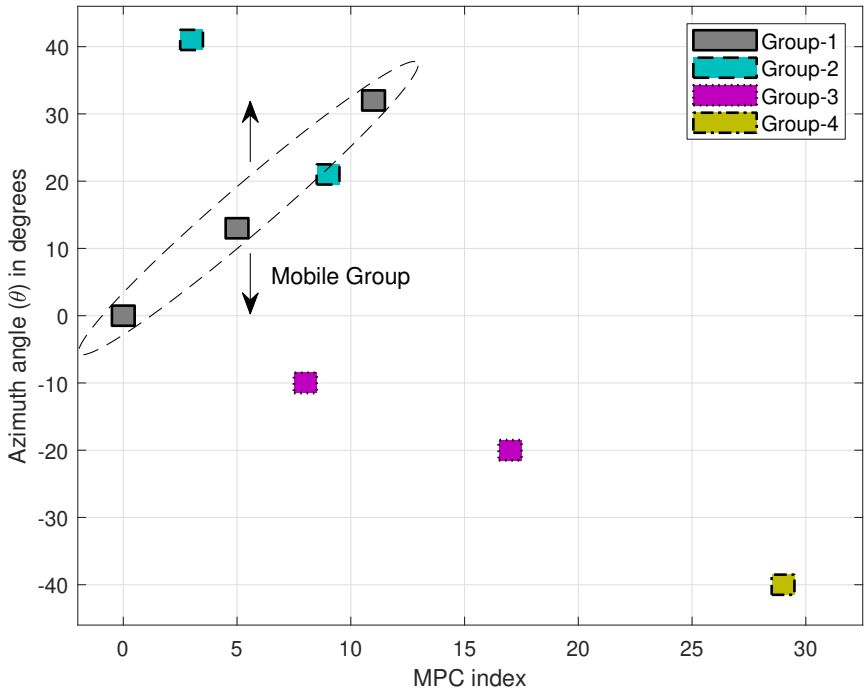

Figure 4.1: Angle-delay map of groups with $\phi = 15°$

are the considered constrained beamformers.

Firstly, we will introduce beampattern metric which shows the power that can be attained at the angle of interest θ for a given analog beamformer. Interference suppression capability of beamformers can be observed by using this metric. Beampattern as a function of θ for given analog beamformer $\mathbf{S}^{(g)}$ can be defined as

$$B(\theta) = \mathbf{u}(\theta)^H \mathbf{S}^{(g)} \left(\left[\mathbf{S}^{(g)}\right]^H \mathbf{S}^{(g)} \right)^{-1} \left[\mathbf{S}^{(g)}\right]^H \mathbf{u}(\theta). \tag{4.27}$$

Fig. 4.2 shows the beampatterns of Group-1 for PE-AM and DFT beamformer with $\phi = 10°$ and $D_1 = 4$ where SNR of each group is set to 40 dB. It is seen that both beamformers can form narrow beams. Although PE-AM does not provide deep nulls, we observed that it can provide moderate suppression for MPCs of other groups whereas DFT beamformer does not consider these MPCs. If beampatterns of PE-AM and DFT beamformer are compared, this suppression appears more significant for interfering angular regions that are close to the angular region of intended group.

Fig. 4.3 shows the average spectral efficiency of Group-1 with changing SNR where

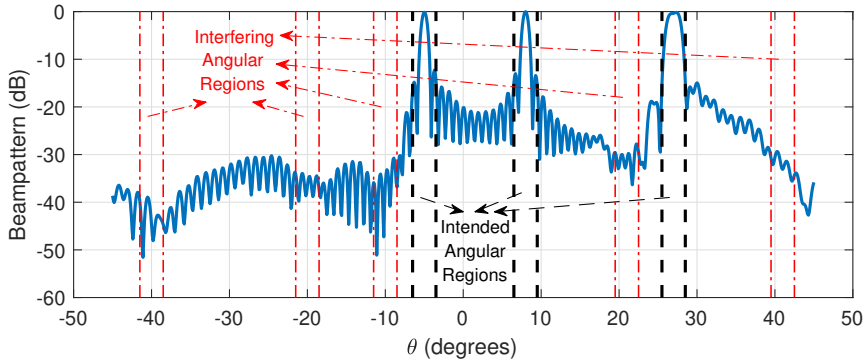

(a) PE-AM

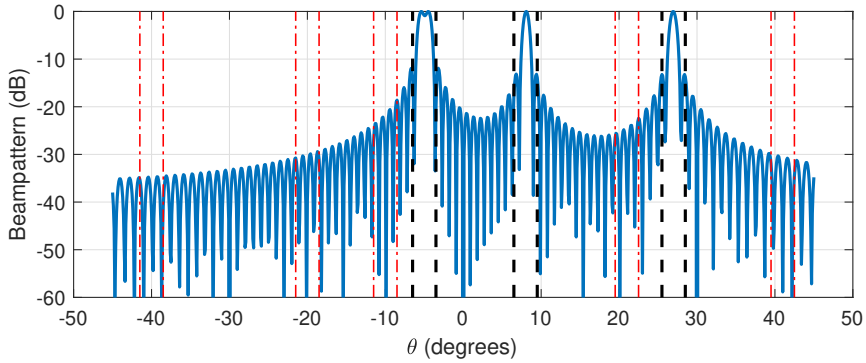

(b) DFT beamformer

Figure 4.2: Beampatterns of Group-1 for fully connected array structures with $\phi = 10°$, $D_1 = 4$ and $SNR^{(g)} = 40$ dB for $\forall g$

SNR of other groups is set to $SNR^{(g')} = 40$ dB for $g' \neq 1$. Note that average spectral efficiency is found by taking the average of ergodic capacity over both users and shifting angle ϕ, i.e., $C_{avg}^{(1)} = \mathsf{E}_{\phi,u}\left\{C_{\phi}^{(1_u)}\right\}$. It can be observed that LMMSE type digital beamformer does not provide a significant improvement over ZF for analog beamformers except DFT beamformer with $D_1 = 2$ since it does not consider inter-group interference. Similarly, there is a significant gap between ZF and LMMSE type beamformers for FD architecture as it does not have any inter-group interference suppression with ZF. However, LMMSE provides improvement for all constrained analog beamformers, especially for DFT beamformer, with $D_1 = 4$ as it can efficiently suppress residual inter-group interference when the number of RF chains is greater than the number of users. It should be noted that LMMSE and ZF type digital beamformers perform the same for GEB at high SNR which shows that there is no

residual interference. Furthermore, it is seen that there is a significant gap between DFT beamformer and other constrained beamformers for $D_1 = 2$, whereas the gap between PE and PE-AM is very small. However, there is a gap between PE and PE-AM for $D_1 = 4$ which is expected since increase in RF chains corresponds to increase in the dimension of the compensation matrix for PE-AM. LMMSE type digital beamformer makes the DFT beamformer perform almost as good as PE for $D_1 = 4$. Moreover, the gap between FD beamformer and GEB is small for $D_1 = 4$, which shows that GEB can achieve the capacity of optimal FD architecture with limited RF chains.

Previous results show the average performance of analog beamformers in the mobile group. However, angular regions of MPCs belonging to Group-1 overlaps with angular regions of MPCs of other groups at certain ϕ values. It is important to observe the degradation in spectral efficiency with different constrained analog beamformers for overlapping situations. In other words, we need to observe the variation in spectral efficiency to obtain the outage capacity. Let the cumulative density function (CDF) of spectral efficiency of Group-1 is defined as $P\big(C_{\phi}^{(g)} < c\big)$ where average spectral efficiency of Group-1 for shifting angle ϕ is denoted by $C_{\phi}^{(1)} = \mathsf{E}_u\Big\{C_{\phi}^{(1_u)}\Big\}$. Then, CDF curves correspond to outage probabilities for given spectral efficiency values. In Fig. 4.4, CDF curves with different analog beamformers are compared for $D_1 = 2$ and $D_1 = 4$ where SNR of each group is set to 40 dB. It is observed that CDF curves of DFT beamformer are wider compared to others which results in higher outage probability. For example, outage probability of PE-AM with $D_1 = 4$ is close to zero at 7 bits/s/Hz while it is above 0.3 for DFT beamformer. On the other hand, GEB has sharp CDF curves for both $D_1 = 2$ and $D_1 = 4$ cases which means that it is a robust analog beamforming method. If CDF curves of GEB and FD beamformer are compared, it can be observed that GEB (even with a significantly reduced number of RF chains) performs very close to FD at low outage probability levels. Furthermore, it is observed that PE and PE-AM has fairly sharp CDF curves especially for $D_1 = 4$ case.

Another performance measure is BER, which can be used to observe the contributions of IB-DFE method over linear equalizers. We considered two different scenarios for BER results. Firstly, we obtained average BER of Group-1 with changing SNR for

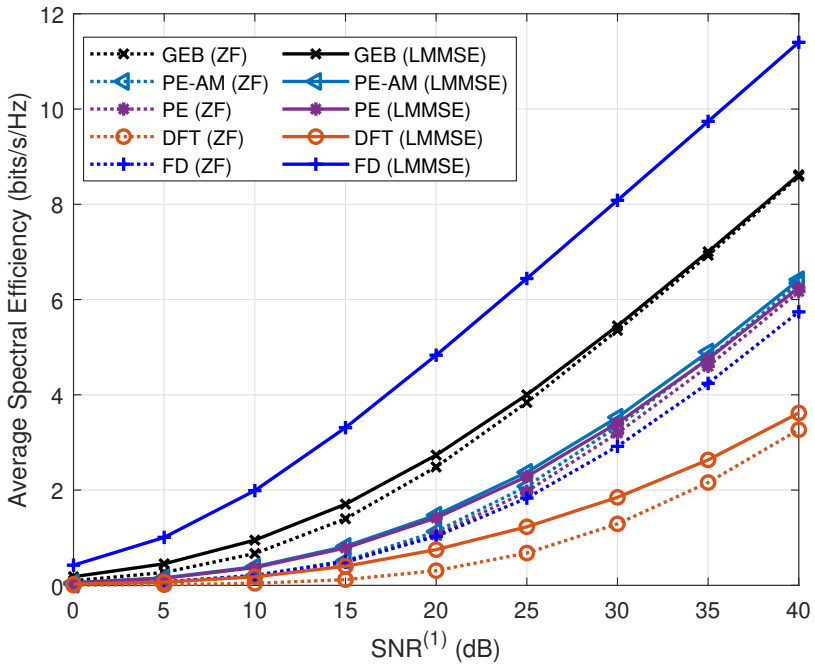

(a) $D_1 = 2$

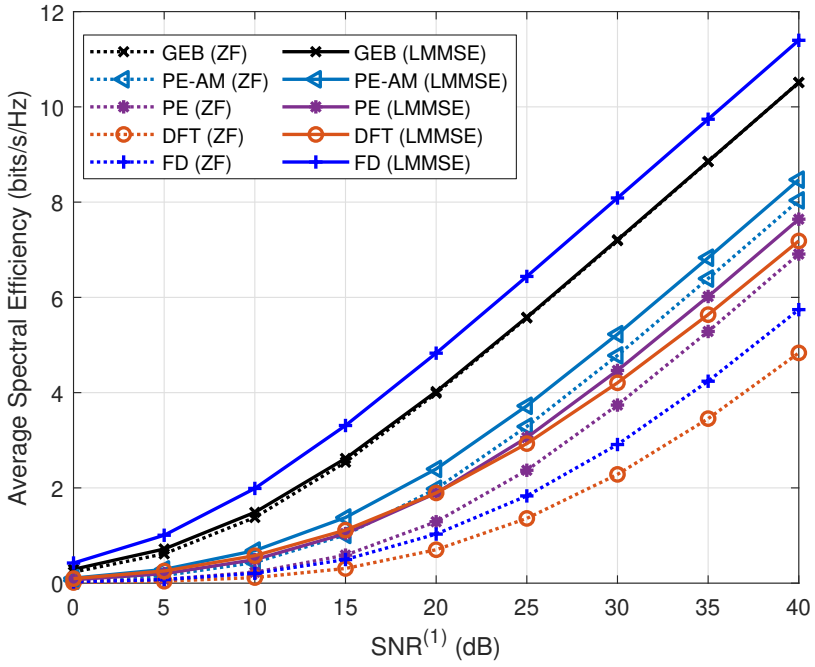

(b) $D_1 = 4$

Figure 4.3: Average spectral efficiency of Group-1 vs. SNR for fully connected array structures with $SNR^{(g')} = 40$ dB for $g' \neq 1$

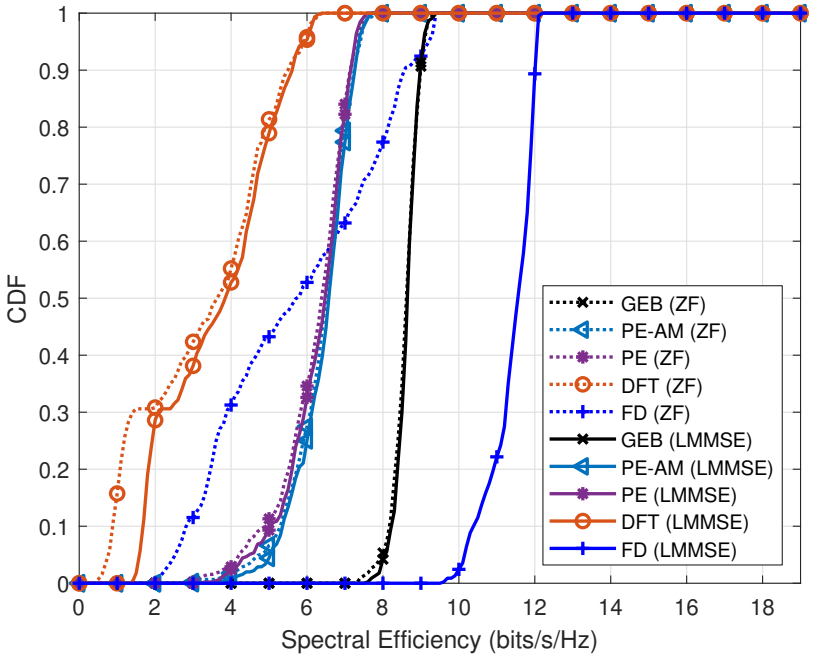

(a) $D_1 = 2$

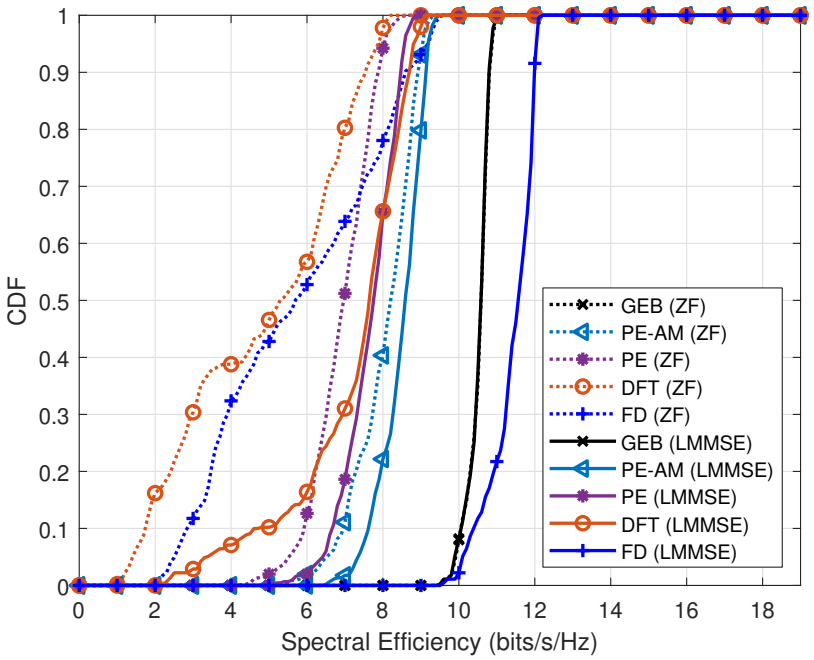

(b) $D_1 = 4$

Figure 4.4: CDF of spectral efficiency of Group-1 for fully connected array structures with $SNR^{(g)} = 40$ dB for $\forall g$

$D_1 = 4$ while keeping SNR of other groups at 30 dB, which is shown in Fig. 4.5a where MFB denotes the asymptotic case with perfect intra-group cancellation. It can be observed that IB-DFE iterations improve the BER of all beamformers compared to linear equalizers, and BER curves of IB-DFE with 2 iterations are very close to MFB curves for FD beamformer, GEB and PE-AM. However, there is still SNR gap between BER curves of MFB and IB-DFE for DFT beamformer. Furthermore, it can be observed that FD beamformer, GEB and PE-AM perform very close to each other, whereas there is 10 dB SNR gap between PE-AM and DFT beamformer with IB-DFE at BER of 10^{-3}. The second scenario is the case where SNR of every group is varied together, which is shown in Fig. 4.5b. It can be observed that DFT beamformer has an error floor even for MFB case, which is expected since perfect intra-group cancellation is utilized with IB-DFE, but DFT beamformer does not consider inter-group interference. Similarly, FD beamformer with ZF does not suppress inter-group interference leading to an error floor. Although PE-AM has an error floor with ZF type digital beamformer, it disappears with IB-DFE iterations. Furthermore, it can be seen that GEB and PE-AM perform very close to each other, which shows that PE-AM preserves the interference suppression capability of GEB. On the other hand, BER results show that interference sensitivity of DFT beamformer could be detrimental although this could not be observed from average spectral efficiency results.

Channel estimation accuracy is another performance measure that is considered in this thesis. Fig. 4.6 shows the average nMSE of Group-1 with $D_1 = 4$ where SNR of other groups is set to $SNR^{(g')} = 40$ dB for $g' \neq 1$. Average of nMSE is taken over shifting angle ϕ, i.e., $nMSE^{(1)}_{avg} = \mathsf{E}_{\phi}\left\{nMSE^{(1)}_{\phi}\right\}$. It can be observed that LMMSE estimator outperforms LS estimator especially with short pilot lengths for all analog beamformers. Moreover, it is important to note that nMSE of DFT beamformer is much higher compared to others even with LMMSE estimator while nMSE of PE-AM is less than nMSE of both PE and DFT beamformer.

In spectral efficiency analysis, DFT beamformer performed close to PE for $D_1 = 4$ with perfect CSI. However, nMSE results show that spectral efficiency performance of DFT would degrade more compared to other ones if the channel estimation errors are considered. Considering the beampattern, outage capacity, BER and nMSE results, it can be concluded that DFT beamformer should be avoided for JSDM frame-

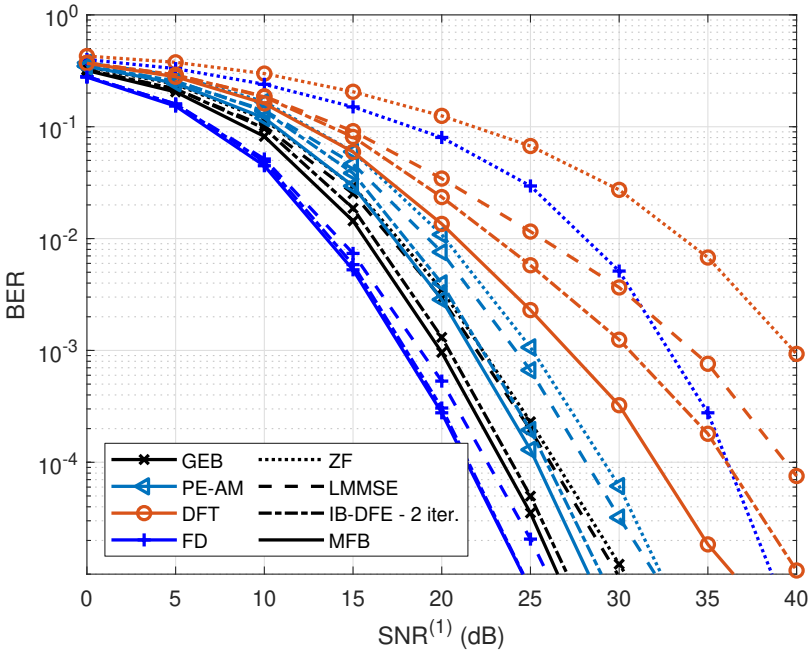

(a) $SNR^{(g')} = 30$ dB for $g' \neq 1$

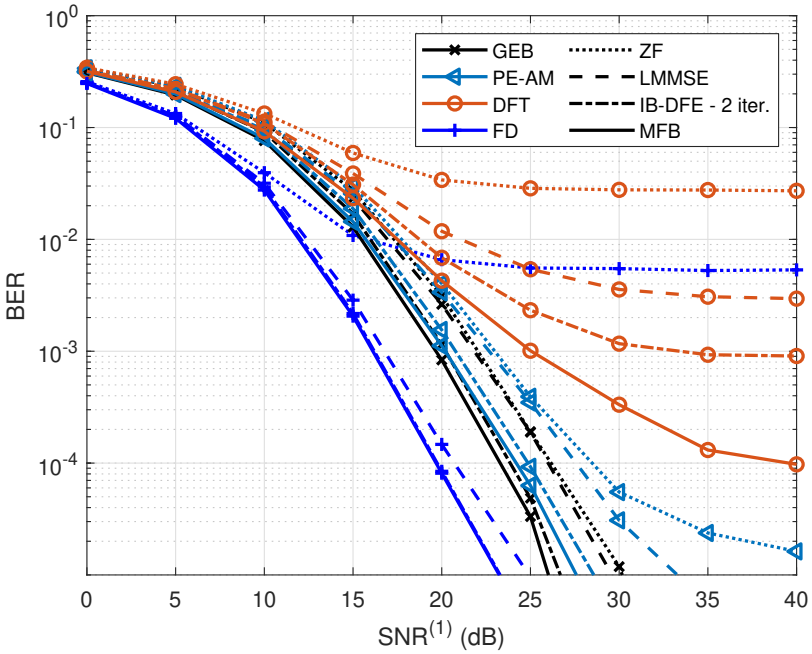

(b) $SNR^{(g')} = SNR^{(1)}$ for $g' \neq 1$

Figure 4.5: Average BER of Group-1 vs. SNR for fully connected array structures with $D_1 = 4$

work especially when the near-far effect is observed as it does not consider MPCs other groups[3]. Furthermore, PE-AM yields better performance than PE especially when the number of RF chains is not highly restricted since dimensions of compensation matrix are determined by this number. Consequently, PE-AM should be preferred to obtain fully connected constrained analog beamformers.

4.3.2 JSDM with Partially Connected Arrays

In this section, partially connected array structures are considered. While SNR of other groups (i.e., inter-group interference) was set to 40 dB for fully connected structures, we consider a moderate interference scenario for partially connected arrays where SNR of interfering groups is set to 20 dB since even constrained analog beamformers with fully connected arrays do not attain the performance of GEB at high interference. Furthermore, we merge Group-1 and Group-2 and denote it by Group-$1'$ which includes 4 users and 5 different MPC clusters. Relative angular regions of MPCs of the merged group is taken as in Fig. 4.1 and the center of the MPCs is swept with shifting angle ϕ from -45° to 45° with increments of 0.1° as in previous part. We want to serve more users with a single analog beamformer which is the reason for merging groups. We will only be interested in the merged group and design a partially connected array for the analog beamformer of this group[4]. Interference originated from Group-3 and Group-4 can be considered as any interference with known covariance matrix. We will consider two different fixed partially connected arrays. The first one is called adjacent or ordered which has a connection matrix $\mathbf{\Pi}_{ord}^{1'} = \mathbf{I}_{D_{1'}} \otimes \mathbf{1}_{M/D_{1'}}$, where $\mathbf{1}_{M/D_{1'}} \in \mathsf{Z}^{M/D_{1'}}$ is a vector of ones. Second type of fixed partially connected arrays is called interlaced which has a connection matrix $\mathbf{\Pi}_{int}^{1'} = \mathbf{1}_{M/D_{1'}} \otimes \mathbf{I}_{D_{1'}}$.

In Fig. 4.7, beampatterns of Group-$1'$ with fixed and dynamic partially connected arrays are given for $D_{1'} = 8$ where MPCs are located as in Fig. 4.1. We selected the number of RF chains as 8 since it is the minimum power of two that is larger than the number of MPCs. SNR of Group-1 and Group-2 before merging was set to 30

[3] The near-far effect stems from the fact that the average received signal strength of different UEs may differ significantly depending on their distance to the BS.

[4] Other groups can be served by using another array at the BS or scheduling them in time and frequency resources.

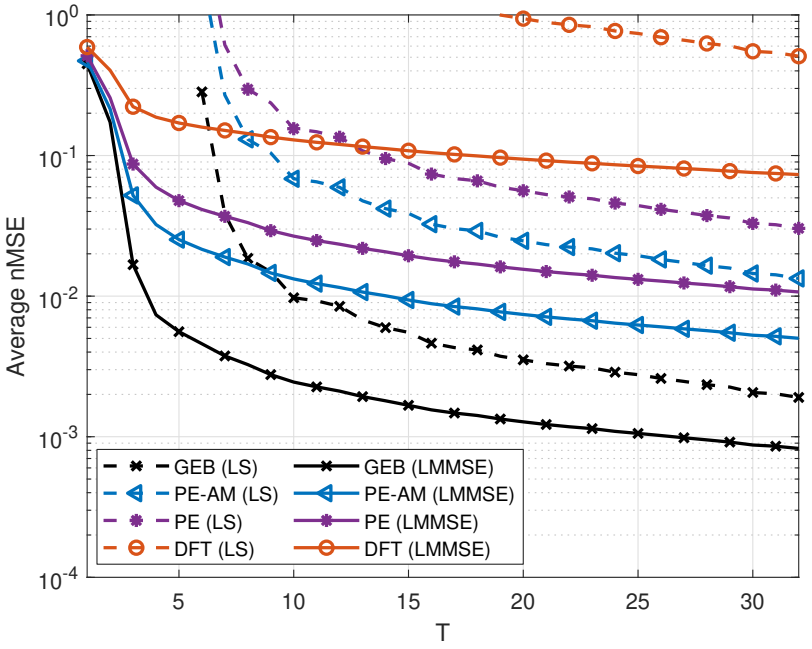

(a) Average nMSE vs. T with $SNR^{(1)} = 30$ dB

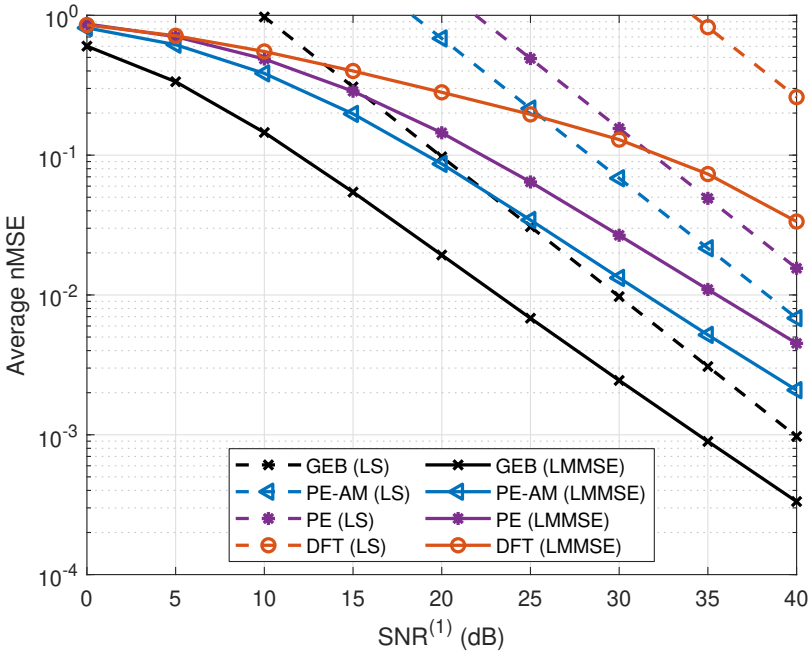

(b) Average nMSE vs. $SNR^{(1)}$ with $T = 10$

Figure 4.6: Average nMSE of Group-1 for fully connected array structures with $D_1 = 4$ and $SNR^{(g')} = 40$ dB for $g' \neq 1$

dB while SNR of other groups is set to 20 dB. We observe that ordered array forms wide beams whereas dynamic subarray can form narrow beams located in the angular regions of Group-$1'$. Hence, dynamic subarray preserved the multipath diversity even though beam power is slightly higher at interfering angular regions. In addition, interference suppression of ordered array would be lost due to wide beams when the MPCs are close to each other in the mobile scenario. On the other hand, interlaced array completely lost interference suppression as it suffers from grating lobe effect which occurs when the antenna spacing of an array is larger than half the wavelength. It is important to note that the proposed dynamic array is seen to effectively compromise between avoiding grating lobes and forming narrower beams.

Average spectral efficiency with changing SNR of Group-$1'$ is given in Fig. 4.8 for $D_{1'} = 8$ where fixed and dynamic subarrays and fully connected PE-AM and GEB are considered while SNR of other groups is set to 20 dB. Firstly, it is important to note that PE-AM performs very close to GEB for this scenario where moderate interference is considered. If we compare partially connected array designs, dynamic subarray outperforms both fixed array structures. Another important point is that the gap between LMMSE and ZF type digital beamformers is smaller for the dynamic subarray which indicates that residual interference after the analog beamformer is smaller compared to fixed subarrays. Moreover, the gap between dynamic and fixed subarrays is larger in this thesis compared to prior work [27, 31]. On the other hand, ordered array has higher average spectral efficiency than interlaced array as expected. We can make similar comments if we compare CDF of spectral efficiency curves which are given in Fig. 4.9. We observe that CDF curves of dynamic subarray are parallel to CDF curves of PE-AM and GEB whereas fixed arrays, especially interlaced structure, has wider CDF curves. This result shows the robustness of the dynamic subarray structure.

Fig. 4.10 shows the average BER of Group-$1'$ with changing SNR for $D_{1'} = 8$ while SNR of other groups is set to 20 dB. It can be noted that BER is improved and MFB can be achieved for all beamformers with IB-DFE method. Furthermore, SNR gap between fully connected beamformers and dynamic subarray is around 3 dB for IB-DFE method at BER of 10^{-3}, while there is 8 dB SNR gap between dynamic and ordered subarrays. It can be seen that performance gap between dynamic and fixed subarrays

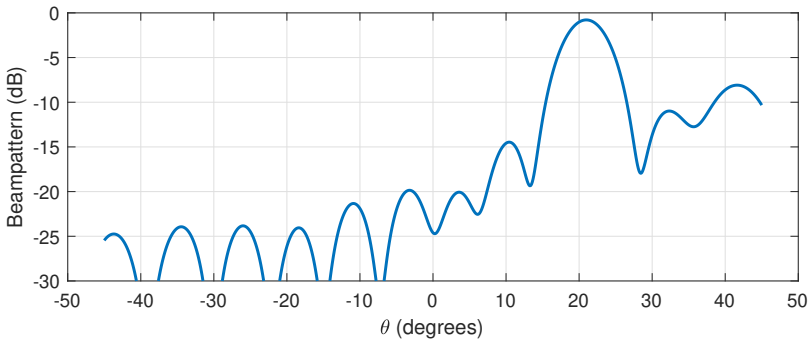

(a) Fixed - Ordered

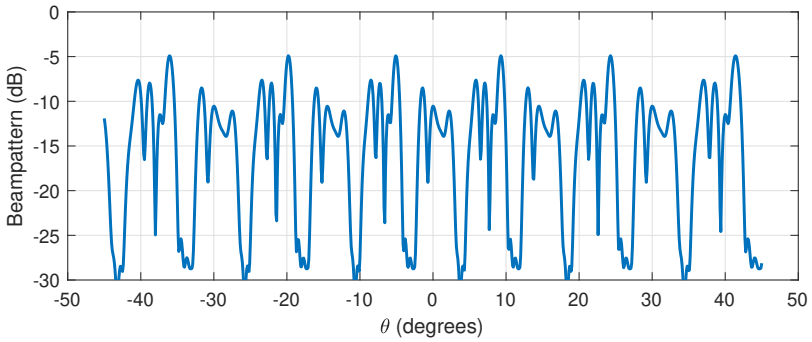

(b) Fixed - Interlaced

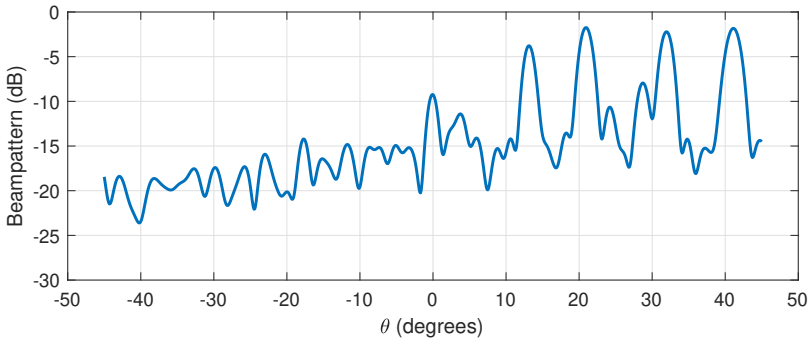

(c) Dynamic

Figure 4.7: Beampatterns of Group-1′ for partially connected array structures with $D_{1'} = 8$, $SNR^{(1)} = SNR^{(2)} = 30$ dB and $SNR^{(3)} = SNR^{(4)} = 20$ dB

is larger than the gap observed from spectral efficiency curves. Therefore, BER results showed the superiority of dynamic subarray against fixed ones more clearly. In conclusion, PE-AM attains the performance of GEB, and proposed dynamic subarray algorithm performs close to fully connected arrays which shows the resilience of proposed algorithms against interference for the moderate interference scenario.

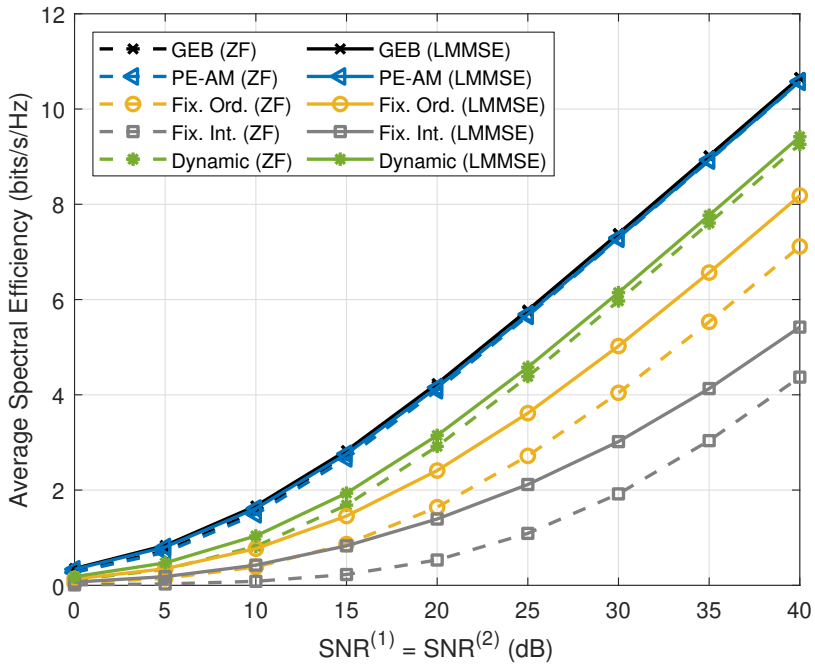

Figure 4.8: Average spectral efficiency of Group-1′ vs. SNR for partially connected array structures with $D_{1'} = 8$ and $SNR^{(3)} = SNR^{(4)} = 20$ dB

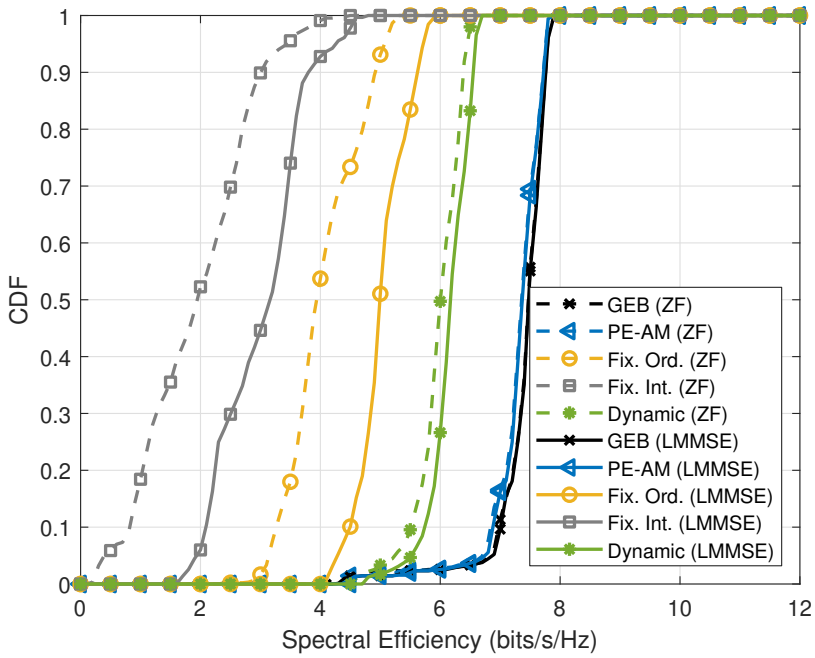

Figure 4.9: CDF of spectral efficiency of Group-1′ for partially connected array structures with $D_{1'} = 8$, $SNR^{(1)} = SNR^{(2)} = 30$ dB and $SNR^{(3)} = SNR^{(4)} = 20$ dB

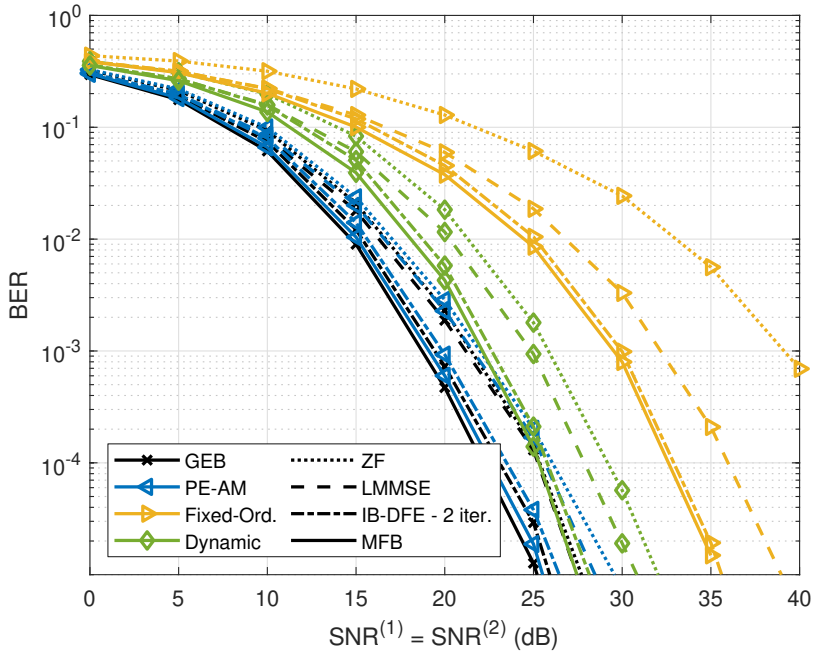

Figure 4.10: Average BER of Group-1′ vs. SNR for partially connected array structures with $D_{1'} = 8$ and $SNR^{(3)} = SNR^{(4)} = 20$ dB

CHAPTER 5

INTRA-GROUP PROCESSING FOR HIGHLY OVERLOADED HYBRID MASSIVE MIMO WITH CODE-DOMAIN NOMA: $U > D$ CASE

In JSDM framework, spatially close users are grouped together. However, users with spatially correlated channels is not the desired case since it degrades the intra-group user separation performance, especially for highly loaded massive MIMO. Code-domain NOMA could be a possible solution to this problem as different codewords are assigned to users, which could potentially provide a better user separation. In this chapter, adaptation of code-domain NOMA to described JSDM architecture is carried out. Initially, relation between code-domain NOMA and transmitted signals of users is defined for SC transmission, and a novel signal wideband-beamspace code-domain NOMA signal model is derived. Then, a code-beamspace IB-DFE receiver is proposed for joint equalization and user separation. Furthermore, modifications to the nearly-optimal GEB and IB-DFE receiver introduced in previous chapters are provided. Lastly, numerical results are discussed with the defined performance metric to show the effectiveness of the proposed design.

5.1 Wideband-Beamspace Code-Domain NOMA Signal Model

We consider a code-domain NOMA scheme, namely MUSA, where users have distinct short spreading sequences transmitted in temporal domain. Let the unit norm spreading code of user u in group g with length N_c be defined as

$$\mathbf{q}^{(g_u)} \triangleq \left[q^{(g_u)}[0]\ q^{(g_u)}[1] \cdots\ q^{(g_u)}[N_c-1]\right]^T, \tag{5.1}$$

where entries of the spreading code $\{q^{(g_u)}[i], i = 0, \ldots, N_c - 1\}$ are randomly selected from the MUSA constellation given in [67]. Then, the relation between NOMA symbols and the transmitted signal of user u in group g at n^{th} time instance can be given as

$$x_n^{(g_u)} \triangleq \sum_{m=0}^{N_s-1} q^{(g_u)}[n - N_c m] a_m^{(g_u)}. \tag{5.2}$$

for $n = 0, 1, \ldots, N$ and $m = 0, 1, \ldots, N_s - 1$, where $N_s = N/N_c$ is the number of symbols transmitted in a block of length N, and $a_m^{(g_u)}$ is the symbol (e.g., QAM symbol) of user u in group g at m^{th} NOMA signaling interval satisfying $\mathsf{E}\{a_m^{(g_u)}(a_{m'}^{(g'_{u'})})^*\} = \frac{E_s^{(g)}}{U_g}\delta_{gg'}\delta_{uu'}\delta_{mm'}$. In this case, average transmit energy of a user signal at any time instance n is given as

$$\mathsf{E}\{x_n^{(g_u)}(x_n^{(g'_{u'})})^*\} = \frac{E_s^{(g)}}{U_g N_c}\delta_{gg'}\delta_{uu'} \tag{5.3}$$

Note that due to the presence of spreading sequences, there will be a correlation among a user's own signals at different time indices, which can be calculated for given spreading sequences.

In order to decode the symbol transmitted at m^{th} interval, we need to observe N_c consecutive received signals. Hence, an equivalent received signal vector $\bar{\mathbf{y}}_m^{(g)} \in \mathsf{C}^{N_c D_g \times 1}$ is obtained by using (2.7) as

$$\begin{aligned} \bar{\mathbf{y}}_m^{(g)} &\triangleq \left[\left[\tilde{\mathbf{y}}_{mN_c}^{(g)}\right]^H \left[\tilde{\mathbf{y}}_{mN_c+1}^{(g)}\right]^H \cdots \left[\tilde{\mathbf{y}}_{(m+1)N_c-1}^{(g)}\right]^H\right]^H \\ &= \sum_{p=0}^{L_{eff}-1} \bar{\mathbf{H}}_{eff,p}^{(g,g)} \bar{\mathbf{x}}_{(m-p)_{N_s}}^{(g)} + \bar{\boldsymbol{\eta}}_m^{(g)}, \end{aligned} \tag{5.4}$$

where, $L_{eff} = \left\lceil \frac{L-1}{N_c} \right\rceil + 1$ is the number of effective MPCs, and $\bar{\mathbf{H}}_{eff,p}^{(g,g)} \in \mathsf{C}^{N_c D_g \times N_c U_g}$

is the augmented effective channel matrix for p^{th} effective MPC which is defined as

$$\bar{\mathbf{H}}_{eff,p}^{(g,g)} \triangleq \begin{bmatrix} \mathbf{H}_{eff,pN_c}^{(g,g)} & \cdots & \mathbf{H}_{eff,(p-1)N_c+1}^{(g,g)} \\ \vdots & \ddots & \vdots \\ \mathbf{H}_{eff,(p+1)N_c-1}^{(g,g)} & \cdots & \bar{\mathbf{H}}_{eff,p}^{(g,g)} \end{bmatrix} \tag{5.5}$$

for $p = 0, 1, \ldots, L_{eff} - 1$. Similar to (5.4), N_c consecutive transmitted signals of users in group g are stacked in a vector $\bar{\mathbf{x}}_m^{(g)} \in \mathsf{C}^{N_c U_g \times 1}$ that is defined as

$$\begin{aligned} \bar{\mathbf{x}}_m^{(g)} &\triangleq \left[\left[\mathbf{x}_{mN_c}^{(g)}\right]^H \left[\mathbf{x}_{mN_c+1}^{(g)}\right]^H \cdots \left[\mathbf{x}_{(m+1)N_c-1}^{(g)}\right]^H \right]^H \\ &= \mathbf{\Gamma}^{(g)} \mathbf{a}_m^{(g)}, \end{aligned} \tag{5.6}$$

where $\mathbf{a}_m^{(g)} \triangleq \left[a_m^{(g_1)}, \ldots, a_m^{(g_{U_g})}\right]^T \in \mathsf{C}^{U_g \times 1}$ is the symbol vector containing the symbols of users in group g at m^{th} signaling interval, and $\mathbf{\Gamma}^{(g)} \in \mathsf{C}^{N_c U_g \times U_g}$ carries the spreading information. By using the relation in (5.2), $\mathbf{\Gamma}^{(g)}$ can be found as

$$\mathbf{\Gamma}^{(g)} = \left[\mathbf{q}^{(g_1)} \otimes \mathbf{e}_1,\ \mathbf{q}^{(g_2)} \otimes \mathbf{e}_2,\ \cdots,\ \mathbf{q}^{(g_{U_g})} \otimes \mathbf{e}_{U_g}\right], \tag{5.7}$$

where $\mathbf{e}_u \in \mathsf{Z}^{U_g \times 1}$ is a vector whose u^{th} entry is one while others are zero. If the equivalent transmitted signal in (5.6) is substituted in (5.4), $\bar{\mathbf{y}}_m^{(g)}$ can be rewritten as

$$\begin{aligned} \bar{\mathbf{y}}_m^{(g)} &= \sum_{p=0}^{L_{eff}-1} \bar{\mathbf{H}}_{eff,p}^{(g,g)} \mathbf{\Gamma}^{(g)} \mathbf{a}_{(m-p)_{N_s}}^{(g)} + \bar{\boldsymbol{\eta}}_m^{(g)} \\ &= \sum_{p=0}^{L_{eff}-1} \mathbf{\Psi}_p^{(g,g)} \mathbf{a}_{(m-p)_{N_s}}^{(g)} + \bar{\boldsymbol{\eta}}_m^{(g)}. \end{aligned} \tag{5.8}$$

where the equivalent channel matrix at p^{th} effective MPC is defined as $\mathbf{\Psi}_p^{(g,g)} = \bar{\mathbf{H}}_{eff,p}^{(g,g)} \mathbf{\Gamma}^{(g)} \in \mathsf{C}^{N_c D_g \times U_g}$. The resultant expression in (5.8) has a similar form with (2.7) since effects of channel vectors and spreading sequences are incorporated in equivalent channel matrices. Therefore, interference cancellation problem for code-domain NOMA is reduced to conventional multiuser detection problem of massive MIMO with SC transmission. In fact, signal model in (5.8) is equivalent to reduced dimensional classical JSDM signal model in (2.7) when $N_c = 1$.

Equalization and multiuser detection can be efficiently performed with the use of IB-DFE method similar to the classical JSDM. Since SC-FDE is considered, normalized DFT of the sequence $\left\{\bar{\mathbf{y}}_m^{(g)}\right\}_{m=0}^{N_s-1}$ should be taken. Noting the circularity in (5.8), one can express the signal after the DFT operation as

$$\bar{\mathbf{y}}_{f,k}^{(g)} = \mathbf{\Lambda}_{f,k}^{(g,g)} \mathbf{a}_{f,k}^{(g)} + \bar{\boldsymbol{\eta}}_{f,k}^{(g)} \tag{5.9}$$

for $k = 0, 1, \ldots, N_s - 1$, where $\left\{\mathbf{a}_{f,k}^{(g)}\right\}_{k=0}^{N_s-1}$ and $\left\{\bar{\boldsymbol{\eta}}_{f,k}^{(g)}\right\}_{k=0}^{N_s-1}$ are normalized DFTs of vector sequences $\left\{\mathbf{a}_m^{(g)}\right\}_{m=0}^{N_s-1}$ and $\left\{\bar{\boldsymbol{\eta}}_m^{(g)}\right\}_{m=0}^{N_s-1}$, respectively. In addition, DFT of equivalent channel matrices are denoted by

$$\mathbf{\Lambda}_{f,k}^{(g,g)} = \sum_{p=0}^{L_{eff}-1} \mathbf{\Psi}_p^{(g,g)} e^{-j\frac{2\pi}{N_s}kp}. \tag{5.10}$$

Similar to the IB-DFE framework introduced in Chapter 4, feedforward and feedback filters of group g for k^{th} frequency bin at i^{th} iteration are denoted by $\mathbf{W}_k^{(g),i} \in \mathsf{C}^{N_c D_g \times U_g}$ and $\mathbf{C}_k^{(g),i} \in \mathsf{C}^{U_g \times U_g}$, respectively. It is important to note that number of rows of feedforward filters are increased by a factor of N_c, compared to the classical JSDM architecture. However, length of the sequences are decreased by a factor of N_c, which directly reduces the number of filters and the size of the DFT operation. Therefore, it can be seen that code-domain NOMA introduces trade-off between the dimension of the feedforward filters and sequence lengths. If we return to the receiver architecture of code-domain NOMA aided JSDM, equalizer output at i^{th} iteration can be expressed as

$$\hat{\mathbf{a}}_{f,k}^{(g),i} = \left[\mathbf{W}_k^{(g),i}\right]^H \bar{\mathbf{y}}_{f,k}^{(g)} - \left[\mathbf{C}_k^{(g),i}\right]^H \tilde{\mathbf{a}}_{f,k}^{(g),i-1}, \tag{5.11}$$

$$\hat{\mathbf{a}}_m^{(g),i} = \frac{1}{\sqrt{N_s}} \sum_{k=0}^{N_s-1} \hat{\mathbf{a}}_{f,k}^{(g),i} e^{j\frac{2\pi}{N_s}km} \tag{5.12}$$

for $k, m = 0, 1, \ldots, N_s - 1$, where time domain estimate of symbols of group g at m^{th} signaling interval for iteration i is denoted by $\hat{\mathbf{a}}_m^{(g),i} \triangleq \left[\hat{a}_m^{(g_1),i}, \ldots, \hat{a}_m^{(g_{U_g}),i}\right]^T$. In (5.11), $\tilde{\mathbf{a}}_{f,k}^{(g),i-1}$ contains soft decisions obtained from the previous iteration.

5.2 Analog Beamforming and Intra-Group Processing for JSDM with Code-Domain NOMA

Equivalent signal model derived for code-domain NOMA aided JSDM differ from the signal model of classical JSDM, even though they have similar forms. The difference between these two signal models is that spreading sequences of code-domain NOMA introduce temporal correlation among the transmitted signals of a user. In this section, we will provide the strategies for analog beamforming and intra group separation by modifying the methods provided for classical JSDM.

5.2.1 Analog Beamforming via GEB

If the optimal analog beamformer is to be computed as in Section (2.3), mutual information between $\bar{\mathbf{y}}_{f,k}^{(g)}$ and $\mathbf{a}_{f,k}^{(g)}$ in (5.9) should be maximized. However, solution of this problem would be dependent on the spreading sequences assigned to users, and it would result in time varying analog beamformers due to the temporal correlation caused by spreading sequences. This solution is not practical and inconsistent with the statistical analog beamforming approach of the JSDM framework. Therefore, we relax the problem by not taking the knowledge of spreading sequences into account. That is, we ignore the temporal correlation of user signals caused by spreading sequences. In that case, the solution would be exactly the same as in the classical JSDM case, which is given in (2.17) that uses the eigenvectors of the generalized eigenvalue problem given in (2.18). However, we need to update the covariance matrices in that problem as

$$\mathbf{R}_{\mathbf{s}}^{(g)} \triangleq \mathsf{E}\Big\{\mathbf{s}_n^{(g)}\big[\mathbf{s}_n^{(g)}\big]^H\Big\} = \frac{E_s^{(g)}}{U_g N_c}\sum_{u=1}^{U_g}\sum_{l=0}^{L-1}\mathbf{R}_l^{(g_u)}, \tag{5.13}$$

$$\mathbf{R}_{\boldsymbol{\eta}}^{(g)} \triangleq \mathsf{E}\Big\{\boldsymbol{\eta}_n^{(g)}\big[\boldsymbol{\eta}_n^{(g)}\big]^H\Big\} = \sum_{g'\neq g}\frac{E_s^{(g')}}{U_{g'} N_c}\sum_{u=1}^{U_{g'}}\sum_{l=0}^{L-1}\mathbf{R}_l^{(g'_u)} + N_0\mathbf{I}_M, \tag{5.14}$$

by considering the modified transmitted signal energy in (5.3). Furthermore, constrained analog beamforming algorithms proposed in Chapter 3 are applicable for

code-domain NOMA aided JSDM, if the GEB is found by using the assumption and modifications above.

5.2.2 Intra-Group Separation via IB-DFE

Intra-group processing for code-domain NOMA aided JSDM is handled with the use of IB-DFE receiver based on (5.9). Frequency-domain augmented channel matrices contain the information of both channels and spreading sequences. Therefore, this approach can be regarded as code-beamspace IB-DFE receiver. The solutions steps are the same as done in Section (4.1). However, we should redefine the covariance matrix of the equivalent signal $\bar{\mathbf{y}}_{f,k}^{(g)}$ in (5.9) as

$$\mathbf{R}_{\bar{\mathbf{y}}_{f,k}^{(g)}} = \mathsf{E}\Big\{\bar{\mathbf{y}}_{f,k}^{(g)}\big[\bar{\mathbf{y}}_{f,k}^{(g)}\big]^H\Big\} = \frac{E_s^{(g)}}{U_g}\mathbf{\Lambda}_{f,k}^{(g,g)}\big[\mathbf{\Lambda}_{f,k}^{(g,g)}\big]^H + \mathbf{R}_{\bar{\boldsymbol{\eta}}_f}^{(g)}. \tag{5.15}$$

It is important to note that statistical knowledge of residual inter-group interference after analog beamformers are taken into account similar to the IB-DFE receiver derived for classical JSDM. However, covariance matrix of the residual interference is dependent on the spreading sequences assigned to the users in other groups. While the covariance matrix of residual interference can be calculated with given spreading sequences, we assume that groups can work asynchronously, and transmitted signals of other users are assumed to be temporally uncorrelated for simplicity. In that case, covariance matrix of interference terms can be expressed as

$$\mathbf{R}_{\bar{\boldsymbol{\eta}}_f}^{(g)} = \mathsf{E}\Big\{\bar{\boldsymbol{\eta}}_{f,k}^{(g)}\big[\bar{\boldsymbol{\eta}}_{f,k}^{(g)}\big]^H\Big\} = \mathbf{I}_{N_c} \otimes \big[\mathbf{S}^{(g)}\big]^H\mathbf{R}_{\boldsymbol{\eta}}^{(g)}\mathbf{S}^{(g)}. \tag{5.16}$$

With the above definitions, feedforward and feedback filters can be computed as done in Section 4.1. However, complexity order of the IB-DFE receiver for code-domain NOMA aided JSDM is different than the IB-DFE receiver of classical JSDM. For code-domain NOMA, matrix inverse operation should be applied to $\mathbf{R}_{\bar{\mathbf{y}}_{f,k}^{(g)}}$ which has a complexity order of $O(N_c^3 D_g^3)$ per frequency bin. Furthermore, inverse of a matrix with size $U_g \times U_g$ is required per frequency bin for the computation of feedback filters as it is seen in (4.4), which would impose a complexity order of $O(U_g^3)$. Therefore,

overall complexity order of this receiver can be given as $O(i_{max}N_s(N_c^3D_g^3 + U_g^3))$. Comparison between complexity orders of IB-DFE receivers of code-domain NOMA aided JSDM and classical JSDM is not trivial since complexity orders depend on various parameters. For example, if the same number of users is considered for both cases, complexity order of code-domain NOMA aided JSDM would be lower. In contrast, if the number of RF chains is kept constant, classical JSDM would require a lower complexity order assuming that the number of users exceed the number of RF chains for code-domain NOMA aided JSDM.

5.3 Performance Analysis

Since an iterative receiver is employed at the receiver, BER is a suitable measure for performance analysis. While BER of the system can be obtained via Monte Carlo simulations, it is possible to find closed-form expressions with some assumptions. Similar to classical JSDM, Bussgang decomposition of the soft output of i^{th} DFE iteration, $\hat{\mathbf{a}}_m^{(g),i}$, can be written as

$$\hat{a}_m^{(g_u),i} = \beta^{(g_u),i} a_m^{(g_u)} + \xi_m^{(g_u),i}, \tag{5.17}$$

for $m = 0, 1, \ldots, N_s - 1$ and $u = 1, 2, \ldots, U_g$, where complex amplitude $\beta^{(g_u),i}$ and power of residual interference $\xi_m^{(g_u),i}$ can be calculated as in Section 4.2. It is observed that complex amplitude and residual interference power do not depend on NOMA signaling index m. Therefore, they can be calculated once at each iteration for the duration of a block. It is important to note that residual interference terms are not Gaussian random variables due to the residual ISI, inter-group interference and soft decisions from previous iterations. However, we can assume that residual interference terms are Gaussian variables with variance $\mathsf{E}\{|\xi_m^{(g_u),i}|^2\}$. Assuming that transmitted symbols are selected from a QAM alphabet $\mathcal{M}$ with cardinality $|\mathcal{M}|$, BER of group g at i^{th} iteration can be expressed as

$$P_b^{(g),i} = \frac{1}{U_g} \sum_{u=1}^{U_g} \alpha \, \mathsf{E}_{\mathbf{H}_l^{(g)}} \left\{ Q\left(\sqrt{\kappa \, SINR_i^{(g_u)}} \right) \right\}, \tag{5.18}$$

where $\alpha = 4\big(1-1/\sqrt{|\mathcal{M}|}\big)/\log_2|\mathcal{M}|$, $\kappa = 3/\big(|\mathcal{M}|-1\big)$, and $Q(.)$ is the Q-function. Furthermore, SINR of user u in group g at the output of i^{th} DFE iteration, $SINR_i^{(g_u)}$, has the same form as in (4.15).

5.4 Numerical Results

We provide BER results for various system parameters. The BS is equipped with $M = 128$ antennas, the block length is $N = 512$, and number of MPCs is set to $L = 32$. Single-antenna users are divided into 4 groups each of them having the same number of users. We consider a stationary angle-delay profile unlike the mobile scenario considered for classical JSDM case where constrained analog beamformers were investigated. However, we provide results for only Group-1 and treat other groups as interfering sources. Table 5.1 shows the angle-delay profile of groups, where active MPCs and associated angular sectors of mean AoAs for each group are given. Mean AoAs of users are selected randomly from given angular sectors. Furthermore, AS $\Delta_l^{(g_u)}$ is set to 3° while $\rho_l^{(g_u)}(\theta)$ is uniform in the AS, and channel gain $\gamma^{(g_u)}$ is set to 1. In addition, user symbols are selected as QPSK symbols, i.e., QAM symbols with cardinality $|\mathcal{M}| = 4$. We use variable number of users for the simulations in this section. Hence, we define a generic SNR as $SNR = E_b/N_0$ since all users have the same bit and symbol energy in all simulations, where the relation between symbol energy of group g and bit energy of any user is expressed as $E_s^{(g)}/U_g = E_b\log_2|\mathcal{M}|$. Finally, we define the MIMO-NOMA user loading in group g with respect to code length N_c and number of RF chains D_g as $\lambda^{(g)} = U_g/(N_cD_g)$.

Fig. 5.1 shows average BER with respect to changing SNR for $U_g = 6$ and $N_c = 4$. We provide the results for GEB and PE-AM, which is the fully connected constant-modulus constrained approximation of GEB proposed in Chapter 3. It is observed that BER curves of final IB-DFE iterations (5 iterations) are close to MFB except for $D_1 = 1$. In other words, MFB is achieved when the MIMO-NOMA loading is below 1, i.e., underloaded case. Moreover, theoretical results obtained with (5.18) are consistent with simulations. Lower BER is obtained with increasing number of RF chains as expected. It is seen that there is no error floor even with $D_1 = 1$ when GEB is utilized. Although PE-AM attains the performance of GEB at low SNR, we observe

Table 5.1: Angle-delay profile of groups for code-domain NOMA aided JSDM

Group	Active MPC (l)	Angular sector for mean AoA $\left(\mu_l^{(g_k)}\right)$
1	0	$[-1°, 1°]$
	5	$[12°, 14°]$
	11	$[31°, 33°]$
2	3	$[40°, 42°]$
	9	$[20°, 22°]$
3	8	$[-11°, -9°]$
	17	$[-21°, -19°]$
4	29	$[-41°, -39°]$

error floor at high SNR for small number of RF chains, even for MFB. The reason is that interference suppression capability of PE-AM is dependent on the accuracy of approximation which is related to the number of RF chains. Nevertheless, we can conclude that the number of users U_g can exceed the number of RF chains D_g, and theoretical bounds can still be achieved with the help of proposed code-beamspace IB-DFE receiver for both unconstrained and constrained analog beamformers.

In Fig. 5.2, average BER vs. SNR plots for $N_c = 8$ and $D_1 = 4$ are provided with LMMSE (first iteration of IB-DFE), IB-DFE and MMSE-SIC receiver for SC-FDE in [68]. We observe that BER performance degrades reasonably with increasing MIMO-NOMA loading, and that IB-DFE outperforms MMSE-SIC especially at high MIMO-NOMA loading (e.g., $\lambda^{(1)} = 1.25, 1.375, 1.5$) since MMSE-SIC receiver suffers from error propagation. Note that MMSE-SIC receiver requires higher computational complexity than IB-DFE for overloaded cases since MMSE-SIC receiver requires construction of MMSE filters and DFT/IDFT operations at each SIC step, whereas IB-DFE converges in a few iterations. On the other hand, LMMSE receiver fails for overloaded cases, i.e., $\lambda^{(1)} > 1$. These results show the necessity of iterative receiver processing for overloaded systems. In addition, proposed code-beamspace IB-DFE receiver is shown to be an efficient iterative receiver for overloaded SC massive MIMO systems in terms of both BER and computational complexity.

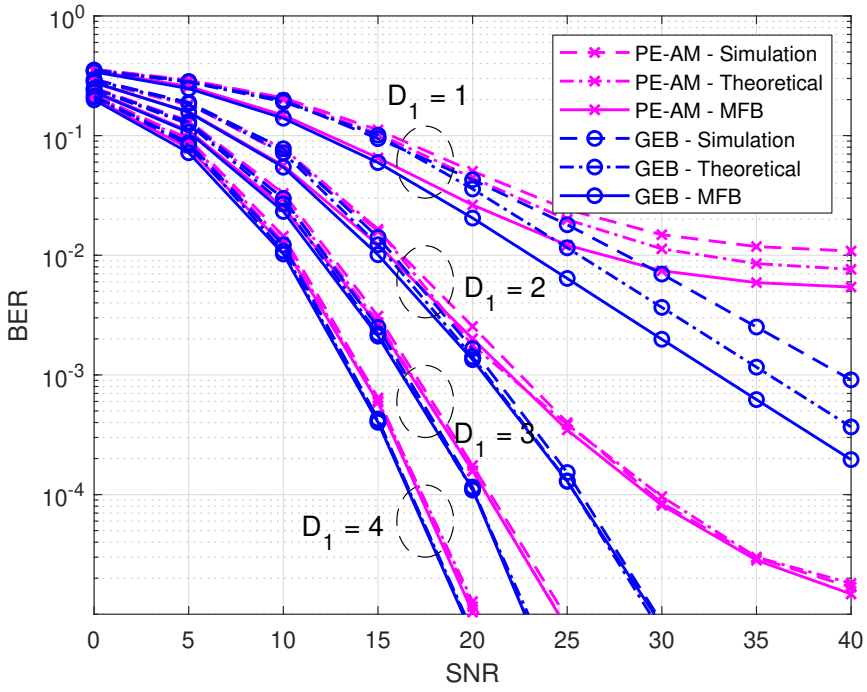

Figure 5.1: Average BER vs. SNR for $U_g = 6$ and $N_c = 4$

Fig. 5.3 illustrates average BER vs. MIMO-NOMA loading at $SNR = 20$ dB. In this figure, the case with $N_c = 1$ is equivalent to classical JSDM scenario. It is observed that BER performance improves with increasing N_c and D_1. Code-domain NOMA aided JSDM clearly outperforms classical JSDM, especially with a reasonable number of RF chains. The performance gap between these two schemes widens with increasing number of RF chains, and with increasing code length. However, we observe that poor BER performance is achieved for all settings when the MIMO-NOMA loading $\lambda^{(1)}$ is increased to 2, whereas significant improvement is observed with code-domain NOMA when MIMO-NOMA loading is around 1. Furthermore, code-domain NOMA provides flexibility since number of users served at the same resources is dependent on N_c. For example, when $D_1 = 3$ and $N_c = 1$, number of users can be $U_g \in \{1, 2 \ldots, 6\}$ for $\lambda(g) \leq 2$. However, when $D_1 = 3$ and $N_c = 4$, number of users can be $U_g \in \{1, 2 \ldots, 24\}$ for the same MIMO-NOMA loading range. Therefore, code-domain NOMA aided JSDM could offer more flexible number of user selection for the same number of RF chains, compared to classical JSDM.

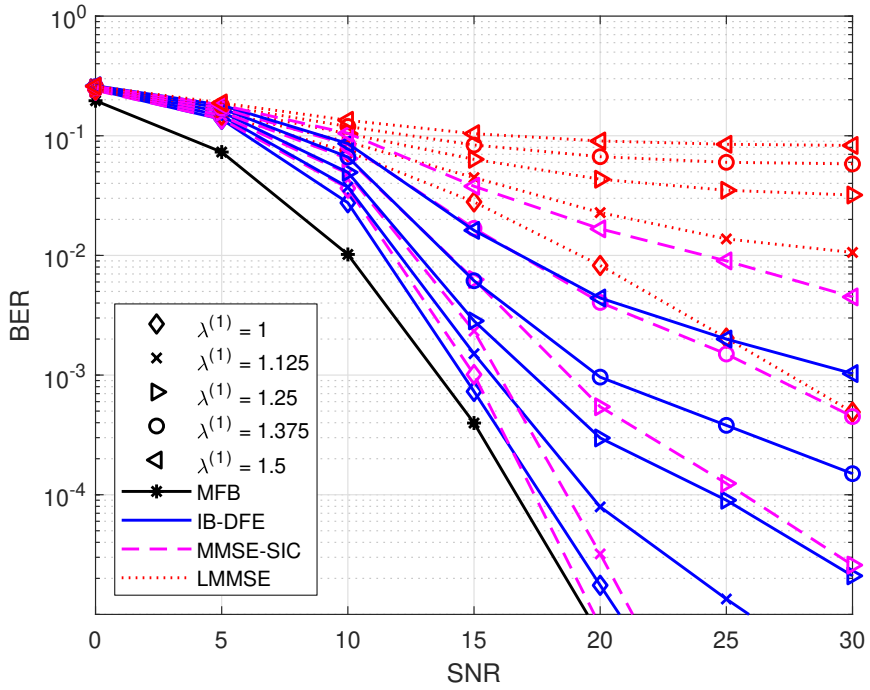

Figure 5.2: Average BER vs. SNR for $N_c = 8$ and $D_1 = 4$

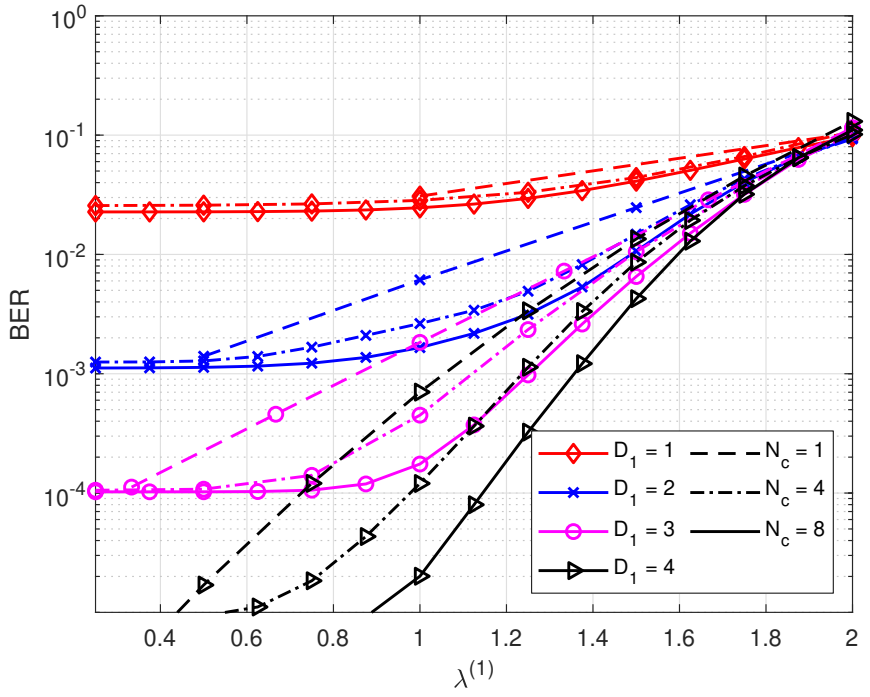

Figure 5.3: Average BER vs. MIMO-NOMA loading at $SNR = 20$ dB

CHAPTER 6

CONCLUSION

6.1 Conclusions

In this thesis, we proposed an interference-aware two-stage beamforming framework, specifically for mm-wave JSDM with SC transmission, where interference is considered in both analog and digital beamforming stages, and subsequently we integrated code-domain NOMA to the proposed framework. In the first part of the thesis, near-optimal slowly varying statistical analog beamformer (i.e., GEB) is designed where inter-group interference suppression is imposed at this stage. GEB is approximated with both fully and partially connected arrays by considering constant-modulus constraint. Furthermore, an algorithm to find the optimal connection structure is proposed for dynamic subarray design. Low-complexity alternating minimization algorithms are employed for obtaining constrained analog beamformers. Superiority of proposed beamformers is shown by using comprehensive analysis tools. It is observed that PE-AM attains the performance of unconstrained GEB with moderate interference strength. Furthermore, this algorithm outperforms commonly used DFT beamformer and phase of GEB. On the other hand, dynamic subarray design performs close to fully connected ones and outperforms fixed subarrays. Moreover, MMSE criterion based IB-DFE type digital beamformers improve the performance of constrained analog beamformers as they take residual interference into account.

In the second part of the thesis, we showed that code-domain NOMA and mm-wave massive MIMO can be efficiently combined for SC transmission with the use of introduced wideband-beamspace signal model. Then, a code-beamspace IB-DFE receiver is proposed for joint equalization and multiuser detection by using the de-

veloped model. Simulation results showed that theoretical bounds can be achieved with the proposed code-beamspace IB-DFE receiver for the underloaded case, while a reasonable degradation is observed for highly loaded case, where IB-DFE outperformed LMMSE and MMSE-SIC receivers. Furthermore, superiority of code-domain NOMA aided massive MIMO over classical massive MIMO is verified. It is clearly shown that code-domain NOMA is beneficial when integrated to mm-wave massive MIMO with limited RF chains and closely spaced users.

6.2 Future Research Directions

Methods that are developed in this thesis has significant implications for physical layer of next generation communication systems. Firstly, interference-awareness is a critical feature for various communication systems. For instance, inter-cell interference can be detrimental, especially for the users on the cell-edge. Proposed interference-aware design can deal with any type of interference with known statistics. Moreover, there are recent studies that consider joint communications and sensing, where sensors (e.g., radars) may cause increase in interference for the communication system. Similarly, our framework can be adapted to such a system in order to provide reliable communication while the interference caused by the sensing unit is suppressed with the interference-aware beamformers. In addition, we have studied a mm-wave massive MIMO system with spatial-narrowband channels. For mm-wave communications, high data rates are achieved with the available vast spectrum at mm-wave bands where spatial-wideband effect is observed, if the bandwidth is excessively wide. Consequently, adaptation of the proposed design to a spatial-wideband scenario could be another research direction.

On the other hand, massive connectivity became a high priority requirement for the communication systems due to the increase in number of smart devices connected to the internet. Proposed integration of code-domain NOMA and mm-wave massive MIMO with user-grouping could be a possible solution to satisfy this requirement. In this work, we have not studied spreading sequence design and we have utilized random sequences. A potential research direction could be to develop more efficient spreading sequences by considering the developed wideband-beamspace code-

domain signal model. Significant improvements could be achieved with optimized spreading sequences, especially for the highly correlated massive MIMO channels. Furthermore, we did not consider the effect of code-domain NOMA while constructing the beamformers. However, performance gains could be achieved by designing beamformers that take spreading sequences into account. Another future research direction could be the joint optimization of beamformers and code-domain NOMA sequences.

With the increasing demand for massive connectivity and high data rates, it is not possible to avoid interference in communication systems. Thus, the design of interference-aware beamformers with practical constraints and the development of architectures that support massive connectivity will play an important role for the communications area in the upcoming years, and this thesis provides a general framework for these goals while offering promising future research directions.

REFERENCES

[1] E. G. Larsson, O. Edfors, F. Tufvesson, and T. L. Marzetta, "Massive MIMO for next generation wireless systems," *IEEE Commun. Mag.*, vol. 52, no. 2, pp. 186–195, 2014.

[2] L. Lu, G. Y. Li, A. L. Swindlehurst, A. Ashikhmin, and R. Zhang, "An overview of massive MIMO: Benefits and challenges," *IEEE J. Sel. Topics Signal Process.*, vol. 8, no. 5, pp. 742–758, 2014.

[3] R. W. Heath, N. Gonzalez-Prelcic, S. Rangan, W. Roh, and A. M. Sayeed, "An overview of signal processing techniques for millimeter wave MIMO systems," *IEEE J. Sel. Topics Signal Process.*, vol. 10, no. 3, pp. 436–453, 2016.

[4] O. E. Ayach, S. Rajagopal, S. Abu-Surra, Z. Pi, and R. W. Heath, "Spatially sparse precoding in millimeter wave MIMO systems," *IEEE Trans. Wireless Commun.*, vol. 13, no. 3, pp. 1499–1513, 2014.

[5] C. Rusu, R. Mèndez-Rial, N. González-Prelcic, and R. W. Heath, "Low complexity hybrid precoding strategies for millimeter wave communication systems," *IEEE Trans. Wireless Commun.*, vol. 15, no. 12, pp. 8380–8393, 2016.

[6] X. Yu, J. Shen, J. Zhang, and K. B. Letaief, "Alternating minimization algorithms for hybrid precoding in millimeter wave MIMO systems," *IEEE J. Sel. Topics Signal Process.*, vol. 10, no. 3, pp. 485–500, 2016.

[7] F. Sohrabi and W. Yu, "Hybrid digital and analog beamforming design for large-scale antenna arrays," *IEEE J. Sel. Topics Signal Process.*, vol. 10, no. 3, pp. 501–513, 2016.

[8] I. Ahmed, H. Khammari, A. Shahid, A. Musa, K. S. Kim, E. De Poorter, and I. Moerman, "A survey on hybrid beamforming techniques in 5G: Architecture and system model perspectives," *IEEE Commun. Surveys Tuts.*, vol. 20, no. 4, pp. 3060–3097, 2018.

[9] A. Adhikary, J. Nam, J. Ahn, and G. Caire, "Joint spatial division and multiplexing—The large-scale array regime," *IEEE Trans. Inf. Theory*, vol. 59, no. 10, pp. 6441–6463, 2013.

[10] A. Adhikary, E. Al Safadi, M. K. Samimi, R. Wang, G. Caire, T. S. Rappaport, and A. F. Molisch, "Joint spatial division and multiplexing for mm-Wave channels," *IEEE J. Sel. Areas Commun.*, vol. 32, no. 6, pp. 1239–1255, June 2014.

[11] N. J. Myers and R. W. Heath, "Message passing-based joint CFO and channel estimation in mmWave systems with one-bit ADCs," *IEEE Trans. Wireless Commun.*, vol. 18, no. 6, pp. 3064–3077, 2019.

[12] S. Wang, Y. Li, and J. Wang, "Multiuser detection in massive MIMO with quantized phase-only measurements," in *Proc. IEEE Int. Conf. Commun.* IEEE, 2015, pp. 4576–4581.

[13] H. G. Myung, J. Lim, and D. J. Goodman, "Peak-to-average power ratio of single carrier FDMA signals with pulse shaping," in *Proc. IEEE 17th Int. Symp. Pers., Indoor and Mobile Radio Commun.*, 2006, pp. 1–5.

[14] F. Pancaldi, G. M. Vitetta, R. Kalbasi, N. Al-Dhahir, M. Uysal, and H. Mheidat, "Single-carrier frequency domain equalization," *IEEE Signal Process. Mag.*, vol. 25, no. 5, pp. 37–56, 2008.

[15] S. Buzzi, C. D'Andrea, T. Foggi, A. Ugolini, and G. Colavolpe, "Single-carrier modulation versus OFDM for millimeter-wave wireless MIMO," *IEEE Trans. Commun.*, vol. 66, no. 3, pp. 1335–1348, 2017.

[16] A. Pitarokoilis, S. K. Mohammed, and E. G. Larsson, "On the optimality of single-carrier transmission in large-scale antenna systems," *IEEE Wireless Commun. Lett.*, vol. 1, no. 4, pp. 276–279, 2012.

[17] X. Song, S. Haghighatshoar, and G. Caire, "Efficient beam alignment for millimeter wave single-carrier systems with hybrid MIMO transceivers," *IEEE Trans. Wireless Commun.*, vol. 18, no. 3, pp. 1518–1533, 2019.

[18] G. M. Guvensen and E. Ayanoglu, "A generalized framework on beamformer design and CSI acquisition for single-carrier massive MIMO systems in millimeter wave channels," in *Proc. IEEE Globecom Workshops*, 2016, pp. 1–7.

[19] A. Kurt and G. M. Guvensen, "An efficient hybrid beamforming and channel acquisition for wideband mm-Wave massive MIMO channels," in *Proc. IEEE Int. Conf. Commun.*, 2019, pp. 1–7.

[20] L. Dai, B. Wang, Y. Yuan, S. Han, C. I, and Z. Wang, "Non-orthogonal multiple access for 5G: Solutions, challenges, opportunities, and future research trends," *IEEE Commun. Mag.*, vol. 53, no. 9, pp. 74–81, Sep. 2015.

[21] Z. Ding, X. Lei, G. K. Karagiannidis, R. Schober, J. Yuan, and V. K. Bhargava, "A survey on non-orthogonal multiple access for 5G networks: Research challenges and future trends," *IEEE J. Sel. Areas Commun.*, vol. 35, no. 10, pp. 2181–2195, 2017.

[22] L. Dai, B. Wang, Z. Ding, Z. Wang, S. Chen, and L. Hanzo, "A survey of non-orthogonal multiple access for 5G," *IEEE Commun. Surveys Tuts.*, vol. 20, no. 3, pp. 2294–2323, 2018.

[23] Y. Jeon, C. Song, S. Lee, S. Maeng, J. Jung, and I. Lee, "New beamforming designs for joint spatial division and multiplexing in large-scale MISO multi-user systems," *IEEE Trans. Wireless Commun.*, vol. 16, no. 5, pp. 3029–3041, 2017.

[24] A. Liu and V. Lau, "Phase only RF precoding for massive MIMO systems with limited RF chains," *IEEE Trans. Signal Process.*, vol. 62, no. 17, pp. 4505–4515, 2014.

[25] J. Choi, G. Lee, and B. L. Evans, "Two-stage analog combining in hybrid beamforming systems with low-resolution ADCs," *IEEE Trans. Signal Process.*, vol. 67, no. 9, pp. 2410–2425, 2019.

[26] S. Park, J. Park, A. Yazdan, and R. W. Heath, "Exploiting spatial channel covariance for hybrid precoding in massive MIMO systems," *IEEE Trans. Signal Process.*, vol. 65, no. 14, pp. 3818–3832, 2017.

[27] S. Park, A. Alkhateeb, and R. W. Heath, "Dynamic subarrays for hybrid precoding in wideband mmWave MIMO systems," *IEEE Trans. Wireless Commun.*, vol. 16, no. 5, pp. 2907–2920, 2017.

[28] S. He, C. Qi, Y. Wu, and Y. Huang, "Energy-efficient transceiver design for hybrid sub-array architecture MIMO systems," *IEEE Access*, vol. 4, pp. 9895–9905, 2016.

[29] J. Jin, C. Xiao, W. Chen, and Y. Wu, "Channel-statistics-based hybrid precoding for millimeter-wave MIMO systems with dynamic subarrays," *IEEE Trans. Commun.*, vol. 67, no. 6, pp. 3991–4003, 2019.

[30] F. Yang, J. B. Wang, M. Cheng, J. Y. Wang, M. Lin, and J. Cheng, "A partially dynamic subarrays structure for wideband mmWave MIMO systems," *IEEE Trans. Commun.*, vol. 68, no. 12, pp. 7578–7592, 2020.

[31] H. Li, M. Li, Q. Liu, and A. L. Swindlehurst, "Dynamic hybrid beamforming with low-resolution PSs for wideband mmWave MIMO-OFDM systems," *IEEE J. Sel. Areas Commun.*, vol. 38, no. 9, pp. 2168–2181, 2020.

[32] R. Magueta, D. Castanheira, A. Silva, R. Dinis, and A. Gameiro, "Hybrid multi-user equalizer for massive MIMO millimeter-wave dynamic subconnected architecture," *IEEE Access*, vol. 7, pp. 79 017–79 029, 2019.

[33] J. Jiang, Y. Yuan, and L. Zhen, "Multi-user hybrid precoding for dynamic subarrays in mmWave massive MIMO systems," *IEEE Access*, vol. 7, pp. 101 718–101 728, 2019.

[34] H. Li, M. Li, and Q. Liu, "Hybrid beamforming with dynamic subarrays and low-resolution PSs for mmWave MU-MISO systems," *IEEE Trans. Commun.*, vol. 68, no. 1, pp. 602–614, 2020.

[35] R. Méndez-Rial, C. Rusu, N. González-Prelcic, A. Alkhateeb, and R. W. Heath, "Hybrid MIMO architectures for millimeter wave communications: Phase shifters or switches?" *IEEE Access*, vol. 4, pp. 247–267, 2016.

[36] S. Buzzi, C. I, T. E. Klein, H. V. Poor, C. Yang, and A. Zappone, "A survey of energy-efficient techniques for 5G networks and challenges ahead," *IEEE J. Sel. Areas Commun.*, vol. 34, no. 4, pp. 697–709, 2016.

[37] M. Vaezi, Z. Ding, and H. V. Poor, *Multiple access techniques for 5G wireless networks and beyond*. Springer, 2019.

[38] W. Yuan, N. Wu, Q. Guo, Y. Li, C. Xing, and J. Kuang, "Iterative receivers for downlink MIMO-SCMA: Message passing and distributed cooperative detection," *IEEE Trans. Wireless Commun.*, vol. 17, no. 5, pp. 3444–3458, 2018.

[39] Y. Chi, L. Liu, G. Song, C. Yuen, Y. L. Guan, and Y. Li, "Practical MIMO-NOMA: Low complexity and capacity-approaching solution," *IEEE Trans. Wireless Commun.*, vol. 17, no. 9, pp. 6251–6264, 2018.

[40] L. Liu, Y. Chi, C. Yuen, Y. L. Guan, and Y. Li, "Capacity-achieving MIMO-NOMA: Iterative lmmse detection," *IEEE Trans. Signal Process.*, vol. 67, no. 7, pp. 1758–1773, 2019.

[41] L. Liu, C. Yuen, Y. L. Guan, Y. Li, and C. Huang, "Gaussian message passing for overloaded massive MIMO-NOMA," *IEEE Trans. Wireless Commun.*, vol. 18, no. 1, pp. 210–226, 2018.

[42] O. Maraqa, A. S. Rajasekaran, S. Al-Ahmadi, H. Yanikomeroglu, and S. M. Sait, "A survey of rate-optimal power domain NOMA with enabling technologies of future wireless networks," *IEEE Commun. Surveys Tuts.*, vol. 22, no. 4, pp. 2192–2235, 2020.

[43] B. Wang, L. Dai, Z. Wang, N. Ge, and S. Zhou, "Spectrum and energy-efficient beamspace MIMO-NOMA for millimeter-wave communications using lens antenna array," *IEEE J. Sel. Areas Commun.*, vol. 35, no. 10, pp. 2370–2382, 2017.

[44] Z. Wei, L. Zhao, J. Guo, D. W. K. Ng, and J. Yuan, "Multi-beam NOMA for hybrid mmWave systems," *IEEE Trans. Commun.*, vol. 67, no. 2, pp. 1705–1719, 2018.

[45] L. Zhu, J. Zhang, Z. Xiao, X. Cao, D. O. Wu, and X.-G. Xia, "Millimeter-wave NOMA with user grouping, power allocation and hybrid beamforming," *IEEE Trans. Wireless Commun.*, vol. 18, no. 11, pp. 5065–5079, 2019.

[46] M. T. P. Le, L. Sanguinetti, E. Bjornson, and M.-G. Di Benedetto, "Code-domain NOMA in massive MIMO: When is it needed?" *IEEE Trans. Veh. Technol.*, pp. 1–1, 2021.

[47] C. Xu, Y. Hu, C. Liang, J. Ma, and L. Ping, "Massive MIMO, non-orthogonal multiple access and interleave division multiple access," *IEEE Access*, vol. 5, pp. 14 728–14 748, 2017.

[48] T. Wang, L. Shi, K. Cai, L. Tian, and S. Zhang, "Non-coherent NOMA with massive MIMO," *IEEE Wireless Comm. Lett.*, 2019.

[49] S. Tang, Z. Ma, M. Xiao, and L. Hao, "Performance analysis for mmwave MIMO-SCMA systems using lens antenna array," in *Proc. IEEE Int. Conf. Commun. Workshops*, May 2019, pp. 1–5.

[50] F. C. Ribeiro, J. Guerreiro, R. Dinis, F. Cercas, and D. N. K. Jayakody, "Multi-user detection for the downlink of NOMA systems with multi-antenna schemes and power-efficient amplifiers," *Phys. Commun.*, vol. 33, pp. 199–205, 2019.

[51] M. Bayraktar and G. M. Guvensen, "A general framework and novel transceiver architecture based on hybrid beamforming for NOMA in massive MIMO channels," in *Proc. IEEE Int. Conf. Commun. Workshops*, 2020, pp. 1–7.

[52] G. M. Guvensen and A. O. Yilmaz, "A general framework for optimum iterative blockwise equalization of single carrier MIMO systems and asymptotic performance analysis," *IEEE Trans. Commun.*, vol. 61, no. 2, pp. 609–619, 2013.

[53] M. Bayraktar and G. M. Guvensen, "An efficient interference-aware constrained massive MIMO beamforming for mm-Wave JSDM," *IEEE Access*, 2021.

[54] J. Nam, A. Adhikary, J. Ahn, and G. Caire, "Joint spatial division and multiplexing: Opportunistic beamforming, user grouping and simplified downlink scheduling," *IEEE J. Sel. Topics Signal Process.*, vol. 8, no. 5, pp. 876–890, 2014.

[55] J. Chen and D. Gesbert, "Joint user grouping and beamforming for low complexity massive MIMO systems," in *Proc. IEEE 17th Int. Workshop on Signal Process. Advances in Wireless Commun. (SPAWC)*, 2016, pp. 1–6.

[56] S. Haghighatshoar, M. B. Khalilsarai, and G. Caire, "Multi-band covariance interpolation with applications in massive MIMO," in *Proc. IEEE Int. Symp. Inf. Theory (ISIT)*, 2018, pp. 386–390.

[57] H. Xie, F. Gao, S. Jin, J. Fang, and Y. C. Liang, "Channel estimation for TDD/FDD massive MIMO systems with channel covariance computing," *IEEE Trans. Wireless Commun.*, vol. 17, no. 6, pp. 4206–4218, 2018.

[58] M. Barzegar Khalilsarai, S. Haghighatshoar, X. Yi, and G. Caire, "FDD massive MIMO via UL/DL channel covariance extrapolation and active channel sparsification," *IEEE Trans. Wireless Commun.*, vol. 18, no. 1, pp. 121–135, 2019.

[59] A. O. Kalayci and G. M. Guvensen, "An efficient spatial channel covariance estimation via joint angle-delay power profile in hybrid massive MIMO systems," in *Proc. IEEE Int. Conf. Commun. Workshops*, 2020, pp. 1–7.

[60] B. Wang, F. Gao, S. Jin, H. Lin, and G. Y. Li, "Spatial- and frequency-wideband effects in millimeter-wave massive MIMO systems," *IEEE Trans. Signal Process.*, vol. 66, no. 13, pp. 3393–3406, 2018.

[61] Y. Chen, Y. Xiong, D. Chen, T. Jiang, S. X. Ng, and L. Hanzo, "Hybrid precoding for wideband millimeter wave MIMO systems in the face of beam squint," *IEEE Trans. Wireless Commun.*, vol. 20, no. 3, pp. 1847–1860, 2021.

[62] Y. Chen, D. Chen, T. Jiang, and L. Hanzo, "Channel-covariance and angle-of-departure aided hybrid precoding for wideband multiuser millimeter wave MIMO systems," *IEEE Trans. Commun.*, vol. 67, no. 12, pp. 8315–8328, 2019.

[63] G. M. Guvensen, C. Candan, S. Koc, and U. Orguner, "On generalized eigenvector space for target detection in reduced dimensions," in *Proc. IEEE Radar Conf.*, 2015, pp. 1316–1321.

[64] P. H. Schönemann, "A generalized solution of the orthogonal procrustes problem," *Psychometrika*, vol. 31, no. 1, pp. 1–10, 1966.

[65] D. Calvetti, L. Reichel, and D. C. Sorensen, "An implicitly restarted Lanczos method for large symmetric eigenvalue problems," *Electron. Trans. Numer. Anal.*, vol. 2, no. 1, p. 21, 1994.

[66] O. T. Demir and E. Bjornson, "The bussgang decomposition of nonlinear systems: Basic theory and MIMO extensions [lecture notes]," *IEEE Signal Process. Mag.*, vol. 38, no. 1, pp. 131–136, 2021.

[67] Z. Yuan, G. Yu, W. Li, Y. Yuan, X. Wang, and J. Xu, "Multi-user shared access for internet of things," in *Proc. IEEE 83rd Veh. Technol. Conf. (VTC Spring)*, 2016, pp. 1–5.

[68] Z. Pan, G. Wu, S. Fang, and D. Lin, "Practical soft-SIC detection for MIMO SC-FDMA system with co-channel interference," in *Proc. Int. Conf. Wireless Commun. Signal Process.*, 2010, pp. 1–5.

[69] S. Noh, M. D. Zoltowski, Y. Sung, and D. J. Love, "Pilot beam pattern design for channel estimation in massive MIMO systems," *IEEE J. Sel. Topics Signal Process.*, vol. 8, no. 5, pp. 787–801, 2014.

Appendix A

COVARIANCE MATRICES IN REDUCED DIMENSION

Covariance matrix of $\tilde{\mathbf{s}}_{f,k}^{(g)}$ is expressed as

$$\begin{aligned}
\mathbf{R}_{\tilde{\mathbf{s}}_f}^{(g)} &= \mathsf{E}\left\{\tilde{\mathbf{s}}_{f,k}^{(g)}\left[\tilde{\mathbf{s}}_{f,k}^{(g)}\right]^H\right\} \\
&= \mathsf{E}\left\{\frac{1}{\sqrt{N}}\sum_{n=0}^{N-1}\tilde{\mathbf{s}}_n^{(g)}e^{-j\frac{2\pi}{N}kn}\sum_{n'=0}^{N-1}\frac{1}{\sqrt{N}}\left[\tilde{\mathbf{s}}_{n'}^{(g)}\right]^H e^{j\frac{2\pi}{N}kn'}\right\} \\
&= \frac{1}{N}\sum_{n=0}^{N-1}\sum_{n'=0}^{N-1}\mathsf{E}\left\{\tilde{\mathbf{s}}_n^{(g)}\left[\tilde{\mathbf{s}}_{n'}^{(g)}\right]^H\right\}e^{j\frac{2\pi}{N}k(n'-n)} \\
&= \frac{1}{N}\sum_{n=0}^{N-1}\sum_{n'=0}^{N-1}\left[\mathbf{S}^{(g)}\right]^H\mathsf{E}\left\{\mathbf{s}_n^{(g)}\left[\mathbf{s}_{n'}^{(g)}\right]^H\right\}\mathbf{S}^{(g)}e^{j\frac{2\pi}{N}k(n'-n)} \\
&= \frac{1}{N}\sum_{n=0}^{N-1}\sum_{n'=0}^{N-1}\left[\mathbf{S}^{(g)}\right]^H\mathbf{R}_{\mathbf{s}}^{(g)}\delta_{nn'}\mathbf{S}^{(g)}e^{j\frac{2\pi}{N}k(n'-n)} \\
&= \frac{1}{N}\sum_{n=0}^{N-1}\left[\mathbf{S}^{(g)}\right]^H\mathbf{R}_{\mathbf{s}}^{(g)}\mathbf{S}^{(g)} \\
&= \left[\mathbf{S}^{(g)}\right]^H\mathbf{R}_{\mathbf{s}}^{(g)}\mathbf{S}^{(g)},
\end{aligned} \tag{A.1}$$

where $\mathbf{R}_{\mathbf{s}}^{(g)}$ is the covariance matrix of intra-group signals of group g whose expression is given in (2.15). Similarly, covariance matrix of $\boldsymbol{\eta}_{f,k}^{(g)}$ can be expressed as $\mathbf{R}_{\tilde{\boldsymbol{\eta}}_f}^{(g)} = \left[\mathbf{S}^{(g)}\right]^H\mathbf{R}_{\boldsymbol{\eta}}^{(g)}\mathbf{S}^{(g)}$ where expression for $\mathbf{R}_{\boldsymbol{\eta}}^{(g)}$, which is the covariance matrix of sum of inter-group signals and noise, is given in (2.16). It is important to note that these covariance matrices are independent of frequency bin.

Appendix B

PROOF OF LEMMA 1

If there are multiple antennas at user u in group g, $\mathbf{h}_l^{(g_u)}$ in (2.3) is replaced with $\mathbf{H}_l^{(g_u)} \in \mathsf{C}^{M \times M_t^{(g_u)}}$ where $M_t^{(g_u)}$ is the number of antennas at the user side. Then, intra-group signals of group g in (2.6) can be rewritten as

$$\mathbf{s}_n^{(g)} = \sum_{u=1}^{U_g} \sum_{l=0}^{L-1} \mathbf{H}_l^{(g_u)} \mathbf{x}_{(n-l)_N}^{(g_u)}, \tag{B.1}$$

where $\mathbf{x}_n^{(g_u)} \in \mathsf{C}^{M_t^{(g_u)} \times 1}$ is the precoded data vector of user u in group g with transmit energy $\mathsf{E}\{||\mathbf{x}_n^{(g_u)}||^2\} = \frac{E_s^{(g)}}{U_g}$. Precoded data vector is defined as $\mathbf{x}_n^{(g_u)} \triangleq \mathbf{V}^{(g_u)} \mathbf{d}_n^{(g_u)}$ where $\mathbf{V}^{(g_u)} \in \mathsf{C}^{M_t^{(g_u)} \times d_t^{(g_u)}}$ is the precoding matrix and $\mathbf{d}_n^{(g_u)} \in \mathsf{C}^{d_t^{(g_u)} \times 1}$ is the data vector with $d_t^{(g_u)}$ streams. Transmitted symbols are assumed to be uncorrelated among streams and time indices which can be expressed as $\mathsf{E}\{\mathbf{d}_n^{(g_u)} [\mathbf{d}_n^{(g_u)}]^H\} = \mathbf{I}_{d_t^{(g_u)}} \delta_{nn'}$.

Assuming that channels obey Kronecker channel model, which is a practical model for spatially correlated MIMO [69], the channel matrices of users can be written as

$$\mathbf{H}_l^{(g_u)} = [\mathbf{R}_l^{(g_u)}]^{1/2} \bar{\mathbf{H}}_l^{(g_u)} \left([\mathbf{\Psi}_l^{(g_u)}]^{1/2} \right)^T, \tag{B.2}$$

where entries of $\bar{\mathbf{H}}_l^{(g_u)} \in \mathsf{C}^{M \times M_t^{(g_u)}}$ are independent zero-mean circularly symmetric complex Gaussian random variables with unit variance. In (B.2), $\mathbf{R}_l^{(g_u)}$ defined in (2.4) expresses the spatial correlation among the receive antenna elements depending on AoAs of MPCs at the BS whereas $\mathbf{\Psi}_l^{(g_u)} \in \mathsf{C}^{M_t^{(g_u)} \times M_t^{(g_u)}}$ shows the spatial correlation among transmit antenna elements depending on angle of departures (AoDs) at the user side. The matrix $\mathbf{\Psi}_l^{(g_u)}$ can be expressed in a similar form as $\mathbf{R}_l^{(g_u)}$. Let $\mathbf{H}_l^{(g_u)}$ matrices be independent for different MPC clusters as in single-antenna user

case. Then, channel statistics for a given MPC can be written as

$$\mathsf{E}\Big\{\mathrm{vec}\Big(\mathbf{H}_l^{(g_u)}\Big)\mathrm{vec}\Big(\mathbf{H}_l^{(g_u)}\Big)^H\Big\} = \mathbf{\Psi}_l^{(g_u)} \otimes \mathbf{R}_l^{(g_u)}, \tag{B.3}$$

which can be obtained after some manipulations starting from (B.2). Moreover, the channel gain can be written as

$$\sum_{l=0}^{L-1} \mathrm{Tr}\Big\{\mathsf{E}\Big\{\mathbf{H}_l^{(g_u)}\big[\mathbf{H}_l^{(g_u)}\big]^H\Big\}\Big\} = \sum_{l=0}^{L-1} \mathrm{Tr}\Big\{\mathbf{\Psi}_l^{(g_u)}\Big\}\mathrm{Tr}\Big\{\mathbf{R}_l^{(g_u)}\Big\} = \gamma^{(g_u)}, \tag{B.4}$$

where $\mathrm{Tr}\big\{\mathbf{\Psi}_l^{(g_u)}\big\}$ is set to 1. Considering the definitions above, covariance matrix of intra-group signals of group g can be calculated as

$$\begin{aligned}\mathbf{R}_{\mathbf{s}}^{(g)} &= \mathsf{E}\Big\{\mathbf{s}_n^{(g)}\big[\mathbf{s}_n^{(g)}\big]^H\Big\} \\ &= \sum_{u=1}^{U_g}\sum_{l=0}^{L-1}\mathsf{E}\Big\{\mathbf{H}_l^{(g_u)}\mathbf{x}_n^{(g)}\big[\mathbf{x}_n^{(g)}\big]^H\big[\mathbf{H}_l^{(g_u)}\big]^H\Big\}.\end{aligned} \tag{B.5}$$

Let the expectation inside the summation in (B.5) is denoted by $\mathbf{\Phi}_l^{(g_u)}$. Then, entry of $\mathbf{\Phi}_l^{(g_u)}$ at i^{th} row and j^{th} column can be expressed as

$$\begin{aligned}\big[\mathbf{\Phi}_l^{(g_u)}\big]_{(i,j)} &= \mathsf{E}\Big\{\big[\mathbf{H}_l^{(g_u)}\big]_{(i,:)}\mathbf{x}_n^{(g)}\big[\mathbf{x}_n^{(g)}\big]^H\big[\mathbf{H}_l^{(g_u)}\big]_{(j,:)}^H\Big\} \\ &= \mathsf{E}\Big\{\mathrm{Tr}\Big\{\mathbf{x}_n^{(g)}\big[\mathbf{x}_n^{(g)}\big]^H\big[\mathbf{H}_l^{(g_u)}\big]_{(j,:)}^H\big[\mathbf{H}_l^{(g_u)}\big]_{(i,:)}\Big\}\Big\} \\ &= \mathrm{Tr}\Big\{\mathsf{E}\Big\{\mathbf{x}_n^{(g)}\big[\mathbf{x}_n^{(g)}\big]^H\Big\}\mathsf{E}\Big\{\big[\mathbf{H}_l^{(g_u)}\big]_{(j,:)}^H\big[\mathbf{H}_l^{(g_u)}\big]_{(i,:)}\Big\}\Big\} \\ &= \mathrm{Tr}\Big\{\mathbf{V}^{(g_u)}\big[\mathbf{V}^{(g_u)}\big]^H\mathbf{\Psi}_l^{(g_u)}\big[\mathbf{R}_l^{(g_u)}\big]_{(i,j)}\Big\} \\ &= \mathrm{Tr}\Big\{\big[\mathbf{V}^{(g_u)}\big]^H\mathbf{\Psi}_l^{(g_u)}\mathbf{V}^{(g_u)}\Big\}\big[\mathbf{R}_l^{(g_u)}\big]_{(i,j)} \\ &= c^{(g_u)}\big[\mathbf{R}_l^{(g_u)}\big]_{(i,j)},\end{aligned} \tag{B.6}$$

where the constant is $c^{(g_u)} = \mathrm{Tr}\big\{\big[\mathbf{V}^{(g_u)}\big]^H\mathbf{\Psi}_l^{(g_u)}\mathbf{V}^{(g_u)}\big\}$. With the result above, co-

variance matrix of intra-group signals can be rewritten as

$$\mathbf{R}_{\mathbf{s}}^{(g)} = \sum_{u=1}^{U_g} \sum_{l=0}^{L-1} \mathbf{\Phi}_l^{(g_u)} = \sum_{u=1}^{U_g} \sum_{l=0}^{L-1} c^{(g_u)} \mathbf{R}_l^{(g_u)}, \tag{B.7}$$

which has a similar form as in (2.15). The only difference is that the constant $c^{(g_u)}$ is dependent on the precoding and slowly varying AoDs at the user side. Furthermore, covariance matrix of sum of inter-group signals and noise $\mathbf{R}_{\boldsymbol{\eta}}^{(g)}$ can be obtained in a similar form as in (2.16) with the usage of constant $c^{(g_u)}$. It is feasible to assume that statistical precoding is utilized at the user side. In this case, the constant $c^{(g_u)}$ becomes a slowly varying parameter which can easily be learned at the BS. Hence, same statistical analog beamforming method proposed in Section 2.3 can be used for the multiantenna user case.

Moreover, proposed digital beamforming and channel estimation scheme would remain the same with the modified effective channel definition which is expressed as

$$\mathbf{H}_{eff,l}^{(g,g_u)} = \left[\mathbf{S}^{(g)}\right]^H \mathbf{H}_l^{(g_u)} \mathbf{V}^{(g_u)}, \tag{B.8}$$

where effects of both the beamformer at the BS and the precoder at the user side are considered. Note that the BS does not require the knowledge of the precoder at the user side during channel estimation phase since effective channels in (B.8) are estimated directly.

Appendix C

EXPECTED SINR IN REDUCED DIMENSION

In reduced dimension, it is possible to find an expected SINR value for each group. Intra-group signal power can be divided by power of sum of inter-group interference and noise in reduced dimension by using (2.7). With this method, expected SINR of group g can be expressed as

$$\begin{aligned}\overline{SINR}^{(g)} &= \frac{\mathsf{E}\left\{\left\|\tilde{\mathbf{s}}_{f,k}^{(g)}\right\|^2\right\}}{\mathsf{E}\left\{\left\|\tilde{\boldsymbol{\eta}}_{f,k}^{(g)}\right\|^2\right\}} = \frac{\mathrm{Tr}\left\{\mathsf{E}\left\{\tilde{\mathbf{s}}_{f,k}^{(g)}\left[\tilde{\mathbf{s}}_{f,k}^{(g)}\right]^H\right\}\right\}}{\mathrm{Tr}\left\{\mathsf{E}\left\{\tilde{\boldsymbol{\eta}}_{f,k}^{(g)}\left[\tilde{\boldsymbol{\eta}}_{f,k}^{(g)}\right]^H\right\}\right\}} \\ &= \frac{\mathrm{Tr}\left\{\mathbf{R}_{\tilde{\mathbf{s}}_f}^{(g)}\right\}}{\mathrm{Tr}\left\{\mathbf{R}_{\tilde{\boldsymbol{\eta}}_f}^{(g)}\right\}} = \frac{\mathrm{Tr}\left\{\left[\mathbf{S}^{(g)}\right]^H\mathbf{R}_{\mathbf{s}}^{(g)}\mathbf{S}^{(g)}\right\}}{\mathrm{Tr}\left\{\left[\mathbf{S}^{(g)}\right]^H\mathbf{R}_{\eta}^{(g)}\mathbf{S}^{(g)}\right\}},\end{aligned} \tag{C.1}$$

where expressions for covariance matrices $\mathbf{R}_{\tilde{\mathbf{s}}_f}^{(g)}$ and $\mathbf{R}_{\tilde{\boldsymbol{\eta}}_f}^{(g)}$ are taken from Appendix A.

Appendix D

ASYMPTOTIC SINR ANALYSIS

Assuming the perfect knowledge of intra-group user symbols, correlation matrices are taken as $\mathbf{P}_1^{(g)} = \mathbf{P}_2^{(g)} = \frac{E_s^{(g)}}{U_g}\mathbf{I}_{U_g}$. In this case, $\mathbf{A}_k^{(g)} = -\left[\mathbf{D}_k^{(g)}\right]^{-1}$ relation can be obtained from (4.9) and (4.10). Then, $\mathbf{A}_k^{(g)}$ can be rewritten as

$$\mathbf{A}_k^{(g)} = \frac{U_g}{E_s^{(g)}}\mathbf{I}_{U_g} + \left[\mathbf{\Lambda}_{eff,k}^{(g,g)}\right]^H \mathbf{R}_{\tilde{\boldsymbol{\eta}}_f^{(g)}}^{-1} \mathbf{\Lambda}_{eff,k}^{(g,g)}, \tag{D.1}$$

if matrix inversion lemma is utilized for (4.9) with asymptotic correlation matrices. Considering the results above, feedback filters in (4.7) can be expressed as

$$\begin{aligned} \mathbf{C}_k^{(g)} &= -\mathbf{I}_{U_g} + \mathbf{A}_k^{(g)}\mathbf{\Delta}^{(g)} \\ &= -\mathbf{I}_{U_g} + \left(\frac{U_g}{E_s^{(g)}}\mathbf{I}_{U_g} + \left[\mathbf{\Lambda}_{eff,k}^{(g,g)}\right]^H \mathbf{R}_{\tilde{\boldsymbol{\eta}}_f^{(g)}}^{-1} \mathbf{\Lambda}_{eff,k}^{(g,g)}\right)\mathbf{\Delta}^{(g)}. \end{aligned} \tag{D.2}$$

Furthermore, feedforward filters can be obtained if (D.2) is substituted in (4.3). After some manipulations that leverage matrix inversion lemma, feedforward filters can be written as

$$\mathbf{W}_k^{(g)} = \mathbf{R}_{\tilde{\boldsymbol{\eta}}_f^{(g)}}^{-1} \mathbf{\Lambda}_{eff,k}^{(g,g)} \mathbf{\Delta}^{(g)}. \tag{D.3}$$

It can be observed from (D.3) that feedforward filters become scaled forms of whitening matched filters for the asymptotic case. That is, feedback filters perfectly cancel the intra-group signals, and the equalizers reduce to optimal whitening matched filters. Finally, it can be shown that asymptotic SINRs of users can be found as in (4.18), if complex amplitude in (4.16) and residual interference power from (4.17)

are computed with the asymptotic feedforward and feedback filters that are defined above.

Appendix E

CHANNEL ESTIMATORS

E.1 LMMSE Type Channel Estimator

LMMSE type channel estimator of group g can be written as

$$\mathbf{Z}^{(g)} = \mathbf{R}^{-1}_{\bar{\mathbf{y}}^{(g)}} \mathbf{R}_{\bar{\mathbf{y}}^{(g)} \bar{\mathbf{h}}^{(g,g)}_{eff}} \tag{E.1}$$

where covariance matrix between $\bar{\mathbf{y}}^{(g)}$ and $\bar{\mathbf{h}}^{(g,g)}_{eff}$ and covariance matrix of $\bar{\mathbf{y}}^{(g)}$ can be computed as

$$\mathbf{R}_{\bar{\mathbf{y}}^{(g)} \bar{\mathbf{h}}^{(g,g)}_{eff}} = \mathsf{E}\Big\{ \bar{\mathbf{y}}^{(g)} \big[\bar{\mathbf{h}}^{(g,g)}_{eff} \big]^H \Big\} = \Big(\mathbf{X}^{(g)} \otimes \mathbf{I}_{D_g} \Big) \mathbf{R}_{\bar{\mathbf{h}}^{(g,g)}_{eff}}, \tag{E.2}$$

$$\begin{aligned} \mathbf{R}_{\bar{\mathbf{y}}^{(g)}} &= \mathsf{E}\Big\{ \bar{\mathbf{y}}^{(g)} \big[\bar{\mathbf{y}}^{(g)} \big]^H \Big\} \\ &= \Big(\mathbf{X}^{(g)} \otimes \mathbf{I}_{D_g} \Big) \mathbf{R}_{\bar{\mathbf{h}}^{(g,g)}_{eff}} \Big(\mathbf{X}^{(g)} \otimes \mathbf{I}_{D_g} \Big)^H + \mathbf{I}_T \otimes \mathbf{R}^{(g)}_{\tilde{\boldsymbol{\eta}}}, \end{aligned} \tag{E.3}$$

where covariance matrix of sum of inter-group interference and noise terms in reduced dimension is denoted by $\mathsf{E}\Big\{ \tilde{\boldsymbol{\eta}}^{(g)}_n \big[\tilde{\boldsymbol{\eta}}^{(g)}_{n'} \big]^H \Big\} = \mathbf{R}^{(g)}_{\tilde{\boldsymbol{\eta}}} \delta_{nn'}$. This covariance matrix can be expressed as $\mathbf{R}^{(g)}_{\tilde{\boldsymbol{\eta}}} = \big[\mathbf{S}^{(g)} \big]^H \mathbf{R}^{(g)}_{\boldsymbol{\eta}} \mathbf{S}^{(g)}$. Other groups are assumed to be in data transmission mode in (E.3) according to Remark 3. That is, $\mathbf{X}^{(g')}$ is taken as a random matrix for $g' \neq g$ which is why $\mathbf{R}^{(g)}_{\tilde{\boldsymbol{\eta}}}$ is used in (E.3). Covariance matrix of the overall

effective channel of group g is expressed as

$$\begin{aligned}\mathbf{R}_{\bar{\mathbf{h}}_{eff}^{(g,g)}} &= \mathsf{E}\left\{\bar{\mathbf{h}}_{eff}^{(g,g)}\left[\bar{\mathbf{h}}_{eff}^{(g,g)}\right]^H\right\} \\ &= \text{blkdiag}\left\{\sum_{l=0}^{L-1}\mathbf{E}_{L,l+1}\otimes\left[\mathbf{S}^{(g)}\right]^H\mathbf{R}_l^{(g_u)}\mathbf{S}^{(g)}\right\}_{m=1}^{U_g}\end{aligned} \tag{E.4}$$

where $\mathbf{E}_{L,l+1} \triangleq \mathbf{e}_{L,l+1}\mathbf{e}_{L,l+1}^H$ and $\mathbf{e}_{L,l+1} \triangleq \left[\mathbf{I}_L\right]_{(:,l+1)}$. It is important to note that due to uncorrelated structure of channel vectors, (E.4) has a block diagonal form where blocks in the diagonals are covariance matrices of effective channels.

E.2 LS Type Channel Estimator

LS type channel estimator of group g can be expressed as

$$\mathbf{Z}^{(g)} = \left(\mathbf{X}^{(g)}\left(\left[\mathbf{X}^{(g)}\right]^H\mathbf{X}^{(g)}\right)^{-1}\right)\otimes\mathbf{I}_{D_g}. \tag{E.5}$$

However, $\bar{\mathbf{h}}_{eff}^{(g,g)}$ has a sparse structure which degrades the performance of LS estimator given in (E.5). We should eliminate the columns of $\mathbf{X}^{(g)}$ corresponding to the inactive MPCs and find the estimator in (E.5). Then, we should insert zero columns to the estimator to make up for the eliminated columns. These zero columns in $\mathbf{Z}^{(g)}$ leads to estimating zero vectors for channels belonging to inactive MPCs. In this way, the dimension of the inverse in the LS estimator is reduced and performance of the estimator is increased.